EFFECT OF INCORPORATING IRIDIUM IN CONJUGATED POLYMERS ON LIGHT-EMITTING AND PHOTOVOLTAIC PROPERTIES

by

Gisela Louisa Schulz
B.Sc. (Hons), McGill University, 2002

THESIS SUBMITTED IN PARTIAL FULFILLMENT OF
THE REQUIREMENTS FOR THE DEGREE OF

DOCTOR OF PHILOSOPHY

In the
Department
of
Chemistry

© Gisela Schulz 2009

SIMON FRASER UNIVERSITY

Spring 2009

APPROVAL

Name: Gisela Louisa Schulz

Degree: Doctor of Philosophy

Title of Thesis: Effect of Incorporating Iridium in Conjugated Polymers on Light-Emitting and Photovoltaic Properties

Examining Committee:

Chair

Dr. Michael H. Eikerling
Assistant Professor, Department of Chemistry

Dr. Steven Holdcroft
Senior Supervisor
Professor, Department of Chemistry

Dr. Erika Plettner
Supervisor
Associate Professor, Department of Chemistry

Dr. Melanie A. O'Neill
Supervisor
Assistant Professor, Department of Chemistry

Dr. Vance E. Williams
Internal Examiner
Associate Professor, Department of Chemistry

Dr. Mario Leclerc
External Examiner
Professor, Department of Chemistry
Laval University

Date Defended/Approved: January 22, 2008

Declaration of
Partial Copyright Licence

efficient photon to electron conversion. In the case of poly(fluorene-co-bithiophene-co-iridium) it is believed that the morphology of the polymer:[6,6]-phenyl C_{61} butyric acid methyl ester blend plays a dominate role in determining photovoltaic properties.

The structure-property relationships identified in this work build on the current understanding of iridium-bound conjugated polymers, and may be relevant to other conjugated polymer systems. The relationships drawn from this work should prove useful for the design of new polymers for light-emitting and photovoltaic applications.

Keywords: conjugated polymers, polyfluorene, iridium complexes, phosphorescence, light emitting devices, photovoltaic devices

Subject Terms: synthesis of conjugated polymers, iridium-bound conjugated polymers, light-emitting properties of conjugated polymers, photovoltaic properties of conjugated polymers.

DEDICATION

To you

ACKNOWLEDGEMENTS

and Mr. Bryan Gormann, for helping with the operation of the thermal evaporator in physics.

My proof readers, Dr. Tim Peckham and Dr. Theresa Kitos.

TABLE OF CONTENTS

LIST OF FIGURES

xii

LIST OF TABLES

GLOSSARY

A	absorbance
EL	electroluminescence
EQE	external quantum efficiency
F8T2	poly(9,9-dioctylfluorene-alt-bithiophene)
F6T2	poly(9,9-dihexylfluorene-alt-bithiophene)
FET	field effect transistor
FF	fill factor
GC	gas chromatography
GPC	gel permeation chromatography
HOMO	highest occupied molecular orbital
I	intensity
ISC	intersystem crossing
ITO	indium tin oxide
IQE	internal quantum efficiency
I-V	current-voltage
λ	wavelength
LED	light emitting device
LUMO	lowest unoccupied molecular orbital
μ	mobility

NMR	nuclear magnetic resonance
P3HT	poly(3-hexylthiophene)
PCBM	[6,6]-phenyl C_{61} butyric acid methyl ester
PCE	power conversion efficiency
PEDOT	poly(3,4-ethylenedioxythiophene)
PF	polyfluorene
PFO	poly(9,9-dialkylfluorene)
PFPy	poly(fluorene-co-pyridine)
PFT	poly(fluorene-co-thiophene)
PL	photoluminescence
PSS	poly(styrenesulphonic acid)
PT	polythiophene
PV	photovoltaic
THF	tetrahydrofuran
TPBI	1,3,5-tris(N-phenylbenzimidazol-2-yl)benzene
UV-vis	ultraviolet-visible

CHAPTER 1: INTRODUCTION

1.1 A General introduction to conjugated polymers

Conjugated polymers (CPs) have been an area of active research since the discovery in the late 1970s of metallic, electrical conductivity in doped poly(acetylene) (PA). The structure of PA is shown in Figure 1.1.[1]
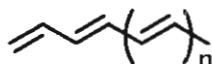
Figure 1.1: Molecular structure of polyacetylene.

Since that initial breakthrough, a wide range of conjugated polymers has been synthesized, for example, poly(p-phenylene), polypyridine, polythiophene and polyaniline. Conjugated polymers are of considerable interest because of their potential to combine the electronic properties of metals and semiconductors with the solution processing and mechanical properties of polymers. This combination of properties yields possibilities for applications that range from light emitting devices (LEDs)[2, 3] to field effect transistors (FETs)[4] to photovoltaic (PV) devices.[5-7]

The structure-property relationship of these diverse polymers has been probed through synthetic and experimental techniques that enable the preparation of a large array of polymers, thus, facilitating the potential fine-tuning of their optical, electronic and mechanical properties. However, only the techniques pertaining to the work described herein will be discussed in subsequent sections. Figure 1.2 presents a few select examples of common CPs.
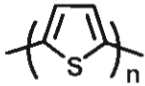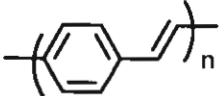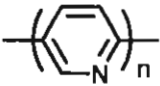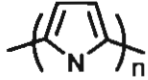
Structure	Name	Abrreviation

 Polythiophene — PT

 Poly(p-phenylene) — PPP

 Poly(p-phenylvinylene) — PPV

 Polypyridine — PP

 Polyaniline — PA

Figure 1.2: Some common conjugated polymers.

The conjugated polymers shown in Figure 1.2 are not soluble in common organic solvents, making them difficult to study. Multiple synthetic approaches are employed to overcome this challenge. First, some of the hydrogen atoms on the repeat units can be replaced with alkyl groups. For example, in the case of PT, alkyl chains can be added to the 3-position, yielding soluble poly(3-alkylthiophene) (P3AT). Alternatively, soluble copolymers can be prepared from repeat units that would typically yield insoluble homopolymers, as long as one of the monomers is able to form a soluble homopolymer. This last strategy was used throughout the work presented here to incorporated iridium complexes into the CP backbone.

1.2 Synthesis of conjugated polymers

The following section highlights a few of the many synthetic techniques available for making conjugated polymers. The work described in this thesis concerns fluorene, thiophene, pyridine and iridium copolymers. Although Suzuki

polymerization was the only method used to prepare the polymers of interest, a brief introduction to some of the other synthetic techniques demonstrates the structural control that is possible with other methods and the motivation for using Suzuki polymerization. Synthetic method development is a very important area within the field of conjugated polymers, however it is not the focus of this work.

1.2.1 Polythiophenes

Poly(3-alkylthiophene)s (P3ATs) are studied extensively in the field of conjugated polymers, various configurational isomers that can form when two 3-alkylthiophenes combine (Figure 1.3).
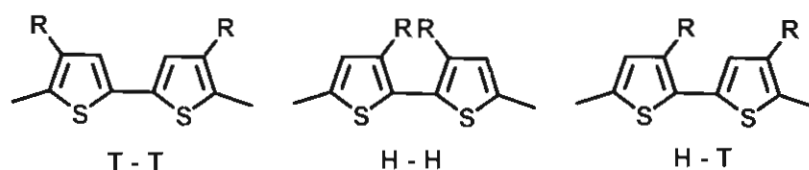
Figure 1.3: Possible configurational isomers formed with two 3-hexylthiophene units.

The steric interactions between the R-groups in a polymer containing all three isomers, compared to a polymer with only the head (H) to tail (T) isomer, are dissimilar, resulting in astonishingly different properties. If the poly(3-alkylthiophene) (P3AT) contains only H-T linkages, the polymer is referred to as regio-regular P3AT. Conversely, if it contains all three types of linkages, it is called regio-random P3AT. The structure-property relationships of P3ATs and in particular poly(3-hexylthiophene) (P3HT) have long been an area of active research within the field of CPs.[8] Various synthetic methods have been developed that yield either regio-regular or regio-random P3AT. For simplicity, only one example of each is given in the discussion below.

1.2.1.1 Chemical Oxidative Coupling

Oxidative coupling is a widely used polymerization method for making regio-random polymers that was developed in the 1960s by Kovacic.[9] The reaction is fast, inexpensive and can be performed on a large scale making it

3

popular for use in industry. One disadvantage of the method is its tendency to produce structural defects in the polymer by causing reactions to occur at both the 2,5- and the 3,4-positions.[10] A variety of catalysts and Friedel-Crafts reagents have been used successfully in oxidative polymerizations. $FeCl_3$ is the most commonly used catalyst (see Figure 1.4 below):
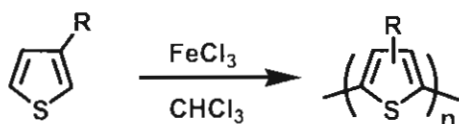
Figure 1.4: Oxidative coupling used to yield regio-random P3HT.

1.2.1.2 The McCullough Method

McCullough developed a synthetic technique to circumvent the formation of H-H linkages.[11] The method is based on a regio-selective synthesis, such as the lithiation of 2-bromo-3-alkylthiophene at the 5-position, followed by metal exchange to obtain the Grignard compound, which is polymerized by cross-coupling using $Ni(dppp)Cl_2$ as the catalyst. See Figure 1.5 below:
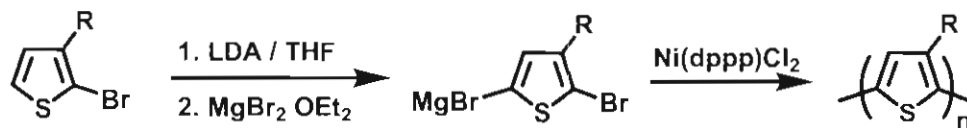
Figure 1.5: McCullough polymerization used to yield regio-regular P3HT.

1.2.2 Polyfluorene and polyfluorene copolymers

In addition to polythiophenes, polyfluorenes (PFs) are another class of CPs that have been a topic of intense research due to their pure blue emission, efficient electroluminescence, high charge carrier mobility and synthetic tunability. The synthesis of PF was first reported by Yoshino in 1989 by oxidatively coupling 9,9-dihexylfluorene using $FeCl_3$.[12] Oxidative coupling produced low molecular weight PF with some structural defects. The quest for well-defined, high molecular weight, defect free polymers became the driving force for developing new techniques for the synthesis of CPs. Polymer chemists

4

adapted three methods used in aromatic "small molecule" coupling reactions for polymer synthesis, leading to Yamamoto,[13] Suzuki[14] and Stille[15] polymerization methods. All three techniques can be used to make high molecular weight homo- or co-polymers. Only the first two techniques will be described here.

1.2.2.1 Yamamoto Coupling

First reported by Yamamoto in 1977, Yamamoto coupling is similar to oxidative coupling in that it produces a regio-random polymer.[13] Although the reaction can be used to make both homopolymers and copolymers, it is sensitive to air and moisture, making it more cumbersome than other methods. In general, Yamamoto coupling involves a nickel-catalyzed coupling of a dihaloaromatic compounds such as 2,7-dibromofluorene, as shown in Figure 1.6.
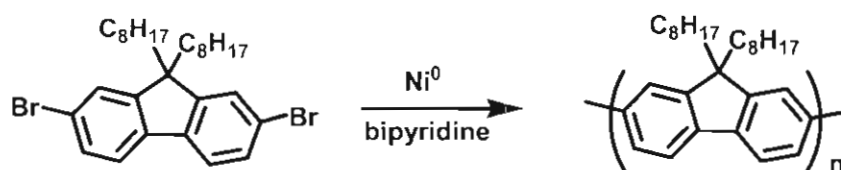
Figure 1.6: Yamamoto coupling used to produce poly(9,9-dioctylfluorene).

1.2.2.2 Suzuki Coupling

Suzuki coupling is a versatile method that is used primarily to make alternating copolymers but can also be used to make homopolymers. It was first reported by Wegner and coworkers in 1989 for the synthesis of poly(p-phenylene)s.[14] Suzuki couplings normally involve a palladium-catalyzed reaction between an organoboronic acid or ester and halides (see Figure 1.7 below). The reaction conditions are milder than those used in Yamamoto coupling, i.e., the reaction is sensitive to the presence of air but not to water.
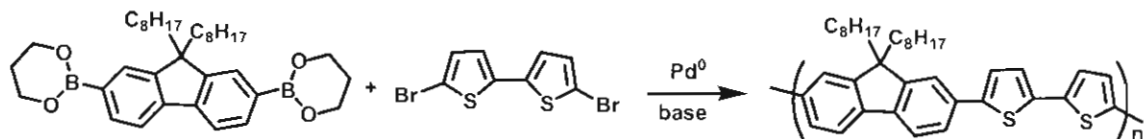
Figure 1.7: Suzuki coupling used to produce poly(fluorene-alt-bithiophene).[16]

1.3 Properties of conjugated polymers

1.3.1 Electronic band gap

The unique optical and electronic properties of CPs originate from their extended π-conjugated system, which is delocalized over a large number of recurring monomer units. Conjugated molecules contain alternating double and single bonds. Starting with ethylene (see Figure 1.8 below), the π-band or orbital is divided into π bonding and π* antibonding orbitals. Since each orbital can hold two electrons per atom, the π orbital is filled and the π* orbital is empty. The energy difference between the highest occupied molecular orbital (HOMO) and the lowest unoccupied molecular orbital (LUMO) is defined as the band gap (E_g). As the number of repeat units in the molecule increases, the band gap becomes narrower. The Hückel approximation predicts that the band gap should approach zero (i.e., that of metallic conductors) as delocalization increases. That is not the case for CPs and can be explained using Peierls distortion theory;[17],[18] which states that there is an electronic instability in one-dimensional metals, and this results in the observed band gap of conjugated polymers.
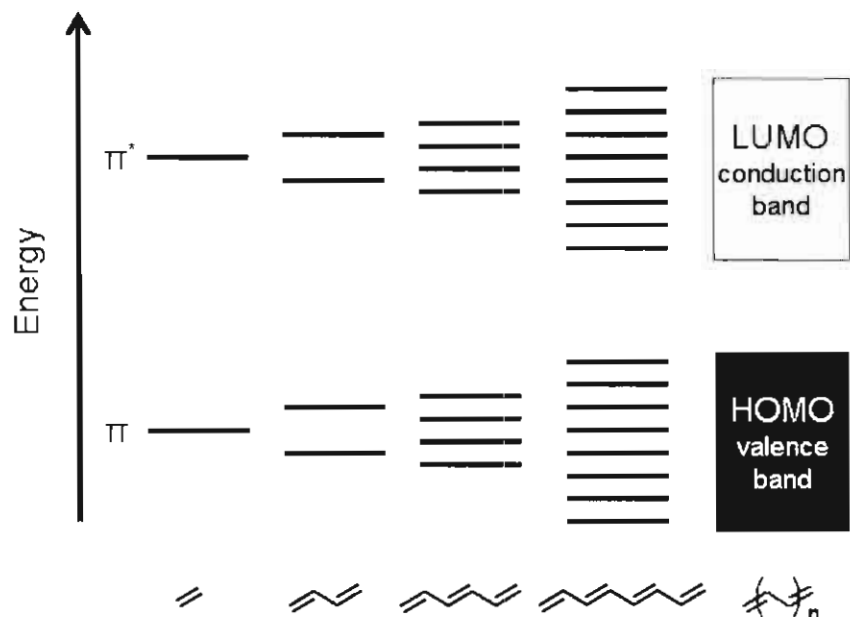
Figure 1.8: Band diagram for the delocalization of electrons in conjugated molecules.

Since the E_g depends on the molecular structure of the repeat unit, it is possible to design polymers that posses different energy gaps.

1.3.2 Energy transfer

Energy transfer is defined as the donation of excitation energy from one molecule or one chromophore to another and is described by Equation 1.1,

Equation 1.1:
$$D^* + A \rightarrow D + A^*$$

where D represents a donor molecule, A represents an acceptor molecule and * denotes electronic excitation. Two types of energy transfer, resonance and exchange, will be discussed.

The main requirement for transfer is spectral overlap between the donor emission and the acceptor absorption. Resonance energy transfer, also called Förster energy transfer, is a long-range transfer process that involves dipole-dipole interactions and transfer distances between 10 to 100 nm.[19] Förster

7

developed Equation 1.2 describing the rate of energy transfer from a donor to an acceptor as a result of dipole-dipole interactions,

Equation 1.2:
$$k_{D^* \to A} = \frac{8.8 \times 10^{-25} \kappa^2 \phi_D}{n^4 \tau_D R^6} \int_0^\infty F_D(v) \varepsilon_A(v) \frac{dv}{v^4}$$

where $k_{D^* \to A}$ is the rate constant for energy transfer, F_d is the donor-acceptor separation, κ^2 is an orientation factor, ϕ_D is the quantum yield for emission from the donor, n is the refractive index of the solvent, τ_D is the mean lifetime of the donor excited state, $F_D(v)$ is the normalized spectral distribution of donor emission, and $\varepsilon_A(v)$ is the molar extinction coefficient of the acceptor as a function of the frequency (v).

In contrast, the short-range process of exchange energy transfer, also called Dexter energy transfer, involves overlap of the electron clouds, which necessitates close proximity of the donor and acceptor to enable energy transfer.[19] Dexter developed Equation 1.3 and 1.4 describing the rate of energy transfer from a donor to an acceptor using the exchange energy transfer mechanism,

Equation 1.3:
$$k_{D^* \to A} = \frac{2\pi}{\hbar} Z^2 \int_0^\infty f_D(v) f_D(v) dv$$

where Z^2 is given by Equation 1.4,

Equation 1.4:
$$Z^2 = K^2 \exp \frac{-2R}{L}$$

where K is a constant with the dimensions of energy, L is a constant called the effective average Bohr radius, $f_D(v)$ is the donor emission spectrum, and R is the donor-acceptor distance. When comparing Equation 1.2 and 1.3, it is clear that the rate constant is more dependant on R in exchange energy

8

transfer than in the case of resonance energy transfer. Both singlet-singlet and triplet-triplet energy transfer can occur by electron exchange. However, the latter is formally forbidden in resonance energy transfer.

A generalized example for energy transfer in a host-guest system is shown in Figure 1.9:
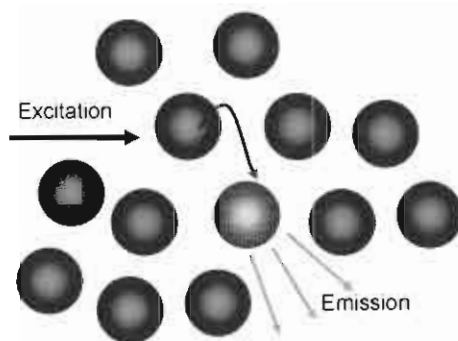
Figure 1.9: General representation of host-guest energy transfer. Blue spheres are the host molecules and the green sphere is the guest.

The fundamental study of energy transfer in conjugated polymers has been on-going for decades and has more recently been applied to the field of LEDs, by way of host-guest systems, in order to increase luminescence efficiencies in conjugated polymer films.[20]

1.3.3 Host-guest systems

'Host-guest' is a term that is used interchangeably with 'donor-acceptor', however the terms are not equivalent. For example, 'host-guest' can describe a system where matrix materials physically isolate the guest molecules from one another, in effect blocking energy transfer. However, such a system would not be described as donor-acceptor, since there is no donor-acceptor interaction between the matrix and the guest molecules. The photophysical and morphological properties of host-guest and donor-acceptor systems have been studied in both molecular-based LEDs (OLEDs) and polymeric-based LEDs (PLEDs). These studies are of interest to further the understanding of the energy

transfer and emission properties of the different host-guest systems. The mechanism for energy transfer is discussed in section 1.3.2.

In both fluorescent and phosphorescent molecular-based systems, only a small concentration of the "guest" is required to enhance solid-state efficiency. Some systems are designed such that an emitter molecule is dispersed in a non-emitting host, as is the case with rhodamine 6G dispersed in poly(methyl-methacrylate).[21] This system shows that concentration quenching can be reduced by physically isolating the guest moieties from one another.

Employing a similar idea, host-guest systems have been studied in films consisting of two different "small molecules", where the emitting guest is dispersed in an emitting host, see Figure 1.10 for a few representative structures. These systems require the host to transport charges and form electronic excited states as a result of either light absorption or charge injection in a LED. The absorption profile of the guest must also overlap with the emission of the host, as discussed previously in section 1.3.2. Phosphorescent OLEDs based on small molecules have received the most attention to date. Organometallic complexes of Pt,[22, 23] Os,[24] Ru[25], Eu,[26, 27] Re[28] and Ir[29, 30] have all been investigated to varying extents as the emitting species in phosphorescent OLEDs. Iridium complexes were chosen for this study on phosphorescent polymers due to their high photoluminescent quantum yields in solution (0.4).[31] For example, 1.5 mol % of tris(2-phenylpyridine)iridium(III) (Ir(ppy)$_3$), doped in 4,4'-bis(N-carbazolyl)-2,2'-biphenyl (CBP) gave a quantum yield of 97± 2 %.[32] Nevertheless, the use of small organic molecules requires vacuum deposition of multilayer structures, and this process increases fabrication costs. In an attempt to mitigate the need for vacuum deposition processes, small molecules have been doped into polymer matrices. These systems are solution processible and, in principle, allow for easy deposition of multiple layers. Examples of such systems include poly(vinylcarbazole) (PVK) doped with Ir(ppy)$_3$,[29] blends of PVK and 2-tert-butylphenyl-5-biphenyl-1,3,4-oxadiazol (PBD) doped with tris(2,5-bis-2'-(9,9-dihexylfluorene)pyridine)iridium(III) (Ir(HFP)$_3$)[33] and poly(9,9-dioctylfluorene) (PFO) doped with Ir(ppy)$_3$.[34]
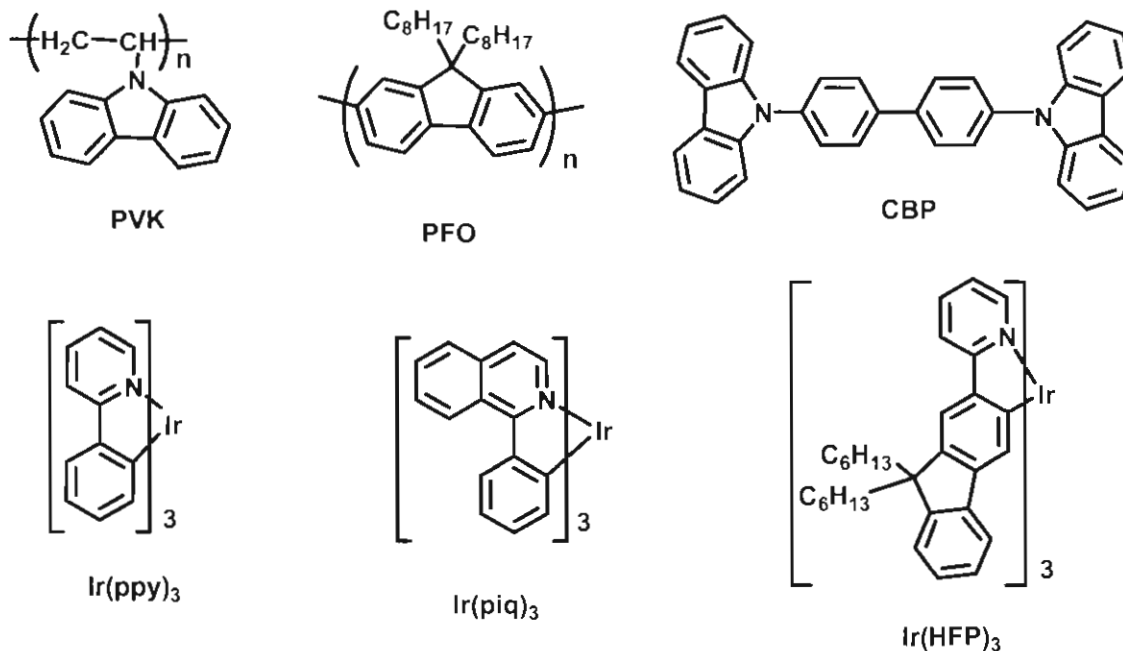
Figure 1.10: Representative chemical structures of host-guest materials used in LEDs.

Other host-guest systems include polymer:polymer blends, such as the poly(fluorene) and poly(phenylenevinylene) (PPV) blends reported by Yang and coworkers. They found that emission spectrum of the blend resembled that of PPV, and the luminous efficiency of LEDs prepared from blends was 70 % higher than that of pristine PPV.[20]

However, all of the above systems suffer from phase segregation over time, which lowers their performance in LEDs[35] and provides motivation for the study and synthesis of copolymers that contain both host and guest moieties. This concept was previously investigated with a study on copolymers of fluorene, 2.5-linked-thiophene and 3,4-linked-thiophene, structure shown in Figure 1.11.[36] It was found that fluorescent quantum yields of films containing copolymers can be increased from 6 % to 42 %, when the mole % of a fluorescent guest in the polymer, fluorene-alt-2,5-linked thiophene was decreased from 100 to 8% within the polymer backbone. Additional examples exist that are similar to this work, wherein the guest is a phosphorescent moiety.[37] The study of phosphorescent

11

groups covalently bound to conjugated polymers is directly related to the work presented in this thesis and is reviewed in the introduction to Chapter 2.
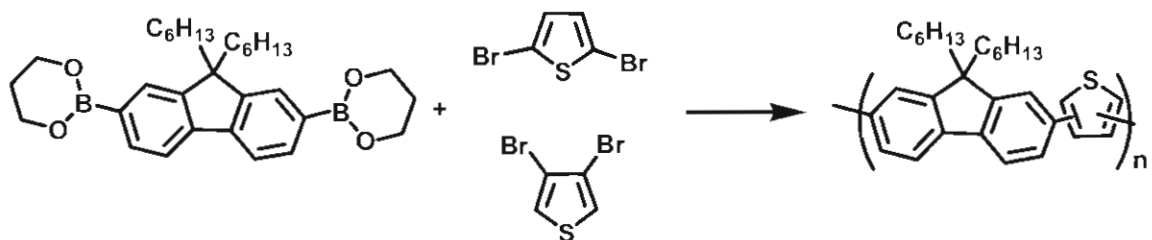
Figure 1.11: Synthetic scheme for PFTs with various feed ratios.[36]

1.3.4 Morphology of conjugated polymer films

Another important property of conjugated polymer films is their morphology, i.e., the molecular packing and orientation in the solid state. Design of conjugated polymers and optimization of processing conditions have allowed for precise control over morphological properties. The knowledge gained through morphology studies has been crucial in the application of conjugated polymers in light emitting and photovoltaic devices.

It has been shown that the structure of poly(3-alkylthiophene)s strongly influences solid state packing, and in turn the crystallinity of the polymer film.[38, 39] For example, it is possible to prepare poly(3-hexylthiophene) (P3HT) with varying amounts of head to head (H-H), tail to tail (T-T) and head to tail (H-T) linkages (see section 1.2.1). It has been shown that regio-regular P3HT (polymers with ~ 80 % H-T linkages) have vastly different film morphologies than regio-random P3HT polymers possessing ~ 50 % H-T linkages. Regio-regular P3HT forms highly ordered, planar, semi-crystalline polymer films, where as films of regio-random P3HT are less ordered due to a higher degree of twisting which is a consequence of the steric hindrance of H-H couplings. Polymer crystallinity is typically probed using X-ray diffraction. An example of a diffraction pattern is shown in Figure 1.12, comparing thin films of 52 % H-T (a), 60 % H-T (b) and 80 % H-T linkages (c). The increased crystallinity is evidenced by the increased peak intensity at 2θ equals ~ 5° for 80% H-T vs. 52 % H-T P3HT in Figure 1.12.
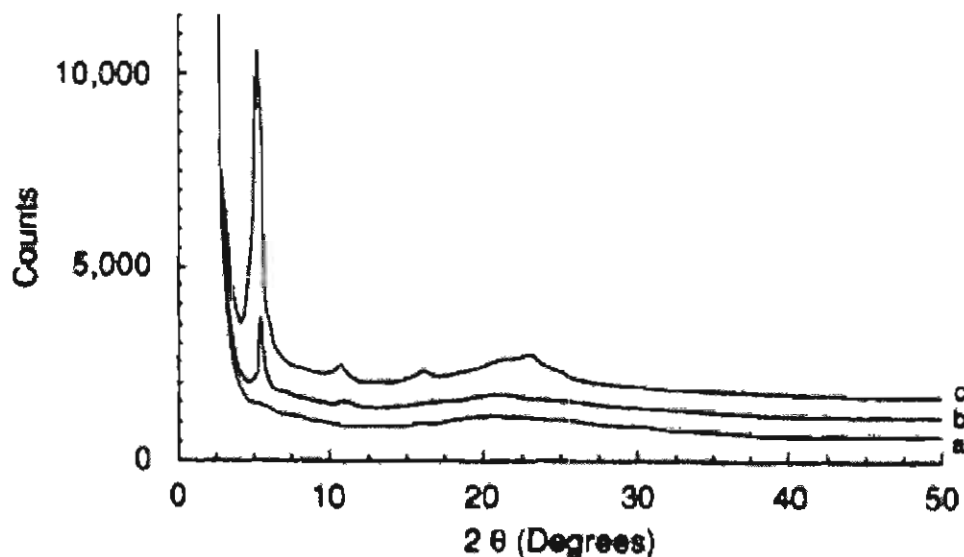
Figure 1.12: X-ray diffraction profiles of P3HT; (a) 52 % H-T, (b) 60 % H-T and (c) 80 % H-T linkages. Reprinted with permission from [39]. Copyright [1993], American Chemical Society.

Interestingly, not all conjugated polymers form semi-crystalline domains, more commonly films are amorphous. Polymers are termed amorphous when the polymer chains are arranged randomly, with no clear long-range order. For example, poly(9,9-dialkylfluorene)s are amorphous polymers.[40] The length and structure of the alkyl substituents do not influence the optical or electronic properties of the polymers in dilute solutions because of the large distance between the C-9 position and the aryl-aryl 2- and 7-positions of the monomer unit. However, the structure of the alkyl chains strongly influences the solid-state packing of the polymers. In some alkyl fluorenes (including PFO) a unique type of aggregation has been observed which has been termed β-phase formation. The β-phase morphology has different absorption and emission properties than the standard PFO, and exhibits red shifted absorption and emission spectra, and well-defined vibronic transitions. Even though PFO does not exhibit semi-crystalline behaviour, control over the film morphology can be used to modify optical properties such as absorption and emission.

1.3.5 Energy levels and photophysics

Knowledge of the energy levels of conjugated polymers is of the utmost importance if the polymers are to be considered for either electroluminescent (EL) or photovoltaic (PV) devices. In EL, the emission wavelength of the polymer is dependant on the band gap, whereas in PV, the absorption of incident light is dependant on the band gap. In EL and PV, device operation requires a small barrier for hole and electron charge injection into the polymer or electrodes; this will be discussed in more detail in section 1.3.6 and 1.3.7. Note that in Figure 1.13, a small energy barrier between the HOMO of the conjugated polymer (P3HT) and the workfunction of the anode (ITO) is shown, allowing for hole injection. A significant amount of effort has been devoted to the structural design of conjugated polymers and its relationship to its band gap, HOMO and LUMO levels, as well as to the correlation between these properties and electroluminescent or photovoltaic properties.[41]

Energy

LUMO	
	2.9 eV
4.7 eV	HOMO
	5.0 eV
ITO	P3HT	Ca
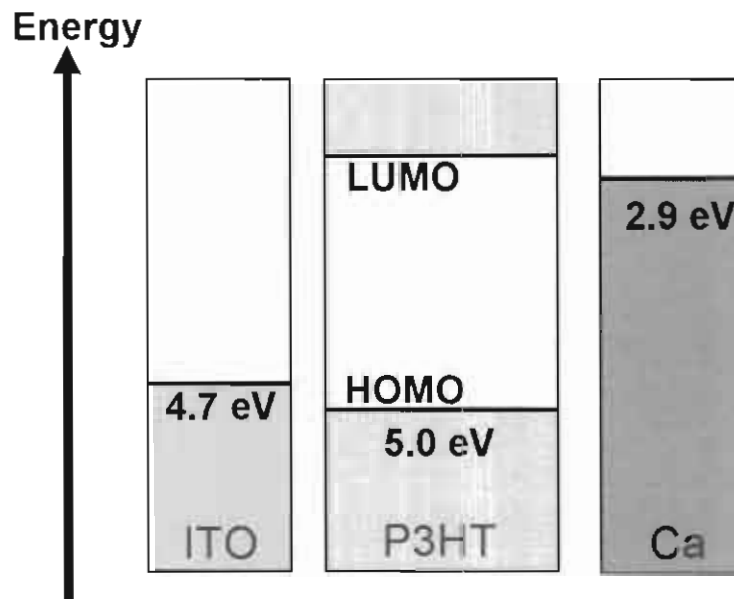
Figure 1.13: Energy level diagram showing the work function of electrodes and HOMO-LUMO levels of P3HT.

In addition to determining the energy of the HOMO and LUMOs of conjugated polymers, much work has involved studying the various

photophysical processes that can occur upon electronic excitation, processes such as energy transfer, fluorescence or non-radiative decay, all of which have been defined in section 1.3.2 and 1.4.1 of this thesis. Figure 1.14 shows some of the possible processes that may occur upon excitation in a phosphorescent polymer. The relative rates of these competing processes will determine the fate of the excited state molecule. For example, phosphorescence by the iridium complex (process (d)) competes with back energy transfer from the iridium triplet to the triplet state of the polymer (process (b)), as well as concentration quenching (process (c)). In Chapter 2, it is shown that modifying the triplet energy level of the conjugated polymer strongly influences the relative rates of back energy transfer, and, in turn, affects its phosphorescence.
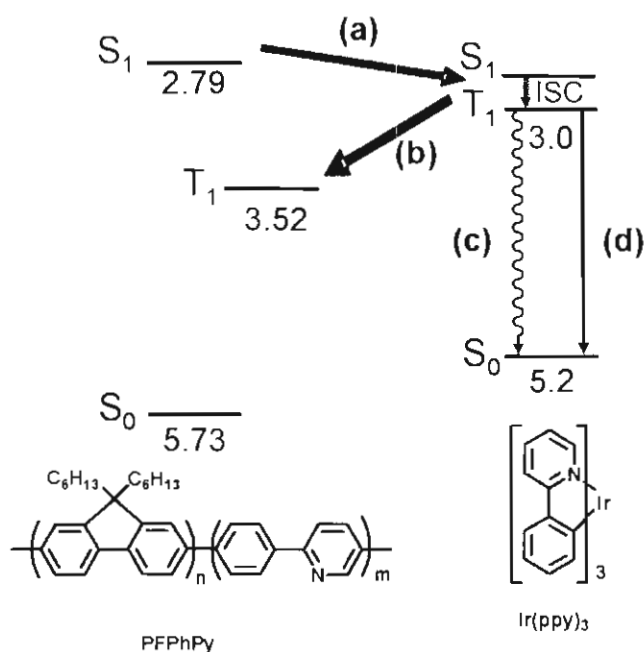
Figure 1.14: Energy level diagram showing (a) energy transfer from the PFPy main chain to the bound Ir complex, (b) triplet quenching of the Ir complex by the PFPy main chain, (c) concentration quenching of the triplet state and (d) phosphorescence of the Ir complex.

When incorporating conjugated polymers in PVs there is at least one additional process that is taken into account since PV devices have a different mechanism of operation than EL devices. This process is photo-induced electron transfer and typically occurs from an electron donor to an electron

acceptor. A variety of materials have been investigated for use as electron acceptors such as fullerenes, perylenes and conjugated polymers with large electron affinities.[42] However, the work presented in this thesis focuses on investigating different conjugated polymers to be used as electron donors and [6,6]-phenyl C_{61} butyric acid methyl ester (PCBM) was used as an electron acceptor. Figure 1.15 demonstrates some of the competing photophysical processes in a phosphorescent polymer blended with PCBM. The energy level diagram shows (a) energy transfer from the PFPhPy main chain to the bound Ir complex, (b) triplet quenching of the Ir complex by the PFPhPy main chain, (c) concentration quenching of the triplet state, (d) phosphorescence of the Ir complex and (e) photo-induced electron transfer from the Ir complex to PCBM.
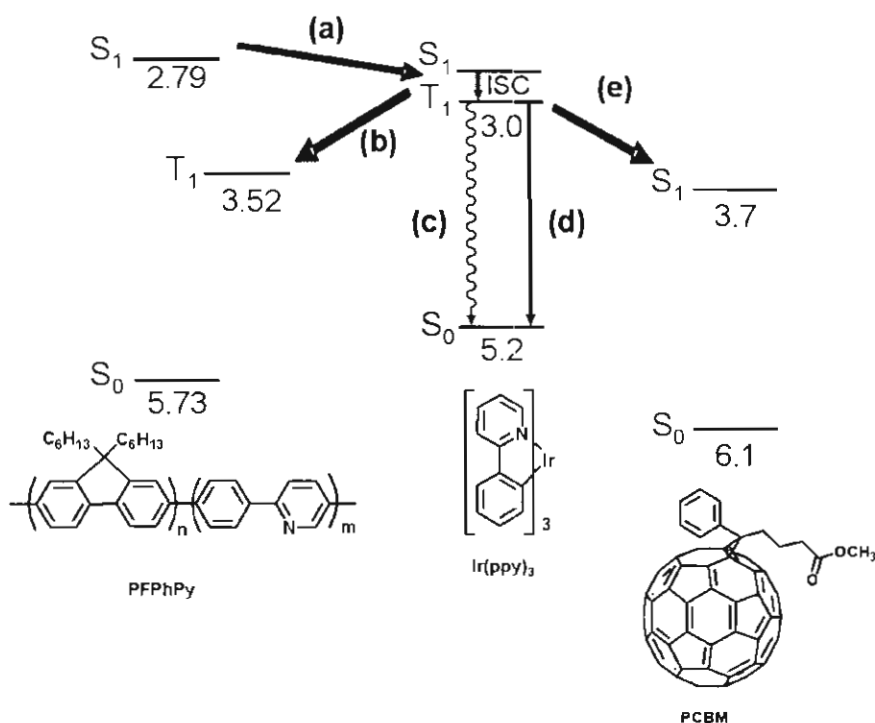
Figure 1.15: Energy level diagram showing (a) energy transfer from the PFPhPy main chain to the bound Ir complex, (b) triplet quenching of the Ir complex by the PFPhPy main chain, (c) concentration quenching of the triplet state, (d) phosphorescence of the Ir complex and (e) photo-induced electron transfer from the Ir complex to PCBM.[43]

Some of the processes that occur during PV operation will be discussed in Chapter 3 in terms of the relative rates of photo-induced electron transfer (e) and

back energy transfer from the triplet state of the iridium complex to the triplet state of the polymer main chain (b). The actual rates of energy transfer and electron transfer were not measured directly, but inferred from the photoluminescence data.

1.3.6 Electroluminescence

Photoluminescent conjugated polymers are of interest because of their potential for applications, such as LEDs. PLEDs are typically made using a sandwich structure, as illustrated in Figure 1.16). Transparent indium tin oxide (ITO) coated glass is used as the anode because of its high work function. On top of the ITO layer, poly(styrene sulfonic acid)-doped poly(ethylenedioxythiophene) (PEDOT:PSS) is spin coated and used as a hole transport layer. This is followed by spin coating of the active layer (conjugated polymer) and finally thermal evaporation of the cathode. The cathode is chosen for its work function, the minimum amount of energy needed to remove an electron from the Fermi energy level into vacuum, and can be Ca, CsF or Mg. Materials that are air sensitive are often coated with aluminum to enhance the stability of the device. To optimize the performance of LEDs, it is important to minimize the barriers for charge injection by choosing electrodes with work functions that are matched to the HOMO and LUMO energy levels of the polymer. Depending on the band gap of the active layer, different emission colors can be obtained, Figure 1.16 shows a photograph of an operating LED made using a polymer described in Chapter 2.
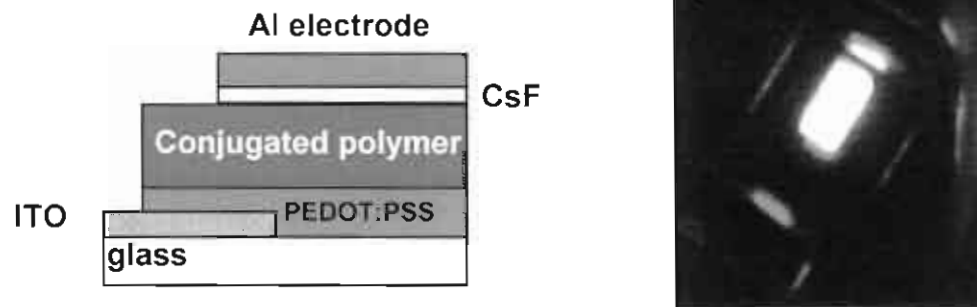
Figure 1.16: Cross section of a typical polymer LED (left) and photograph of an operating LED made using PFTIr10 (Chapter 2, right).

When a potential is applied across the device, charge injection occurs at the electrodes with holes injected by the anode and electrons by the cathode, as shown in Figure 1.18a. A hole is defined as the vacancy created when an electron is excited from the valence band into the conduction band, and is illustrated schematically for polyacetylene in Figure 1.17 by a white circle. An electron carries a negative charge, whereas a hole carries a positive charge.
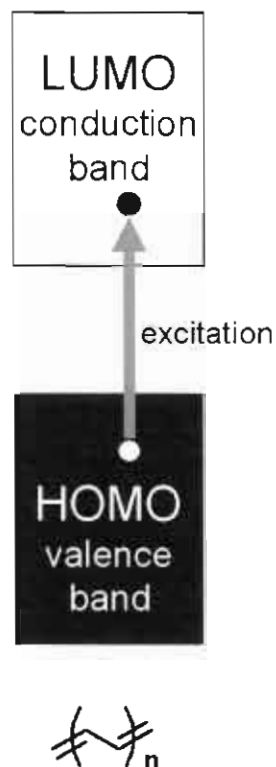
Figure 1.17: Excitation of an electron and hole formation in polyacetylene. The white circle represents a hole and black circle represents an electron.

Recombination of a hole and an electron produces an exciton, which, upon relaxation, emits light through the transparent anode (see Figure 1.18c and the photograph of an operating PLED device in Figure 1.16, left). Characterization of these devices is done primarily by measurement of current-voltage (I-V) and brightness-voltage behaviour, as well as by electroluminescence (EL) and is described in more detail in section 1.4.5.
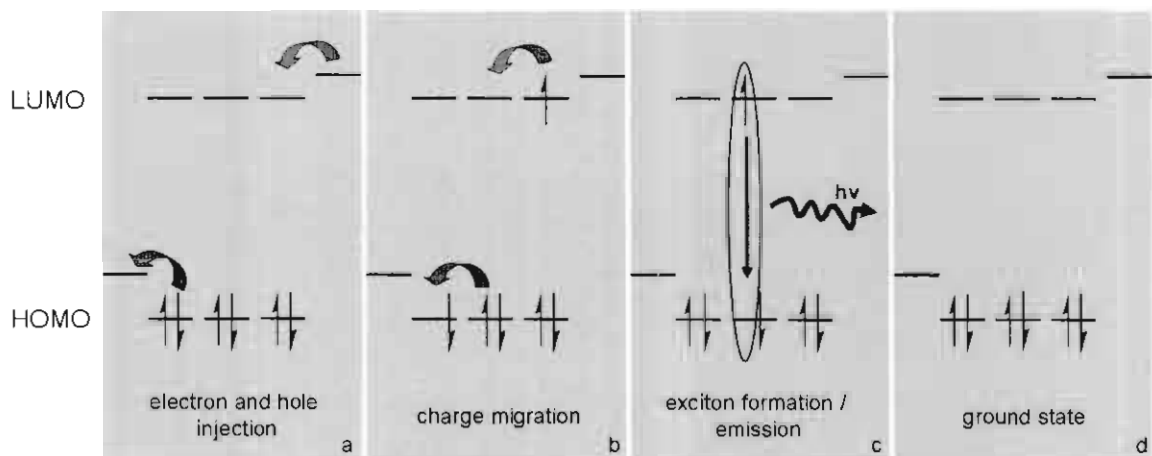
Figure 1.18: Schematic diagram illustrating electron and hole injection (a), charge migration (b), exciton formation and emission (c), and the molecular ground state (d), during LED operation.

1.3.7 Photovoltaics

Conjugated polymers can also be used as the active material in photovoltaic (PV) devices. Bulk-heterojunction polymer PV devices are typically made using a sandwich structure similar to LEDs, as illustrated in Figure 1.19. Indium tin oxide (ITO) is used as the anode and PEDOT:PSS is spin coated on top of this and used as a hole transport layer. The active layer, which consists of a blend of an electron donor (conjugated polymer) and electron acceptor (typically a C_{60} derivative), is spin coated on top of the PEDOT:PSS. The large interfacial area between the donor and acceptor promotes ultrafast charge generation in the device. Light from different regions in the solar spectrum can be captured, depending on the chemical structure of the active layer. The final step in this process is thermal evaporation of the cathode, a component that is chosen for its work function and can be, for example, Ca or Al. In photovoltaic devices, air sensitive metals are often coated with aluminum to enhance the stability of the electrode.
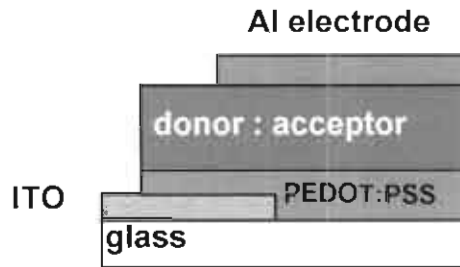
Figure 1.19: Cross section of a typical polymer photovoltaic device.

When the PV device is illuminated, absorption occurs and excitons are generated, as shown in Figure 1.20a. If an exciton diffuses to the donor-acceptor interface, electron transfer can occur, resulting in the generation of a hole on the donor and an electron on the acceptor, shown in Figure 1.20b. Electron transfer is followed by electron and hole transport to the cathode and anode, respectively, as shown in Figure 1.20c. In order for holes and electrons to be transported efficiently, a specific morphology must be formed in the donor–acceptor blend.
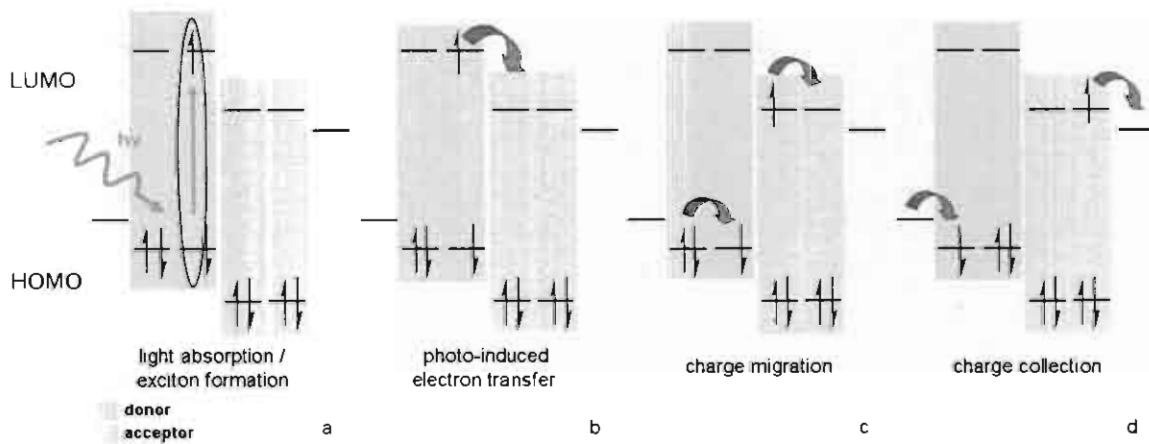
Figure 1.20: Schematic diagram illustrating exciton formation (a), photo-induced electron transfer (b), charge migration (c), and charge collection (d), during PV operation.

In bulk heterojunction PV devices, the structure-morphology relationship is complicated by the introduction of a two component (donor-acceptor) system compared to a single layer polymer LED. The active layer is typically spin coated

21

from a blend of an electron donating polymer and electron accepting fullerene derivative. The morphology of the resulting film is of utmost importance in terms of device operation. To achieve high quantum efficiency in PV devices, a significant fraction of photogenerated excitons must reach and dissociate at a donor-acceptor interface; and subsequently the created charges must drift to their respective electrodes. The dissociation of the bound electron-hole pair (exciton) is termed electron transfer and takes place on the ps time scale.[44] The morphology of the blend will determine, in part, the fate of the excitons and if the above mentioned processes can occur. Morphology is dictated largely by the chemical structure of the materials, but the following parameters have also been found to influence the morphology of the polymer blends on the nanoscale: the solvent used, the composition of the blend, the solution concentration and crystallization induced by annealing.[45] For example, in the case of blends of poly(3-hexylthiophene) (P3HT, electron donor) and [6,6]-phenyl C_{61} butyric acid methyl ester (PCBM, electron acceptor), the blend morphology is strongly influenced by thermal annealing.[46] Yang et. al. reported that annealing the blend results in an increase in crystallinity, mainly for the P3HT phase but also for the PCBM.[47] It was observed that upon annealing, the fibrillar P3HT crystals grow in length and new PCBM domains are developed. As a result, the charge transport improved yielding higher device efficiencies.

One of the primary limitations of a heterojunction photovoltaic device is that singlet excitons have short diffusion lengths (~ 10 nm), therefore only the fraction of incident light absorbed in a thin region near the donor acceptor interface results in the conversion of excitons into charges (i.e., low charge generation). Only the excitons generated within a diffusion length of the interface produce charges. The relatively short diffusion length of singlet excitons are illustrated in Figure 1.21a by the thin black lines separating the donor and acceptor phases. The formation of triplet excitons in photovoltaic devices was investigated in Chapters 3 and 4, using phosphorescent conjugated polymers because the inherent lifetime of triplet excitons is longer than singlet excitons. The longer lifetime of the triplet exciton are expected to increase the diffusion

length assuming the mobility of the exciton is not compromised. The thick black lines Figure 1.21b illustrate the enhanced diffusion length of triplet excitons, which would result in increased charge generation.
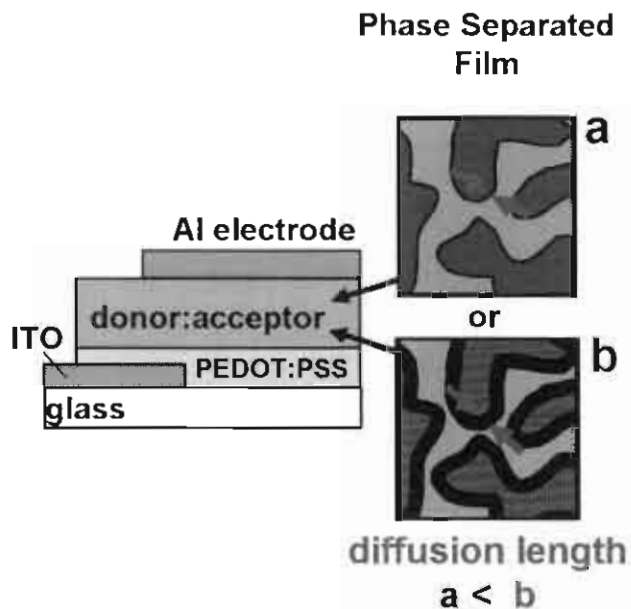
Figure 1.21: Illustration showing the phase separated morphology of a singlet material and its diffusion length represented by the thin black lines at the donor acceptor interface (a) and a triplet material with a longer diffusion length represented by the thicker black lines (b).

1.4 Characterization of conjugated polymers

Conjugated polymers synthesized for the work reported herein were characterized using UV-vis, photoluminescence, ^{1}H NMR, ^{13}C NMR, elemental analysis, cyclic voltammetry, X-ray fluorescence and gel permeation chromatography, as well as with light emitting, photovoltaic and hole-only devices. The techniques of ^{1}H NMR, ^{13}C NMR and elemental analysis are considered routine and, thus, will not be explained here in detail.

1.4.1 Optical techniques

UV-vis spectroscopy allows the quantification of the amount of light transmitted or absorbed by a particular material as a function of wavelength. Absorbance (A) is described by Equation 1.5:

Equation 1.5: $$A = -\log(T) = \log\frac{P_0}{P}$$

where T is the transmittance, P_0 is the incident power of radiation and P is the power of radiation after the light has passed through the sample.[48]

Photoluminescence (PL) is a general term used to describe either fluorescence or phosphorescence and is illustrated in Figure 1.22.[48] In both processes, excitation is caused by the absorption of photons. In fluorescence, an electron is promoted to the excited singlet state (S_1), followed by relaxation from S_1 to the singlet ground state, resulting in emission. The lifetime of the excited state is typically on the order of nanoseconds. In contrast, phosphorescence occurs when the electrons in the excited singlet state undergo intersystem crossing to the triplet state (*i.e.*, change in electron spin), followed by relaxation from T_1 to the singlet ground state. Phosphorescent lifetimes are longer than fluorescent lifetimes, typically on the order of micro to milliseconds.

Conjugated polymers do not normally phosphoresce at room temperature because the change in electron spin (shown as intersystem crossing in Figure 1.22) is formally forbidden. The process becomes partially allowed when heavy atoms such as transition metals are present. The work presented in this thesis will show that phosphorescence occurs in conjugated polymers that have iridium complexes bound to the polymer main chain.
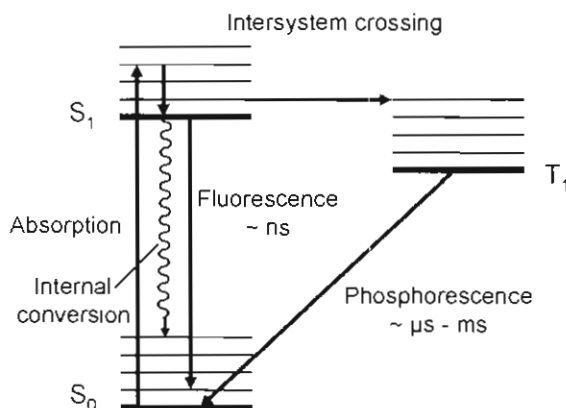
Figure 1.22: Jablonski diagram depicting the process of fluorescence and phosphorescence.

The quantum yield or quantum efficiency of photoluminescence (Φ) is the ratio of emitted photons to absorbed photons. The process of photoluminescence competes with internal conversion (Figure 1.22), an intermolecular process that involves the non-radiative decay of excited electronic states. The competition of rates is reflected in the definition of quantum yield, which is described by Equation 1.6.

Equation 1.6: $$\Phi = \frac{n_{em}}{n_{abs}} = \frac{k_r}{k_r + k_{nr}}$$

where n_{em} is the number of emitted photons, n_{abs} is the number of absorbed photons, k_r is the rate of radiative decay, and k_{nr} is the rate of non-radiative decay.

Two methods are used to measure the quantum yield of photoluminescence.[49] The method of relative standards estimates the quantum yield of a given material based on its fluorescence intensity relative to that of a compound of known fluorescence. The quantum yield is calculated using Equation 1.7,

Equation 1.7: $$\Phi_u = \frac{A_s \times F_u \times n^2}{A_u \times F_s \times n_0^{2}} \times \Phi_s$$

where the subscript u and s refer to the unknown and the standard, respectively; F is the integrated emission area, n is the refractive index of the solvent containing the unknown; and n_0 is the index of refraction of the solvent containing the standard. The emission from the sample is assumed to be uniform in all directions, which is true for dilute solutions, however, for anisotropic films, the emission intensity has an angular dependence, making the determination of the quantum yield more difficult.

The second method for assessing the quantum yield of photoluminescence is a direct measurement using an integrating sphere, which allows for the quantification of both the absorption and emission. The

measurement involves two scans of the photoluminescent spectrum: the first (scan 1 in Figure 1.23) is collected with a blank in the sample holder and is used to obtain a background scan and to determine the intensity of the lamp, while the second (scan 2 in Figure 1.23) performed with sample, measures the reduction of the lamp intensity and the emission profile. The absorption of the sample is calculated by subtracting scan 1 from scan 2 and peak area is calculated to determine the number of photons absorbed by the sample (I_a). The number of photons emitted by the sample is determined by first calculating the ratio of the intensity of scan 2 over that of scan 1, $r = I_{scan\ 2}/ I_{scan\ 1}$, followed by multiplying the computed ratio by scan 1 and subtracting the resulting curve from scan 2. The residual spectrum is the photoluminescence of the sample with the dark and light background noise subtracted (corrected emission in Figure 1.23). The corrected curve is integrated over the range of the emission to give the area (I_p) and the quantum yield is given by I_p/I_a.
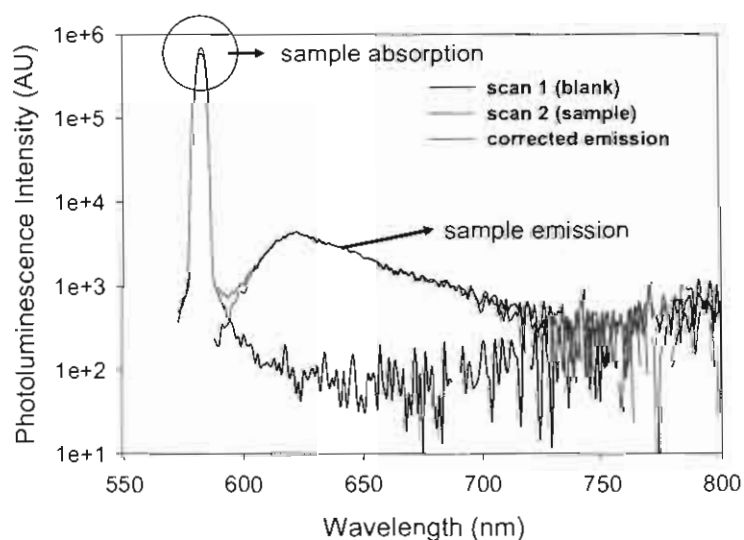
Figure 1.23: Photoluminescence spectra of cresyl violet standard and blank

The integrating sphere system used in this work, tested using a cresyl violet standard, gave a quantum yield of 0.50 ± 0.05, a value that is similar, within experimental error, to the previously reported value of 0.54 ± 0.03.[50]

1.4.2 X-ray fluorescence

X-ray energy spectroscopy (XES), or X-ray fluorescence, is a useful, non-destructive method for quantitative elemental analysis of many different types of samples.[51] This technique was used in the present study to quantify the amount of iridium present in films of conjugated polymers. The principle of X-ray fluorescence is straightforward and similar to the process of fluorescence that was described earlier. When X-rays of sufficient energy strikes an inner shell electron (shown as a in Figure 1.24), an electron is ejected from the atom (shown as b in Figure 1.24), resulting in a vacancy within the inner atomic electron core (K, L, M shells). Following electron rearrangement within the shell (i.e., filling of the vacancy), X-rays are emitted (shown as c in Figure 1.24), and with energy that is characteristic of the element. The total number of emitted X-rays depends upon the concentration of that element in the sample.
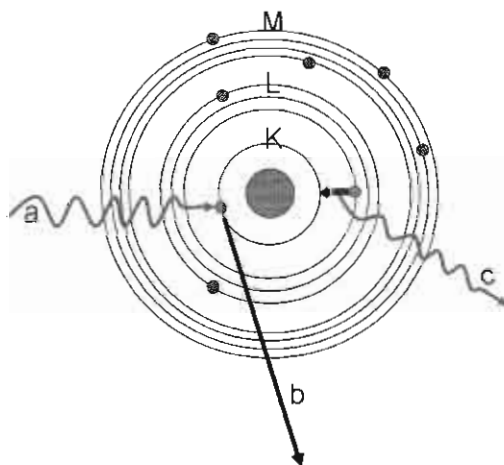
Figure 1.24: Diagram depicting the process of X-ray fluorescence. K,L and M are inner electron shells. An X-ray strking an inner shell electron (process a), electron ejection (process b) and X-ray emission (process c).

1.4.3 Cyclic voltammetry

Cyclic voltammetry (CV) is a technique that is widely used for acquiring information about electrochemical reactions.[52] CV offers rapid estimation of reduction and oxidation potentials of materials, including conjugated polymers. In brief, CV consists of scanning linearly the potential of a stationary working

electrode. During the potential sweep, shown schematically in Figure 1.25, the potentiostat measures the current that results from the applied potential. The plot of current vs. potential is termed a cyclic voltammogram, an example of which is shown for ferrocene in Figure 1.26.
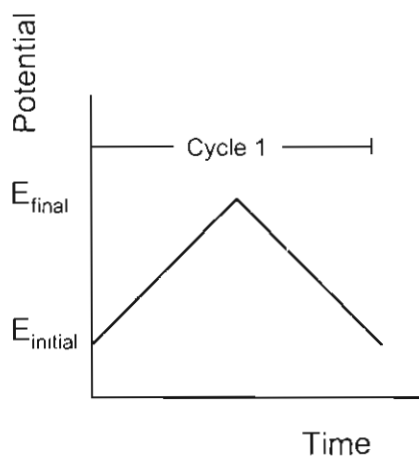
Figure 1.25: Potential vs. time in a cyclic voltammetry experiment.
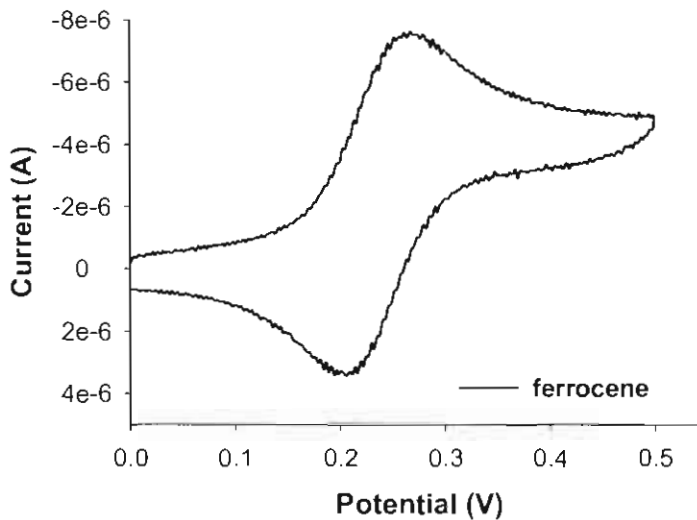
Figure 1.26: A cyclic voltammogram of ferrocene.

As a part of the work for this thesis, cyclic voltammograms were obtained for conjugated polymer films. From the onset of the reduction potential for the n-

doping process and oxidation potential for the p-doping process, it was possible to estimate the LUMO and HOMO energy levels, respectively. All potentials were measured against the ferrocene/ferrocenium redox couple, and the energy levels were estimated using Equation 1.8 and Equation 1.9, where

Equation 1.8: $$IP = -(4.8 + E_{onset}(oxidation))$$

Equation 1.9: $$EA = -(4.8 + E_{onset}(reduction))$$

IP represents the ionization potential (HOMO), EA is the electron affinity (LUMO) and E_{onset} is the potential onset of either the n-doping or p-doping process in the cyclic voltammogram.[53] 4.8 eV is the energy required to remove one electron from ferrocene relative to the vacuum level and must be taken into account when the cyclic voltammograms are measured relative to the ferrocene/ferrocenium redox couple.

1.4.4 Gel permeation chromatography

Size exclusion chromatography is a chromatographic method in which particles are separated based on their size or more specifically, hydrodynamic volume. It is called gel permeation chromatography (GPC) when the column is packed with particles that swell in the presence of solvent and form a gel in which the space between cross-links in the gel surface generates pores of varying diameter.[54] The underlying principle of this method is that particles of different sizes will elute through the column at different rates. Smaller particles enter the smaller pores and "explore" the narrow pore space in the column. However, larger particles cannot enter the narrow pores and therefore pass through the column more quickly. Therefore, smaller particles take a longer time to elute than larger particles. A UV-vis detector monitors the eluent absorption at 254 nm as it exits the column, generating a plot of absorbance vs. time. Weight average and number average molecular weights are calculated using Equation 1.10 and

Equation 1.11, respectively. The ratio of which is defined as the polydispersity index (PDI, Equation 1.12).

Equation 1.10:
$$M_w = \sum_i \frac{n_i M_i^2}{n_i M_i}$$

Equation 1.11:
$$M_n = \frac{\sum_i n_i M_i}{\sum_i n_i}$$

Equation 1.12:
$$PDI = \frac{M_w}{M_n}$$

Where n_i is the number of molecules of molecular weight M_i.

1.4.5 Light emitting devices

The device physics and method of fabrication of polymer light emitting devices (PLEDs) are described in section 1.3.6. To summarize, PLEDs are typically made using a sandwich structure, where the conjugated polymer is sandwiched between a high and low work function electrode. When a potential is applied across the device, charge injection occurs at the electrodes with holes injected by the anode and electrons by the cathode. Charge recombination produces an exciton, which, upon relaxation, emits light through the transparent anode. Characterization of these devices is done primarily by measurement of current-voltage (I-V) and brightness-voltage behaviour, as well as by electroluminescence (EL). EL is the process of light emission as a result of an electrical current passing through a material. The turn-on voltage is the voltage at which the luminance of the device reaches 0.2 cd/m^2.[55] Luminance (L) is a measure of the brightness or luminous intensity of light, usually expressed in units of candelas per square meter (cd/m^2). A luminance of 0.2 cd/m^2 was visible

to the human eye and therefore chosen as the turn-on voltage. Luminous efficiency (LE, cd/A) is calculated using Equation 1.13,

Equation 1.13:
$$LE = \frac{L}{J}$$

where J is the current density. As a point of reference the luminance of a 60 W light bulb is 10^5 cd/m^2 and the luminous efficiency is 600 cd/A.[56, 57] Luminous power efficiency (PE) is described by Equation 1.14:

Equation 1.14:
$$PE = \frac{\pi \times L}{J \times V}$$

The external quantum efficiency (EQE) is calculated and used to normalize the luminous efficiency by the sensitivity of the eye. The EQE is the ratio of emitted photons to the number of electrons injected into the LED and is calculated Equation 1.15,

Equation 1.15:
$$EQE = \frac{5 \times 10^3}{h\nu \times \theta(\lambda)} \times LE$$

where hv is the photon energy in eV of emission and θ (λ) is the photopic luminosity function, which describes the response of the human eye to light.[58, 59] The response of the eye must be accounted for since LEDs are meant to be used for display applications.

1.4.6 Photovoltaic devices

The device physics and method of fabrication of bulk heterojunction organic photovoltaic (PV) devices is described in section 1.3.7. To summarize, PV devices are typically made using a sandwich structure, where a conjugated polymer:fullerene blend is sandwiched between a high and a low work function electrode. When the PV device is illuminated, absorption occurs and excitons are generated. If an exciton diffuses to the donor-acceptor interface, electron

transfer can occur, resulting in the generation of a hole on the donor and an electron on the acceptor. Electron transfer is followed by electron and hole transport to the cathode and anode, respectively. Characterization of these devices is done by measuring the I-V behaviour under white light illumination and in the dark, i.e., no illumination, as well as by measuring the action spectrum under monochromatic illumination. The I-V curve measured in the dark shows that very little current is generated without light, as shown in Figure 1.27.
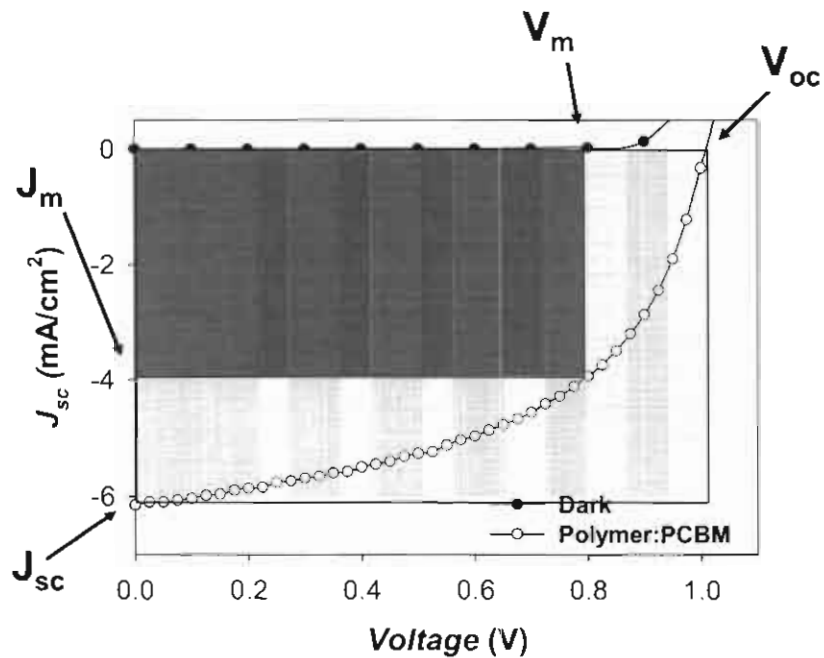
Figure 1.27: Graph of a typical I-V curve for a PV device.

Many useful parameters can be identified from the I-V curve, for example, J_{sc} defined as the short circuit current density, and its magnitude is dependant on charge generation and light absorption. The open circuit potential (V_{oc}) is a parameter whose value is influenced by the energy difference between the HOMO of the donor and the LUMO of the acceptor, as well as by the morphology of the active layer.[60] The fill factor (FF) is defined as the ratio between the maximum power delivered to an external circuit (blue rectangle in Figure 1.27) and the potential power (pink rectangle in Figure 1.27), it is calculated using Equation 1.16,

Equation 1.16:
$$FF = \frac{I_m \times V_m}{I_{SC} \times V_{OC}}$$

where I_m is the current and V_m is the voltage that corresponds to the maximum power obtained from the device. The fill factor is influenced by the absorption, as well as the charge transport in the device, and the larger the value, the better the charge transport.[6] Another value of interest is the power conversion efficiency (PCE). It is calculated using Equation 1.17,

Equation 1.17:
$$PCE = \frac{I_m \times V_m}{P_o} \times 100$$

and is the ratio of the power produced by the photovoltaic device to the power of the white light illumination (P_o).

The action spectrum is the current produced by the device as a function of the wavelength of illumination. The current is used in Equation 1.18 to determine the external quantum efficiency (EQE), *i.e.*, the ratio of electrons generated to the incident photons.

Equation 1.18:
$$EQE = \frac{n_e}{n_{ph}} = \frac{hc \times I_{SC}}{\lambda e \times P_o} \times 100$$

I_{sc} is the short-circuit current, h is Planck's constant, c is the speed of light, λ is the wavelength of light illuminated on the device, e is the charge of an electron and P_o is the incident optical power. Further insight into the operation of the PV device is gained when the EQE is divided by the light absorbed by the device (A). This yields the internal quantum efficiency (IQE) and is defined as the conversion efficiency of photons absorbed to current produced.

Equation 1.19:
$$IQE = \frac{EQE}{A} = \frac{EQE}{1 - T - R}$$

The amount of light absorbed by the active layer is calculated using the transmission (T) through the polymer film and the reflection (R) of light by the ITO

anode. The transmittance is obtained from the UV-vis absorption profile of the active layer and calculated using Equation 1.5. Whereas the reflection is estimated by comparing the amount of light that reaches a power meter light with and without a piece of ITO coated glass in the optical path.

1.4.7 Hole-only devices

The device structure used to make LEDs or PV devices can be modified such that when operating, hole transport dominates. Devices are commonly termed "hole-only" devices and are used to measure hole or positive charge mobilities. They are typically made using a sandwich structure, wherein the conjugated polymer:fullerene derivative film is sandwiched between two high work function materials, as depicted in Figure 1.28. The Al layer used in polymer photovoltaic devices is replaced with a higher work function metal such as Pd or Au.[61]

Pd electrode
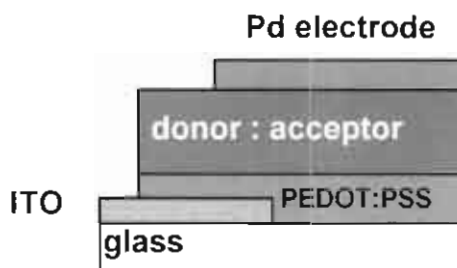
Figure 1.28: Schematic of a typical polymer hole-only device.

Characterization of these devices is done by measuring the I-V behavior in the dark. A typical plot is shown in Figure 1.29. This technique is based on the formation of space-charge limited current (SCLC) and is sometimes referred to a SCLC technique. Hole mobilities are calculated using the Mott-Gurney law,[62] shown in Equation 1.20,

Equation 1.20:
$$J = \frac{9}{8}\varepsilon_r\varepsilon_0\mu_h\frac{V^2}{d^3}$$

where ε_0 is the permittivity of free space, ε_r is the relative permittivity of the material, μ_h is the hole mobility and d is the thickness of the active layer. The curve in Figure 1.29 is plotted in a log-log representation of the current density *vs.* voltage, corresponding to hole injection through the ITO|PEDOT electrode under forward bias. Three distinct regions are identifiable in the plot: region A has a slope = 1, corresponding to the Ohmic region; region B has a slope > 2, which corresponds to the trap filling region; and region C has a slope ~ 2, corresponding to the trap free space charge limiting current region (TFSCLC). Mobilities can be extracted from the experimental data in the region of TFSCLC, *i.e.*, where the obtained slope in the double log plot is equal to 2.
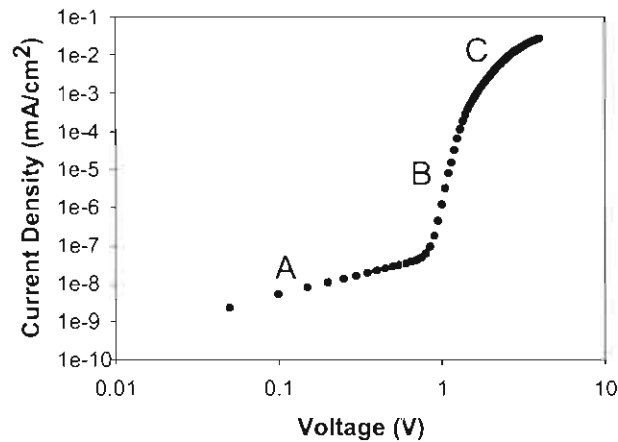
Figure 1.29: Forward dark current voltage characteristics of hole-only ITO|PEDOT|P3HT|Al devices, in double logarithmic scale.

1.5 Conjugated Polymers used in Electroluminescent and Photovoltaic Devices

Over the past decade a wide range of conjugated polymers have been applied in light-emitting devices. Blue-emitting polymers such as polyfluorenes and polycarbazoles, as well as green-emitting polymers such as polyphenylvinylenes and red-emitting polymers such as polythiophenes.[63] Copolymers of various monomeric units have also been used to obtain all the

35

colours in the visible range. Figure 1.30 below shows the polymer structures of some typical examples from the literature.
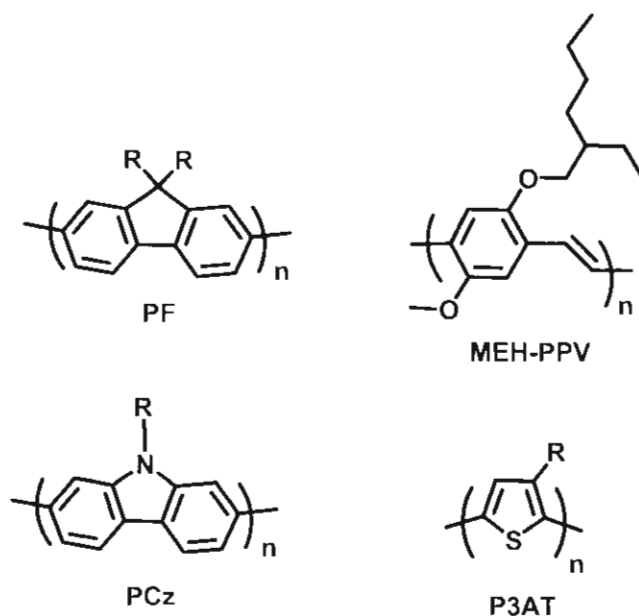
Figure 1.30: **Examples of conjugated polymers used in electroluminescent devices from the literature.**

Each class of polymers have resulted in a variety of derivatives. For example, polyfluorenes have been synthesized with different side chains, from alkyl chains, to alkoxy chains, to phenyl groups (spiro fluorene) as well as with a ketone group at the C-9 position.[40] Numerous studies have investigated the replacement of the C-9 carbon atom with a Si atom (polysilafluorenes)[64] or a nitrogen atom (polycarbazoles)[41].

Analogous to the field of light-emitting devices, a range of conjugated polymers with different absorption profiles have been applied in organic photovoltaic devices. Very few of the reported polymers investigated absorb primarily blue light due to their poor spectral overlap with the solar spectrum (see Figure 4.1). The PPV derivatives were among the first polymers to be investigated for photovoltaic applications, followed shortly thereafter by the investigation of polythiophenes. It was quickly realized that longer wavelengths could be captured by low band gap polymers and much effort has been invested

in the development of polymers with bandgaps < 2.0 eV, i.e., absorbing light with wavelengths longer than 620 nm. A common approach has been to make copolymers containing various combinations of the following groups: fluorene, carbazoles, benzothiadiazoles, or thiophenes, [45, 65, 66] Figure 1.31 below shows a few examples of conjugated polymers that have been reported for use in organic photovoltaics.
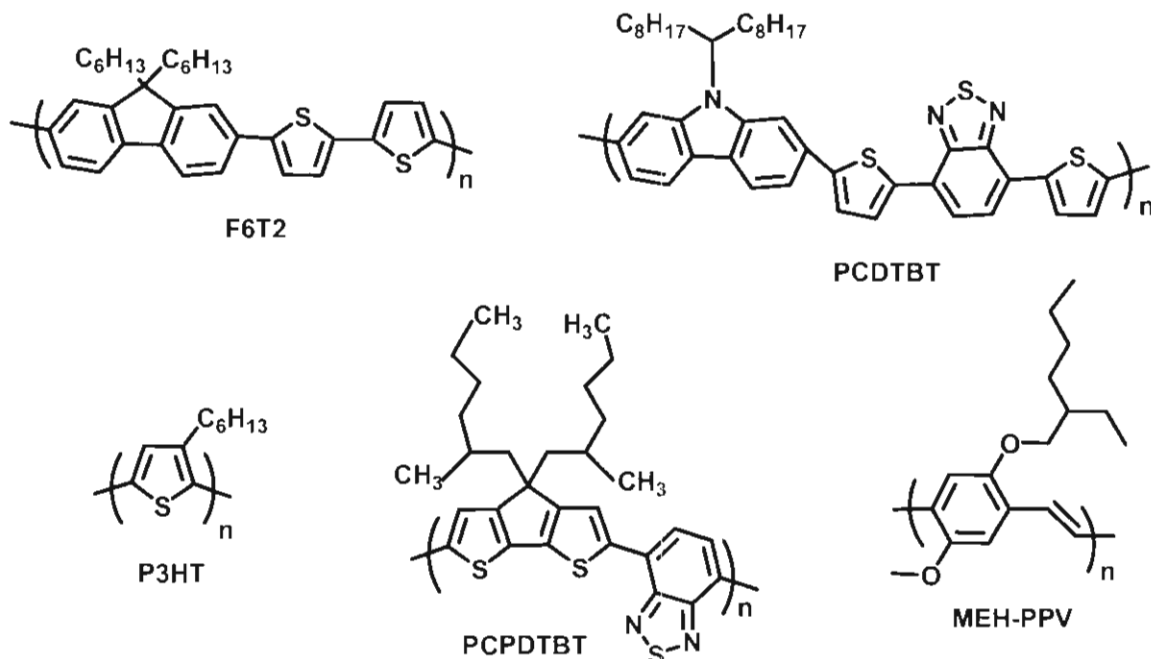
Figure 1.31: Examples of conjugated polymers used in photovoltaic devices from the literature.

1.6 Research Perspective and Thesis Outline

The design and fabrication of polymer LED based displays is a multidisciplinary area that presents a challenging task for chemists, material scientists, physicists and electronic engineers. The use of phosphorescent materials in LEDs has been of increasing interest due to their potentially high EL efficiencies resulting from emission from both the singlet and triplet excitons. Devices made from blends of polymers and "small-molecule" phosphors have been shown to suffer from poor stability after prolonged operation as a result of unstable blend morphologies. This led to the strategy of attaching

phosphorescent moieties, such as iridium complexes, to conjugated polymers. Some researchers elected to attach iridium *via* polymer side chains, while others attached the phosphors to the main chain.[35, 55, 67-70]

The work described in this thesis uses the aforementioned strategy and investigates the structure-property relationship in host-guest phosphorescent conjugated polymers. Chapter 1 contains a brief overview of conjugated polymers, highlighting pertinent synthetic techniques and physico-chemical properties. The application of conjugated polymers in light-emitting and photovoltaic devices is discussed and a brief description of the methods used to characterize the polymers presented in the thesis is included.

Chapter 2 presents a study of two series of conjugated polymers: poly(fluorene-alt-pyridine) and a poly(fluorene-alt-thiophene), both of which have varying amounts of phosphorescent iridium complexes bound to the polymer main chain. Exchanging the 2,5-linked pyridine group with the 3,4-linked thiophene group was investigated in terms of its effect on energy levels, photophysical properties and LED performance.

The design and fabrication of polymer-based PV devices is also a challenging task. The use of conjugated polymers in photovoltaics requires understanding of their optical and electronic behaviour. Poly(alkylthiophene)s, most commonly poly(3-hexylthiophene) (P3HT), have been extensively studied in organic photovoltaic devices.[71] State-of-the-art devices have been made from blends of P3HT and [6,6]-phenyl C_{61} butyric acid methyl ester (PCBM) (1:0.8 wt. ratio), producing devices with power conversion efficiencies (PCEs) > 5 % and external quantum efficiencies (EQEs) > 80 %. The high efficiencies observed in these devices are attributed to the superior hole transporting ability of P3HT which results from its semi-crystalline morphology and the nano-sized phase separation of P3HT and PCBM.[72] The ability to form nano-phase separated morphology has emerged as a requirement for efficient charge transport of singlet excitons because of their short lifetimes. This strict requirement may be lifted if triplet excitons are formed and extent the diffusion length of the exciton.

As described in section 1.3.7, triplet excited states possess inherently longer lifetimes relative to singlet excited states and triplet excitons are expected to possess longer diffusion lengths, thereby increasing the percentage of excitons that reach a donor/acceptor interface, *i.e.*, increasing the efficiency of charge generation.

The advantages of phosphorescent polymers for PVs is their solution processablity, reduced phase segregation over time and the expected longer diffusion lengths of triplet excitons. Chapter 3 reports on the effect of incorporating iridium complexes into the conjugated polymer main chain of a polyfluorene derivative on the photophysical, redox and photovoltaic properties. Two polymers were investigated: poly(fluorene-co-phenylpyridine) and poly(fluorene-co-phenylpyridine) with bound iridium complexes. Photovoltaic performance is correlated to the polymer structure and the formation of triplet excitons.

Finally, Chapter 4 investigates two different approaches to red-shift conjugated polymer absorption profiles relative to the polymers presented in Chapter 3, in order to capture a greater portion of the solar spectrum. Iridium complexes were incorporated into a poly(fluorene-alt-bithiophene) main chain and the effect of iridium content on interchain interactions, photophysical, redox and photovoltaic properties was studied.

CHAPTER 2: ENHANCEMENT OF PHOSPHORESCENCE DUE TO INCREASING THE TRIPLET LEVEL OF THE MAIN CHAIN OF IRIDIUM-BOUND, CONJUGATED POLYMERS

Sections of this Chapter have been reproduced in part with permission from Macromolecules, 2006, 39 (26) 9157-9165. Copyright 2006, American Chemical Society.

2.1 Introduction

Recently, much effort has been invested into developing organic light emitting devices (OLEDs). Conjugated polymers are attractive for such applications because of their solution processability, mechanical flexibility, color tunability, and low operating voltage.[73, 74] Commonly, light emission from conjugated polymers is fluorescent; however, systems that emit phosphorescence have gained interest because of the potential for higher EL efficiencies resulting from emission of both singlet and triplet excitons. Heavy metal complexes promote spin-orbit coupling of electronic states resulting in rapid intersystem crossing (ISC), short triplet state lifetimes, and stronger phosphorescent emission at room temperature.

As discussed in section 1.3.3, phosphorescent OLEDs based on small molecules have received the most attention to date. Organometallic complexes of Pt, Ir, Ru, Re and Os have all been investigated to varying extents as the emitting species in phosphorescent OLEDs.[25, 75-78] However, the use of small organic molecules requires vacuum deposition of multilayer structures, and this process increases fabrication costs. In an attempt to mitigate the need for vacuum deposition processes, small molecules have been doped into polymer

matrices. These systems are solution processible and, in principle, allow for easy deposition of multiple layers. Examples of such systems, depicted in Figure 2.1, include poly(vinylcarbazole) (PVK) doped with Ir(ppy)$_3$,[29] blends of PVK and 2-tert-butylphenyl-5-biphenyl-1,3,4-oxadiazol (PBD) doped with tris(2,5-bis-2'-(9,9-dihexylfluorene)pyridine)iridium(III) (Ir(HFP)$_3$)[33] and poly(9,9-dioctylfluorene) (PFO) doped with Ir(ppy)$_3$.[34]
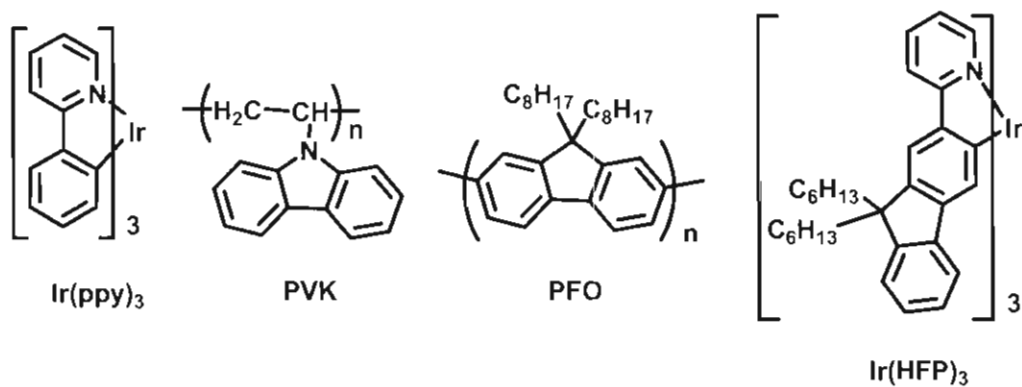
Figure 2.1: Representative chemical structures of host-guest systems used in solution processible LEDs.

Although significant improvements in device efficiencies using blended systems are reported, their performance can suffer from aggregation of the phosphor, phosphorescent quenching,[67] phase separation, and inefficient energy transfer.[68] In efforts to overcome these shortcomings, a new class of materials, in which phosphorescent groups are covalently attached to a conjugated polymer backbone, are being investigated. Examples of some chemical structures that have been reported in the literature are shown in Figure 2.2. Chen et al.[55] reported the first synthesis of such materials, and showed that polyfluorene with pendant iridium complexes (Ir(ppy)$_2$acac and Ir(btp)$_2$(acac)) and charge transport moieties (carbazole) have comparable efficiencies to Ir complex-based OLEDs. Jiang et al.[69] developed a similar system of fluorene-alt-carbazole polymers with various ligands bound to iridium pendant groups attached to the N-position of the carbazole, for example, 1-phenylisoquinoline, 2-naphthylpyridine and 2-phenylquinoline. They attribute the observed increase in device performance to the high triplet energy of carbazole and efficient charge

41

injection due to a more favorable position of the HOMO and LUMO levels. Sandee et al. developed a synthetic strategy to covalently attach phosphorescent emitters [Ir(ppy)$_2$(acac) and Ir(btp)$_2$(acac)] to a poly(9,9-dioctylfluorene) backbone.[67] The latter confirmed work by Sudhakar (using a fluorene trimer) that revealed the importance of the relative triplet energy levels of the donor and acceptor on the intensity of phosphorescent emission.[79] A similar study by Zhen et al.[68] describes the synthesis and characterization of poly(fluorene-co-carbazole) containing varying mole fractions of iridium phosphors attached to the polymer backbone. This study emphasized the improvement of iridium-bound polymers compared to their corresponding blend systems, attributing the improvement to the more efficient intramolecular energy transfer of the former versus intermolecular energy transfer of the latter. Work by Yang et al.[80] described hyper-branched and linear substituted poly(p-phenylene)s based on Ir(ppy)$_3$ and (mppy)$_2$Ir(acac) complexes. In addition, a conjugated fluorene-based polymer with an iridium complex covalently attached to the polymer main chain was described by Ito et al.[70] The iridium content in this system was optimized by its blending with 4,4'-N,N'-carbazole-biphenyl (CBP) and 2-tert-butylphenyl-5-biphenyl-1,3,4-oxadiazol (PBD). The work presented in this chapter builds on the current knowledge of the photophysics of iridium-bound conjugated polymers with respect to quenching of the triplet of the phosphor by the conjugated polymer.
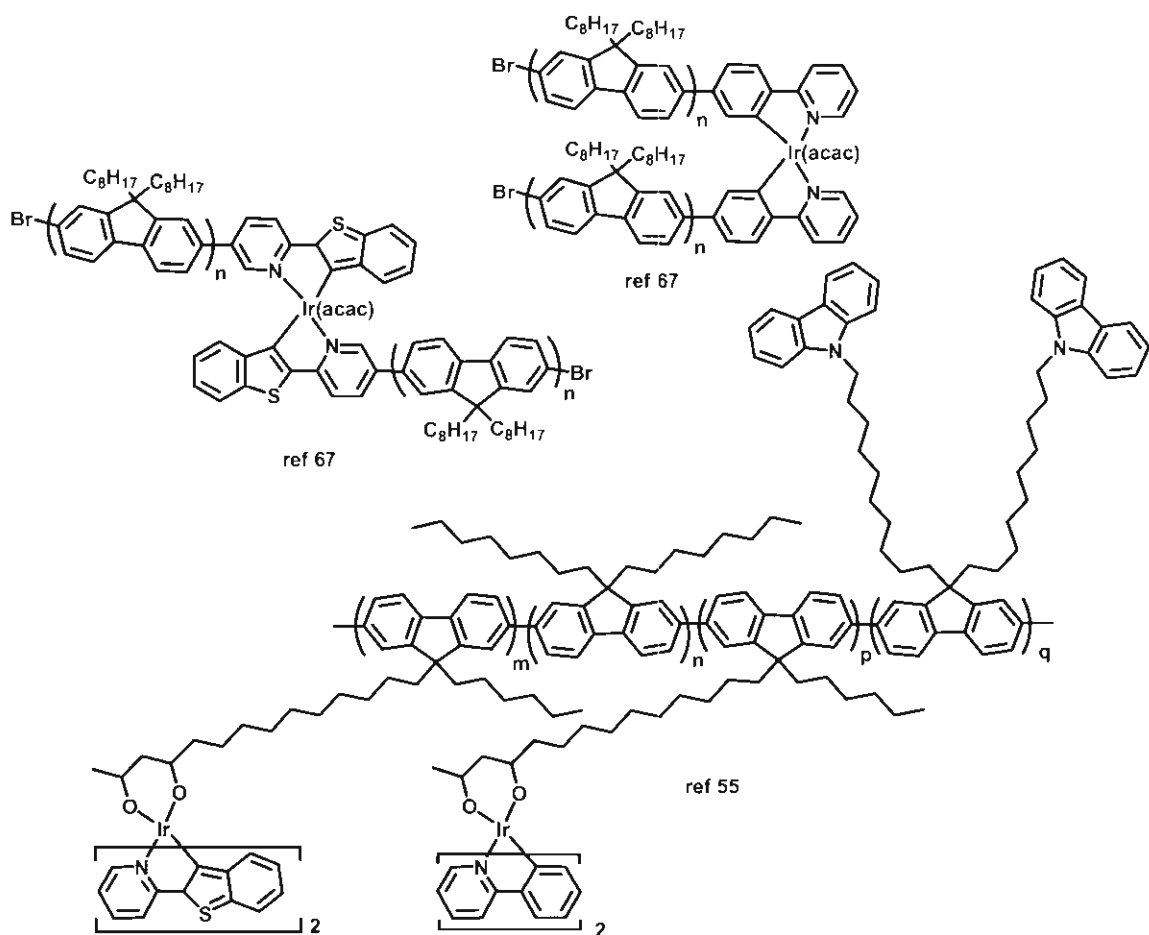
Figure 2.2: Examples of iridium-bound conjugated polymers from the literature.

Understanding quenching pathways of phosphorescent species by main chain, conjugated polymer triplet states is necessary in order to refine the design of highly efficient systems. Several studies have examined the role of the triplet energy of the phosphor on the efficiency of quenching but *none* have examined the role of modifying the energy levels of the main chain. In this chapter, the effect of modifying the triplet energy of the polymer main chain with a view to reduce triplet quenching of phosphorescent complexes by the main chain is examined, process (b) *vs.* process (c) shown in Figure 2.3. Reduction in quenching is achieved through the design and synthesis of polymer structures of the type below (Figure 2.4), wherein an iridium complex, of varying mole fractions, is attached to the main chain of a conjugated polymer. The conjugated polymer is designed with and without 3, 4- linked thienyl groups which, when

43

incorporated, are expected to lower conjugation along the backbone,[81] thereby increasing the electronic energy levels (both singlet and triplet) of the main chain. Energy transfer from the polymer to the phosphor and its effect on phosphorescent quantum yield was investigated by changing the mole fraction of the iridium incorporated into the polymer.
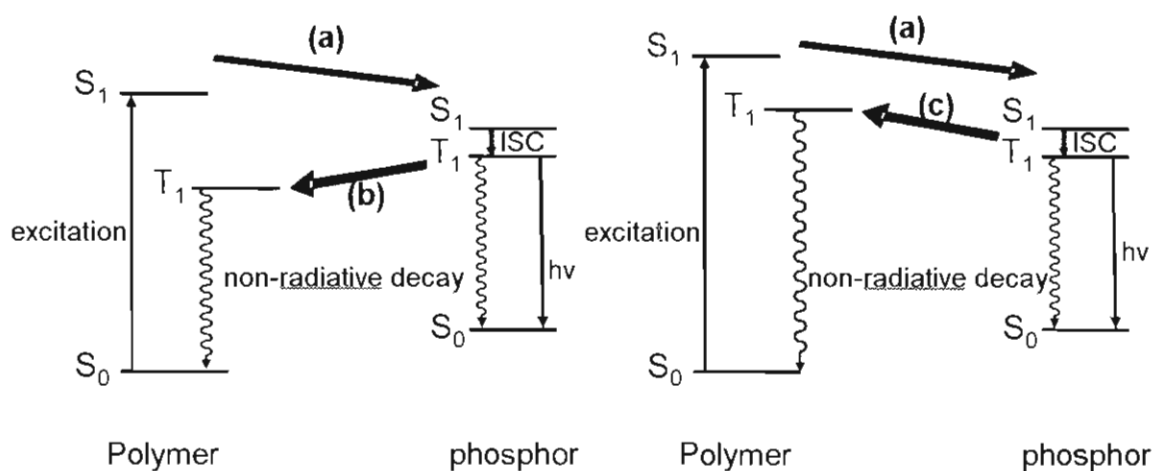
Figure 2.3: Depiction of energy transfer between a conjugated polymer and a pendent phosphor (a) and subsequent quenching of the phosphor triplet state by a lower energy polymer triplet (b) and a higher energy polymer triplet (c).

PFPyIr

PFTIr
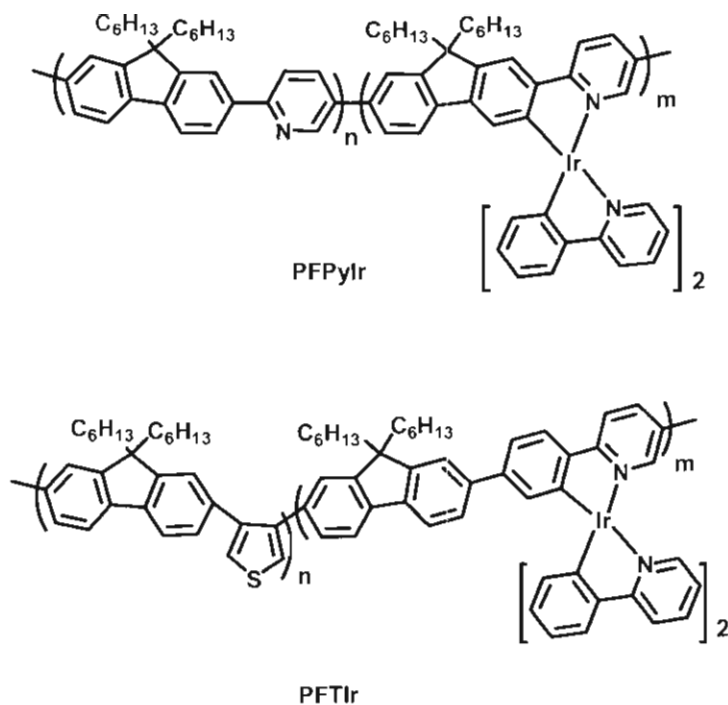
Figure 2.4: Generalized structures of the polymers used in this study.

2.2 Experimental

2.2.1 Materials

Materials and Chemicals. 9,9-dihexylfluorene-2,7-bis(trimethyleneborate), 2,5-dibromopyridine, 3,4-dibromothiophene, tetrakis(triphenylphosphine)palladium ($Pd(PPh_3)_4$), 2,5-dibromobenzene, iridium (III) chloride trihydrate and cresyl violet perchlorate were purchased from either Sigma-Aldrich Co. or Acros Organics. THF and ether were dried over sodium and freshly distilled before use. Poly(styrene sulfonic acid)-doped poly(ethylenedioxythiophene) (PEDOT:PSS, Baytron P CH 8000) was purchased from Bayer Corp.

Synthesis of PFPyIr. 9,9-dihexylfluorene-2,7-bis(trimethyleneborate) was copolymerized with 2,5-dibromopyridine by Suzuki coupling to produce an alternating copolymer, **PFPy**. The polymers were subject to two postfunctionalization reactions in order to attach the iridium complex, and produce **PFPyIr** (Figure 2.5).

Synthesis of PFTIr. Iridium (III) chloride trihydrate was reacted with 2-phenyl pyridine to produce a chloride-bridged dimer. The product was then reacted with two equivalents of 1,4'-dibromo-2-phenylpyridine to yield $(ppy)_2Ir(BrPhPyBr)$. 9,9-dihexylfluorene-2,7-bis(trimethyleneborate) was copolymerized with a varying ratio of 3,4-dibromothiophene and $(ppy)_2Ir(BrPhPyBr)$ using Suzuki coupling to produce the alternating copolymer, **PFTIr** (Figure 2.6).

Poly(9,9-dihexylfluorene-alt-pyridine) (PFPy) was synthesized *via* Suzuki polycondensation according to Figure 2.5.[82] 9,9-Dihexylfluorene-2,7-bis(trimethyleneborate) (1.0 g, 2.0 mmol) and 2,5-dibromopyridine (0.47 g, 2.0 mmol) were dissolved in THF (12.5 mL, deoxygenated); to which, a solution of K_2CO_3 (0.19 g/mL, 2 mL) was added, together with $Pd(PPh_3)_4$ (0.076 g, 3 mole% based on fluorene). The resulting mixture was sealed in a glass vial and heated for 24-72 hours at 80°C in an oil bath. End capping of the polymer was carried out as the last step in synthesis. Phenyl boronic acid (0.012 g, 5 mole %) was added and the solution was heated (80°C, 8 h). This was followed by the addition of bromobenzene (0.016 g, 5 mole %), and the temperature was maintained at 80 °C (16 h). Once cooled to room temperature, the THF was removed and the residue was dissolved in chloroform. This was followed by washing with water (3 times) and drying over anhydrous magnesium sulfate. After filtration, the volume of chloroform was reduced and the concentrated solution was passed through an alumina column. The volume of the resulting solution was again reduced and precipitated in methanol (~50 mL) to yield 0.58 g of the product (78%). A weight average molecular weight (M_w) of 44 000 Daltons and a PDI of 1.6 was obtained. ^1H NMR (CD_2Cl_2) δ (ppm) 9.09 (s, 1H), 8.20-7.75 (m, 8H), 2.13 (br. β-CH_2), 1.15-0.78 (m, CH_2 and CH_3). Anal. Calcd. for $(C_{25}H_{32})_{0.5}(C_5H_3)_{0.5}$: C, 87.97; H, 8.61; N, 3.42. Found: C, 87.56; H, 8.61; N, 3.52.

General procedure for the synthesis of PFPyIr5, PFPyIr10, PFPyIr15, PFPyIr20 and PFPyIr30 using PFPyIr5 as an example.[83] Poly(9,9-dihexylfluorene-alt-pyridine) (43.5 mg, 0.106 mmol) was reacted with $Ir(acac)_3$

46

(2.6 mg, 0.0053 mmol) in *m*-cresol (10 mL, degassed) at 250°C for 10 h. After cooling, 2-phenylpyridine (1.6 mg, 0.011 mmol) was added to the solution and reacted for an additional 10 hours at 250 °C.[21] The volume of the obtained solution was reduced to ~1 mL and precipitated from methanol 3 times. Purification was carried out using flash chromatography using silica gel and a mixture of dichloromethane and pyridine as the eluent. ^{1}H NMR (CD$_2$Cl$_2$) δ (ppm): 9.09 (s), 8.20-7.75 (m), 2.13 (br. β-CH$_2$), 1.15-0.78 (m, CH$_2$ and CH$_3$). A weight average molecular weight (M$_w$) of 28 500 Daltons and a PDI of 2.1 was obtained.

PFPyIr10. ^{1}H NMR (CD$_2$Cl$_2$) δ (ppm): 9.09 (s), 8.20-7.75 (m), 2.13 (br. β-CH$_2$), 1.15-0.78 (m, CH$_2$ and CH$_3$). A weight average molecular weight (M$_w$) of 44 000 Daltons and a PDI of 1.7 was obtained.

PFPyIr15. ^{1}H NMR (CD$_2$Cl$_2$) δ (ppm): 9.09 (s), 8.20-7.75 (m), 2.13 (br. β-CH$_2$), 1.15-0.78 (m, CH$_2$ and CH$_3$). A weight average molecular weight (M$_w$) of 47 000 Daltons and a PDI of 1.9 was obtained.

PFPyIr20. ^{1}H NMR (CD$_2$Cl$_2$) δ (ppm): 9.09 (s), 8.20-7.75 (m), 2.13 (br. β-CH$_2$), 1.15-0.78 (m, CH$_2$ and CH$_3$). A weight average molecular weight (M$_w$) of 35 000 Daltons and a PDI of 1.9 was obtained.

PFPyIr30. ^{1}H NMR (CD$_2$Cl$_2$) δ (ppm): 9.09 (s), 8.20-7.75 (m), 2.13 (br. β-CH$_2$), 1.15-0.78 (m, CH$_2$ and CH$_3$). A weight average molecular weight (M$_w$) of 25 300 Daltons and a PDI of 2.6 was obtained.

Figure 2.5: Synthetic route for PFPyIr
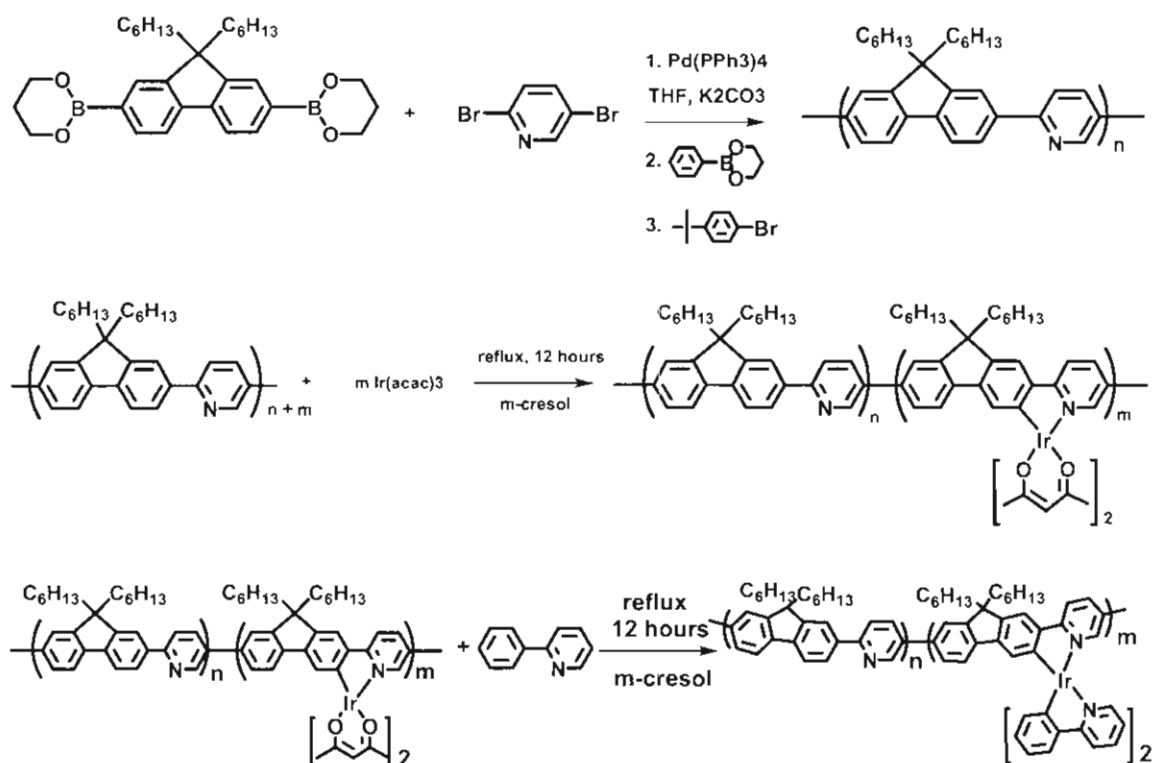
Feed ratio	PFPy	PFPyIr5	PFPyIr10	PFPyIr15	PFPyIr20	PFPyIr30
n/ m	1/ 0	0.95/ 0.05	0.90/ 0.10	0.85/ 0.15	0.80/ 0.20	0.70/ 0.30

[(ppy)₂IrCl]₂. [(ppy)$_2$IrCl]$_2$ was synthesized according to a modified published procedure.[84] Iridium (III) chloride trihydrate (0.150 g, 0.502 mmol) and 2-phenylpyridine (0.779 g, 5.02 mmol) were dissolved in ethylene glycol (10 mL). The reaction flask was subjected to microwave energy (2450 MHz, 480 W) under nitrogen for 35 minutes. After cooling, the solvent volume was reduced under vacuum to yield a yellow precipitate, which was collected on a glass filter frit. The precipitate was washed with 95% ethanol (20 mL) and acetone (20 mL) and dissolved in dichloromethane (30 mL). Toluene (12 mL) and hexanes (5 mL) were added to the dichloromethane, which was then reduced in volume and cooled to yield dark yellow crystals (0.160 g, 60 %). ^{1}H NMR (CD$_2$Cl$_2$) δ (ppm):

9.23 (d, 1H), 7.78 (d, 1H), 7.67 (t, 1H), 7.39 (d, 1H), 6.67 (m, 2H), 6.50 (t, 1H), 5.90 (d, 1H). MS (MALDI): m/z 1070.87 (M/z), 1034.99 (M/z – Cl), 501.19 (M/z – Cl$_2$Ir(ppy)$_2$).

1,4'-dibromo-2-phenylpyridine was synthesized according to published procedures.[85] To a suspension of magnesium turnings (0.230 g, 9.4 mmol) in 5 mL of ether, 1,4-dibromobenzene (2.170 g, 9.2 mmol) in 10 mL of ether was added dropwise at room temperature. The resulting mixture was stirred at room temperature until all the magnesium was consumed (~ 4 h). The mixture was then added to a mixture of 2,5-dibromopyridine (2.298 g, 9.7 mmol) and PdCl$_2$ (dppb) (0.061 g, 0.10 mmol) at room temperature and stirred overnight. The solvent was removed and water was added to the residue (100 mL), followed by dilute HCl until the pH of the solution reached 5. The product was extracted with chloroform (3 x 30 mL), washed with water and dried over anhydrous magnesium sulfate. Column chromatography was used to isolate the product (silica gel, hexane and a mixture of hexane and ether, 15:1), which was recrystalized from a mixture of chloroform and hexane. Fluffy, white crystals were obtained (0.9755 g, 33%). ^{1}H NMR (CDCl$_3$) δ (ppm): 8.73 (d, 1H), 7.88 (dd, 1H), 7.85 (s, 1H), 7.83 (s, 1H), 7.59-7.61 (s, 3H). MS (EI): m/z 315, 313, 311 (M$^+$, 1:2:1).

(ppy)$_2$Ir(BrPhPyBr) was synthesized according the published procedures.[86] [(ppy)$_2$IrCl]$_2$ (0.150 g, 0.14 mmol) and 1,4'-dibromo-2-phenylpyridine (0.109 g, 0.35 mmol) were dissolved in glycerol (10 mL) with K$_2$CO$_3$ (0.193 g). The reaction was carried out under an inert atmosphere at 200°C for 22 hours. After cooling, deionized water (20 mL) was added to the reaction mixture, which resulted in precipitation of the product, which was subsequently washed with ether and hexanes. Further purification was performed using flash chromatography (silica gel, CH$_2$Cl$_2$). Addition of methanol to the chromatographed solution followed by removal of the dichloromethane resulted in precipitation of an orange powder (0.090 g, 40% yield). ^{1}H NMR (CD$_2$Cl$_2$) δ (ppm): 7.84 (d, 1H), 7.59 (m, 2H), 7.48 (m, 1H), 6.84 (m, 2H), 6.67 (m, 2H). MS (MALDI): m/z 807.26 (M/z), 655.23 (M/z – ppy).

Poly(9,9-dihexylfluorene-alt-3,4-thiophene) (PFT) was synthesized *via* Suzuki polycondensation according to Figure 2.6.[81, 87] 9,9-dihexylfluorene-2,7-bis(trimethyleneborate) (0.53 g, 1.00 mmol) and 3,4-dibromothiophene (0.26 g, 1.00 mmol) were dissolve in THF (10 mL, degassed), to which, a solution of K_2CO_3 (0.19 g/mL, 2 mL) was added, together with $Pd(PPh_3)_4$ (0.036 g, 3 mole % based on fluorene). The resulting mixture was sealed in a glass vial and heated for 24-72 hours at 80°C in an oil bath. The solution obtained was washed with water (3 times) and dried over anhydrous magnesium sulfate. After filtration, the volume of chloroform was reduced and passed through an alumina column. The volume of the resulting solution was reduced, and precipitated in methanol (~25 mL) to give 0.332 g (yield, 80%). A weight average molecular weight (M_w) of 8100 Daltons and a PDI of 1.3 was obtained. ^{1}H NMR (CD_2Cl_2) δ (ppm): 7.7-7.1 (8H, fluorene and thiophene), 1.7 (4H, β-CH_2), 1.05 (12H, CH_2), 0.70 (6H, CH_3), 0.55 (4H, CH_2). Peaks were assigned using the ^{1}H NMR spectra of 9,9-dihexylfluorene-2,7-bis(trimethyleneborate) and 3,4-dibromothiophene. Anal. Calcd. for $(C_{25}H_{32})_{0.5}(C_4H_2S)_{0.5}$: C, 84.0; H, 8.26. Found: C, 84.23; H, 8.20.

General procedure for the synthesis of PFTIr2, PFTIr5, PFTIr10 and PFTIr20 using PFTIr5 as an example. Suzuki polycondensation. 9,9-dihexylfluorene-2,7-bis(trimethyleneborate) (0.307 g, 0.61 mmol), 3,4-dibromothiophene (0.140 g, 0.58 mmol) and $(ppy)_2Ir(BrPhPyBr)$ (0.024 g, 0.03 mmol) were dissolve in THF (10 mL, degassed), to which, a solution of K_2CO_3 (0.19 g/mL, 2 mL) was added, together with $Pd(PPh_3)_4$ (0.022 g, 3 mole % based on fluorene). The resulting mixture was sealed in a glass vial and heated for 24-72 hours at 80°C in an oil bath. End capping of the polymer was carried out as the last step in synthesis. Phenyl boronic acid (0.004 g, 5 mole %) was added and the solution was heated (80 °C, 8 h). This was followed by the addition of bromobenzene (0.016 g, 5 mole %) and which was heated at 80 °C, for 16 h. The solution was washed with water (3 times) and dried over anhydrous magnesium sulfate. After filtration, the volume of chloroform was reduced and passed through an alumina column. The volume of the resulting solution was again reduced and precipitated in methanol (~50 mL) to yield 0.100 g product

(yield, 37%). ^{1}H NMR (CD$_2$Cl$_2$) δ (ppm): 7.93-6.75 (m, 9H), 1.69 (br. 4H), 1.15-0.52 (m, 22H). Peaks were assigned using the ^{1}H NMR spectra of 9,9-dihexylfluorene-2,7-bis(trimethyleneborate), 3,4-dibromothiophene and Ir(ppy)$_3$. A weight average molecular weight (M$_w$) of 3300 Daltons and a PDI of 1.9 was obtained.

PFTIr2. Yield of 0.100 g (32%). ^{1}H NMR (CD$_2$Cl$_2$) δ (ppm): 7.93-6.75 (m, 9H), 1.69 (br. 4H), 1.15-0.52 (m, 22H). A weight average molecular weight (M$_w$) of 5700 Daltons and a PDI of 2.1 was obtained.

PFTIr10. Yield of 0.175 g (53%). ^{1}H NMR (CD$_2$Cl$_2$) δ (ppm): 7.93-6.75 (m, 9H), 1.69 (br. 4H), 1.15-0.52 (m, 22H). A weight average molecular weight (M$_w$) of 7000 Daltons and a PDI of 1.9 was obtained.

PFTIr20. Yield of 0.217 g (69%). ^{1}H NMR (CD$_2$Cl$_2$) δ (ppm): 7.93-6.75 (m, 9H), 1.69 (br. 4H), 1.15-0.52 (m, 22H). A weight average molecular weight (M$_w$) of 6600 Daltons and a PDI of 2.0 was obtained.
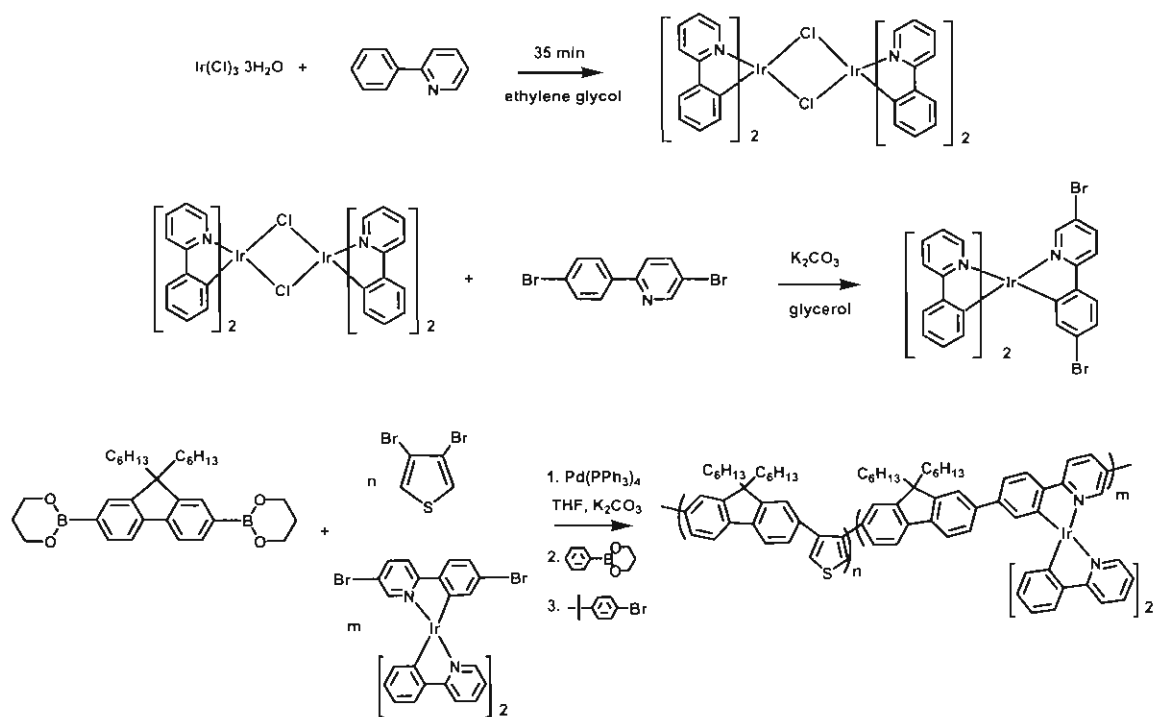
Feed ratio	PFT	PFTIr2	PFTIr5	PFTIr10	PFTIr20
n/ m	1/ 0	0.98/ 0.02	0.95/ 0.05	0.90/ 0.10	0.80/ 0.20

Figure 2.6: Synthetic route for PFTIr

2.2.2 Methods and Instrumentation

Solutions of the polymers used for acquiring absorption and fluorescence spectra were prepared using freshly distilled THF. Chloroform (spectro-grade, Caledon Laboratories Ltd.) was used to prepare solutions (4 mg/mL) for film casting. Films were spin-cast on either quartz or glass slides at 1500 rpm for 60 s. NMR spectroscopy was performed using a 400 MHz Brucker AMX400 spectrometer. Elemental analyses were performed using a Carlo Erba model 1106 CHN analyzer. Ir content was determined using a Kristalloflex 2H X-ray fluorescence (XRF) spectrometer made by Siemens. Samples were excited with

Mo X-rays, operated at 40 kV and 5 mA. A calibration curve was made using Ir(acac)$_3$ as a standard and yttrium as an internal standard. Samples were prepared by drop casting films on ultra thin mylar sheets. Molecular weight determinations were performed using gel permeation chromatography (Waters Model 1515 isocratic pump). Polymers were eluted with THF using a flow rate of 1 mL/min and monitored with a UV-vis detector (Waters 2487). Microwave synthesis was performed using an in-house modified Panasonic Inverter Microwave (model no NN-S614, see Appendix C). Absorption and fluorescence spectra were collected using Cary 3E and PTI spectrophotometers, respectively. Quantum yield measurements were performed using an integrating sphere. Electroluminescence spectra were collected using a Jobin Yvon Horiba, Fluoromax-3 fluorescence spectrometer. Mass spectrometry was performed using a Voyager DE Perceptive biosystems MALDI Spectrometer. Cyclic voltammograms were measured on polymer films drop cast on a Pt disk electrode (1.5 mm) in acetonitrile containing 0.1 M Bu$_4$NClO$_4$, a Pt wire counter electrode, and a scan rate of 50 mV/s. Potentials were measured against an Ag/AgCl reference electrode and reported against ferrocene/ferrocenium using a potentiostat/galvanostat (PAR 263A). Quantum yields of the iridium containing polymers were measured using the method of relative fluorescence, which is explained in the detail in section 1.4.1. Cresyl violet perchlorate was selected as the standard. Its quantum yield is reported to be 0.54 +/- 0.03 in methanol.[9]

The following electroluminescent device configurations were used: ITO| PEDOT:PSS| conjugated polymer| CsF (2.0 nm)| Al (60 nm) and ITO| PEDOT:PSS| conjugated polymer| TPBI (30nm)| CsF (2.0 nm)| Al (60 nm). ITO patterned glass was pre-cleaned, followed by O$_2$ plasma treatment (45 W, 193 mbar, 5 min). PEDOT:PSS (Bayer) was spin coated at 2000 rpm for 90 s, and the layer dried under vacuum for 1 h at 140 °C. Solutions of the conjugated polymers were spin coated on the PEDOT:PSS layer from CHCl$_3$ solutions (~ 8 mg/mL) to yield films 800 to 1100 Å thick. CsF and Al layers were thermally evaporated at a pressure < 10^{-6} Torr, yielding thicknesses of 2.0 and 60 nm, respectively. The electrical and luminescence properties of devices were

measured using a Keithley power supply (model 238) and a luminescence meter (BM8 from TOPCON), respectively. Polymer thicknesses were determined using a Tencor P-10 surface profiler. The active area of the diode was ~10 mm^2.

2.3 Results and Discussion

2.3.1 Synthesis and Properties of PFPyIr

Figure 2.5 depicts the Suzuki polycondensation reaction that yielded poly(9,9-dihexylfluorene-alt-pyridine). Two subsequent post-functionalization reactions attached the iridium complex with the desired ligands. The feed ratios of iridium complexes in the post-functionalization reaction were 0, 5, 10, 15, 20 and 30 mol%; the corresponding polymers are termed **PFPy**, **PFPyIr5**, **PFPyIr10**, **PFPyIr15**, **PFPyIr20** and **PFPyIr30**, respectively. X-ray fluorescence (XRF) spectroscopy determined the actual amount incorporated was 0, 2, 2, 3, 3, 6 mol% for **PFPy**, **PFPyIr5**, **PFPyIr10**, **PFPyIr15**, **PFPyIr20** and **PFPyIr30**, respectively. ^{1}H NMR spectra were collected for all of the polymers. Examples spectra for **PFPy** and **PFPyIr15** are shown in Appendix A. Peak assignments were done using the ^{1}H NMR spectra of the monomers and polymer spectra from the literature. The weight average molecular weights were determined to be between 25 000 and 47 000 with polydispersity ranging from 1.6 and 2.6.

2.3.2 Absorption and Photoluminescent Properties of PFPyIr

Absorption and emission wavelengths of poly(9,9-dihexylfluorene) (PF) and poly(9,9-dihexylfluorene-alt-2,5-pyridine) (**PFPy**), listed in Table 2.1, are similar (385 vs. 394 nm and 422 vs. 428 nm for solid state absorption and photoluminescence, respectively) indicating that the pyridine groups do not significantly perturb the energy gap of polyfluorene. The solid state absorption and photoluminescence spectra are slightly red shifted relative to those obtained in solution due to aggregation.[88] Peak assignments were made by comparing the absorption spectra of poly(fluorene), **PFPy** and **PFPyIr** and Ir(ppy)$_3$ (Figure 2.7). The absorption maximum of PF, **PFPy** and the iridium containing polymers

(**PFPyIr**) (Figure 2.7 and Table 2.1) are similar but that of Ir(ppy)$_3$ differs. Ir(ppy)$_3$ has a strong absorption in the UV region attributed to the π-π* transition.[75, 89] In addition, weaker ^{1}MLCT and ^{3}MLCT bands are observed for Ir(ppy)$_3$ at 390 and 455 nm, respectively.[75, 90] Since **PFPy** and **PFPyIr** exhibit a single absorption peak at 391 and 396 nm in the solution and solid state, respectively, it is concluded that the polymer backbone is responsible for absorption in these systems. Figure 2.8 shows emission spectra of **PFPyIr** polymers illustrating that the luminescence intensity associated with fluorescence from the backbone decreases with increasing iridium content. For polymers bearing iridium complexes, an emission peak is observed at 610 nm in solution and 613 nm in the solid state. This peak is due to phosphorescence from the iridium complex [67] which is a result of energy transfer from the excited singlet state of the polymer backbone to the excited singlet state of the Ir complex, followed by intersystem crossing to the triplet state of the Ir complex, and subsequent emission (phosphorescence) from this state,[33] as depicted in Figure 2.3. Quantum yields of phosphorescence are too low for accurate measurement in solution but they increase considerably in the solid state. However, the quantum yield of phosphorescence from these films is relatively low (~ 0.05), regardless of the iridium content in the polymer (see Table 2.1).

Figure 2.7: **Absorption spectra of PFPyIr in THF (a) and as a film (b).**
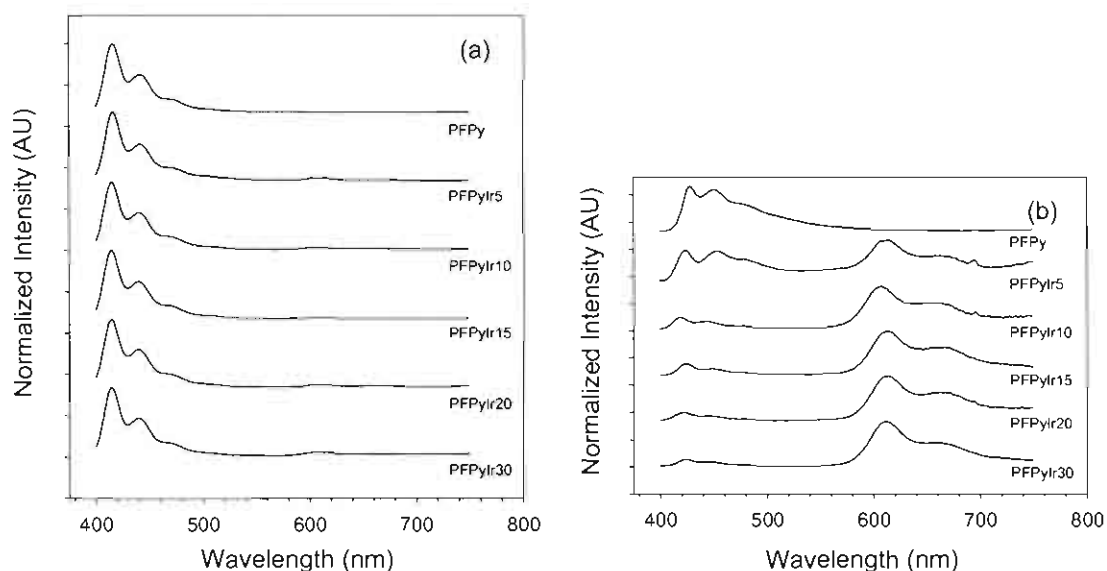
Figure 2.8: Photoluminescence spectra of PFPyIr in THF (a) and as a film (b). λ_{ex}=390 nm.

Table 2.1: Summary of photophysical data for PFPyIr.

Polymer	Solution		Film		
	Absorption λ_{max} (nm)	Emission λ_{max} (nm)	Absorption λ_{max} (nm)	Emission λ_{max} (nm)	Φ_{film}^{*}
PF[23,28]	379	415	385.5	422	0.12
PFPy	391	416 (442)	394	428 (453)	-
PFPyIr5	391	416 (442, 610)	396	613 (423,453,665)	0.040
PFPyIr10	391	416 (442, 610)	396	613 (423,665,453)	0.050
PFPyIr15	391	416 (442, 610)	396	613 (423,665,453)	0.037
PFPyIr20	391	416 (442, 610)	396	613 (423,665,453)	0.045
PFPyIr30	391	416 (442, 610)	396	613 (423,665,453)	0.045
Ir(ppy)$_3$[3]	385 (450)	515	390 (455)	518	0.12

* triplet emission, except PF and PFPy.

2.3.3 Triplet Energy Levels of PFPyIr

The HOMO energy level of **PFPy**, depicted in Figure 2.9, was estimated using cyclic voltammetry (as described in section 1.4.2) and was found to be in agreement with previously reported values.[91] The LUMO energy level was

56

calculated from the HOMO energy level and the onset of the absorption. The triplet energy gap of the polymer was estimated using the following equation: $T_1 = (1.13\ S_1 - 1.43) \pm 0.25$ eV.[92] The ground state energy level of the iridium complex attached to PFPy is approximated to be between 5.2 eV $(Ir(ppy)_3)$[93] and 4.73 eV $(Ir(HFP)_3$ (tris(2,5-bis-2'-(9,9-dihexylfluorene)pyridine)iridium(III)),[33] due to the similarity of their chemical structures. The structure of one of the ligands bound to the iridium center is similar to that in HFP and the other two ligands are identical to ppy. The triplet energy of the phosphor was estimated from the phosphorescent emission wavelength (609 nm, 2.04 eV). Figure 2.9 indicates the triplet energy of **PFPy** to be 2.13 eV. It is believed that this low energy gap results in quenching of the excited triplet state of the iridium complex by energy transfer to the triplet of the polymer backbone. This would result in quenching of emission from the phosphor and explains the corresponding low quantum efficiencies (0.05) for the **PFPyIr** series. Previous work[79] indicates that the emission quenching of the phosphor may be reduced by decreasing the triplet energy of the phosphor (guest) relative to the polymer (host). We have taken a different approach and modified the **PFPy** series with aim of increasing the triplet energy of the host polymer so that triplet energy transfer from the phosphor to the triplet backbone is less favorable. A new series of Ir-containing polymers containing a 3,4-linked thienyl moiety, **PFTIr** was designed to test this hypothesis. As will be demonstrated in the following sections, the triplet energy of the conjugated polymer backbone was raised by 0.75 eV, as illustrated in Figure 2.9.
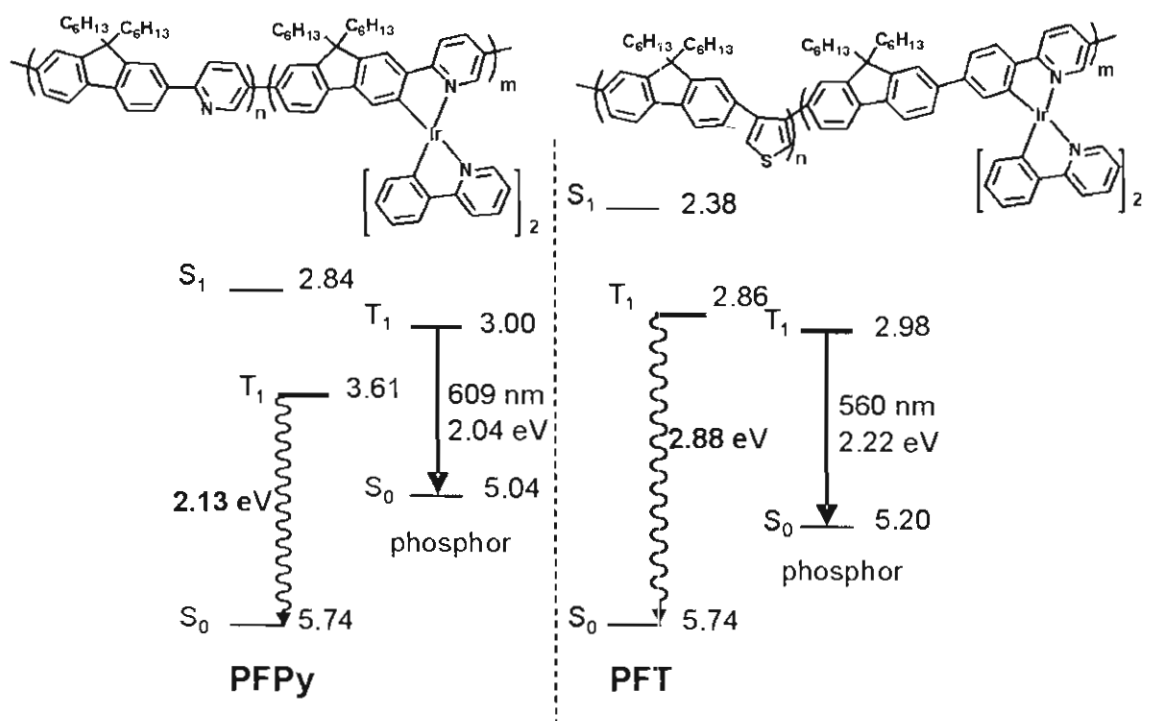
Figure 2.9: Energy level diagram of PFPyIr and PFTIr.

2.3.4 Synthesis and Properties of PFTIr

Figure 2.6 depicts the synthetic route used to prepare iridium-containing monomers *via* the corresponding iridium chloride-bridged dimers. Monomer synthesis was carried out using an in-house modified microwave oven. The Suzuki polycondensation method was used to prepare polymers with the following iridium contents: 0, 2, 5, 10 and 20 mol %. The corresponding polymers were named **PFT**, **PFTIr2**, **PFTIr5**, **PFTIr10** and **PFTIr20**, respectively. X-ray fluorescence (XRF) spectroscopy determined the actual amount incorporated was 0, 10, 20, 14, and 25 mol% for **PFT**, **PFTIr2**, **PFTIr5**, **PFTIr10** and **PFTIr20**, respectively. ^{1}H NMR spectra were collected for all of the polymers. Examples spectra for **PFT** and **PFTIr10** are shown in Appendix A. Peak assignments were done using the ^{1}H NMR spectra of the monomers and polymer spectra from the literature. The weight average molecular weights were determined to be between 3300 and 8100 with polydispersity ranging from 1.3 and 2.1. The low molecular weights of the **PFT**s are believed to be due to the

58

low reactivity of the 3,4-dibromothiophene relative to the 2,5-dibromopyridine. Previous reports of poly(fluorene-co-thiophene)s had similar molecular weights.[81, 94]

2.3.5 Absorption and Photoluminescent Properties of PFTIr

Incorporation of a less conjugated thienyl moiety into the polymer backbone led to a significant change in spectroscopic properties relative to poly(9,9-dihexylfluorene-alt-pyridine) (**PFPy**). These spectroscopic changes are not believed to be due to the lower molecular weight of the **PFT**s compared to the **PFPy**s (5000 vs. 40000 Da). Work by Miller and Klaerner[95] support this claim in their study of the effect of molecular weight on absorption and emission of oligo and poly(fluorene)s. As n, the number of repeat units, increases from 5 to 10, a small red shift is observed in the absorption maxima and there is no change in the emission maxima. When n > 10 there is essentially no change in the absorption or emission maxima. The UV-vis absorption of **PFT** was blue shifted relative to **PFPy** by 68 nm in both the solution and solid state (323 vs. 391 nm and 326 vs. 394 nm for **PFT** and **PFPy**). For the **PFTIr** series of materials, UV-vis absorption is dominated by the host polymer (**PFT**) since both materials absorb at 323 nm, while a small red shift is observed for films of the polymer (323 nm vs. 326 nm). The photoluminescent properties were also affected by the presence of the thienyl group. The emission maxima were blue shifted relative to **PFPy** by 36 and 38 nm in solution and solid state, respectively (380 vs. 416 nm and 390 vs. 428 nm for **PFT** and **PFPy**). Incorporation of iridium complexes into the polymer chain resulted in very little change in the solution or solid state absorption spectra (323 nm and 328 nm respectively); however significant changes are observed in the emission spectra (Figure 4). In solution, a broad weak emission peak can be seen ~ 590 nm while in the solid state, a strong emission is observed between 553 and 573 nm, depending on the content of iridium in the polymer. It should be noted that the fluorescence peak seen at 390 nm did not show any red shift as the iridium content increased, whereas the phosphorescence peak red shifted by up to 20 nm. The latter is believed to be

59

caused by an increase in conjugation length that does not appear to affect the fluorescence emission wavelength. It is concluded that the less conjugated thienyl segments isolate the emission from the fluorene-backbone moiety. The increase in quantum yields of the **PFTIr** series relative to the **PFPyIr** series supports the hypothesis that emission quenching is reduced by changing the relative triplet energies of the host polymer and the phosphorescent guest.
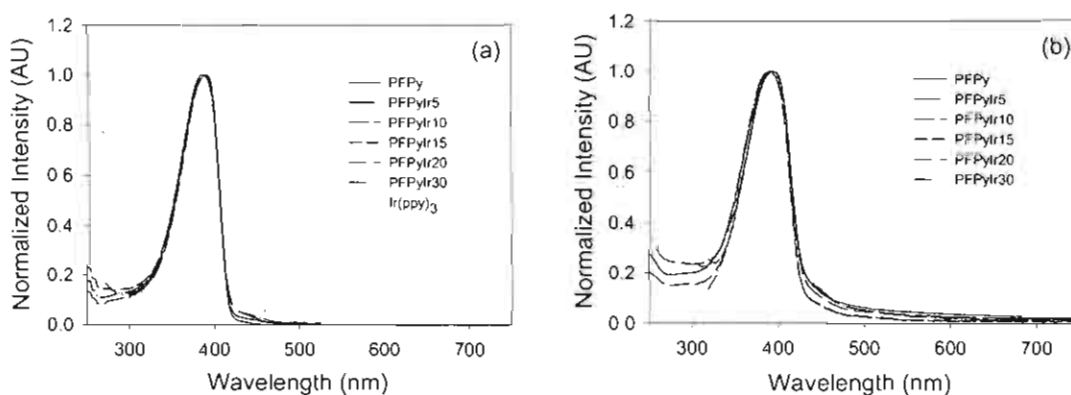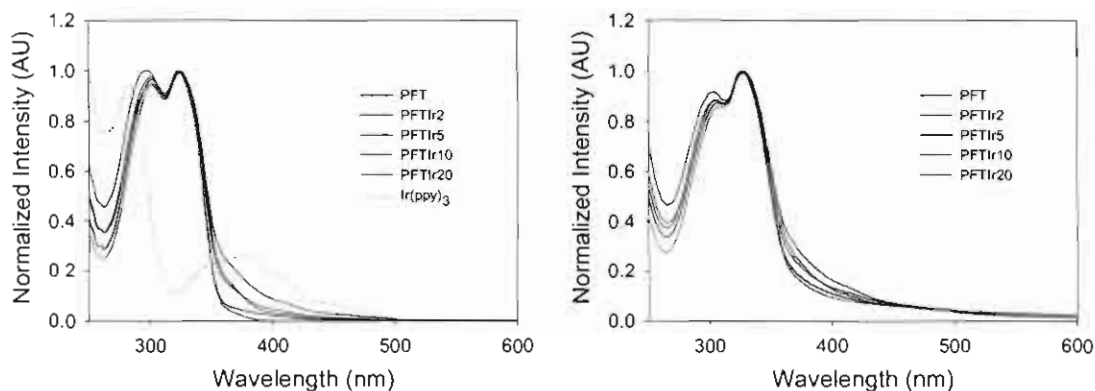

Figure 2.10: Absorption spectra of PFTIr in THF (a) and as a film (b).
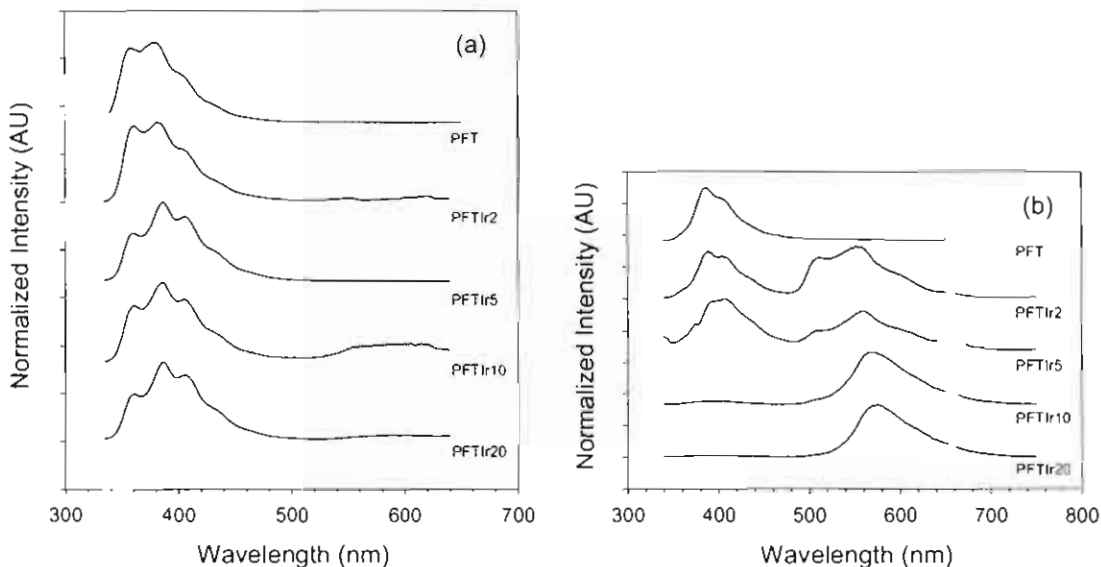
Figure 2.11: Photoluminescence spectra of PFTIr in THF (a) and as a film (b). λ_{ex}=330 nm.

Table 2.2: Summary of photophysical data for PFTIr series.

Polymer	Solution		Film		
	Absorption λ_{max} (nm)	Emission λ_{max} (nm)	Absorption λ_{max} (nm)	Emission λ_{max} (nm)	Φ_{film} *
PFT	323	380	326 (304)	390 (410)	0.07
PFTIr2	323 (300)	382	328 (306)	553 (390,410)	0.14
PFTIr5	325 (300)	386	327 (306)	554 (410)	0.21
PFTIr10	323 (300)	386	327 (306)	570	0.22
PFTIr20	324 (300)	387	329 (303)	573	0.23
Ir(ppy)₃[7]	385 (450)	515	390 (455)	518	0.12

* triplet emission, except **PFT**.

2.3.6 Triplet Energy Levels of PFTIr

The HOMO and LUMO energy levels of **PFT** (Figure 2.9) were estimated as previously described in as described in section 1.4.2. The ground state energy level of the iridium complex attached to **PFT** is approximated by that of Ir(ppy)₃ (5.2 eV)[92], due to the similarity of their chemical structures. The triplet energy of the phosphor was estimated from the phosphorescent emission wavelength (560 nm, 2.22 eV).

As illustrated by Figure 2.9, the triplet energy of **PFPy** is lower than that of **PFT**. It should be noted that the triplet energies of the polymers are only approximations; it is the relative difference between triplet energies that are important and not their absolute values. The triplet state energy of **PFT**, incorporating the 3,4- linked thienyl, is ~0.7 eV larger than the corresponding triplet energy of the phosphor. Thus the possibility of triplet energy transfer from an excited state phosphor to the non-emitting triplet state of the backbone is reduced. In support of this hypothesis, the quantum yields of phosphorescence from **PFTIr** materials are found to be ~ three times greater (0.20) than the corresponding **PFPyIr** polymers.

2.3.7 Electroluminescence of PFPyIr and PFTIr

Electroluminescence (EL) of the host polymer, **PFPy**, exhibits an emission maximum at 490 nm, which is red-shifted by 62 nm compared to its PL maximum (428 nm), as shown in Figure 2.12 and reported in Table 2.3. This is in agreement with previous reports in the literature[96] and may be explained by exciplex formation at the interfacial region when the emission wavelength becomes voltage dependant (Figure 2.12).[94] Incorporation of the iridium complex into the **PFPy** backbone results in a red shifted emission at 610 nm which originates from the metal complex. At lower iridium concentrations, a subpeak at 490 nm is observed, as shown in Figure 2.12. The EL of the host polymer for the **PFTIr** series, PFT, has an emission maximum at 402 nm (see Table 2.1 and Figure 2.13). Incorporation of iridium complex results in emission from the lowest energy state of the system, the iridium complex. The emission maximum increases from 550 to 570 nm, as the iridium content increases. Polymer **PFTIr5** also displays a weak emission between 400 and 450 nm, due to incomplete energy transfer. The PL and EL maximum emission wavelengths for all the polymers (Table 2.3) are quite similar with the exception of **PFPy**. However the relative intensities of polymer host and the iridium complex are different.

EL can be generated by charge trapping or energy transfer,[97] which may result in significant differences in PL and EL emission for a given material. When the PL and EL spectra are similar it can be concluded that the dominant mechanism generating luminescence is energy transfer, i.e., from the excited state of the polymer backbone to the emitting species. If the PL and EL spectra are different, as observed in the present system, then the dominant mechanism leading to luminescence is charge trapping. This may occur in a system with two different segments of differing energy levels; electrons or holes may be trapped on the lower energy segment. This causes a build up of local charge density, which can in turn enhance the possibility of attracting the opposite charge carriers.[98] In addition to direct charge trapping, excitons formed on higher energy segments can undergo energy transfer to the lower energy sites. Direct

and indirect charge trapping results in an increase in emission intensities from the emitting guest, relatively to the polymer backbone, as observed in Figure 2.12 and Figure 2.13.
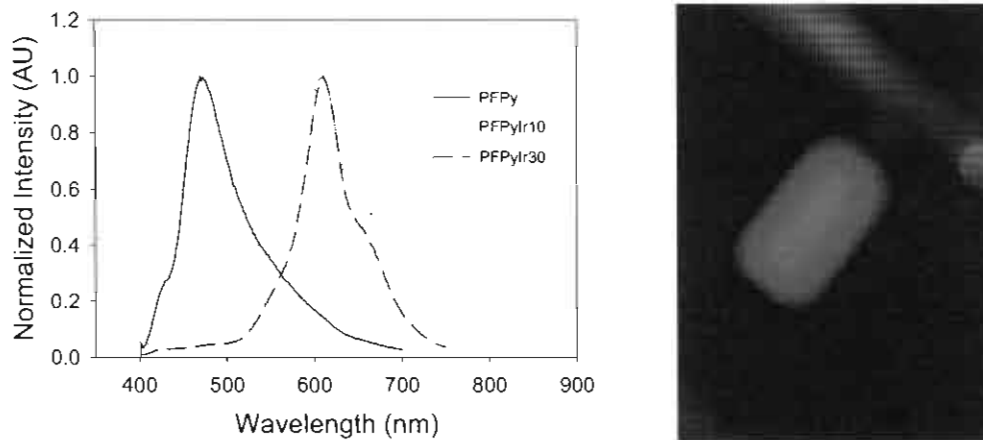
Figure 2.12: EL spectra PFPyIr-based devices (left) and photo of an operating device made from PFPyIr30 (right).
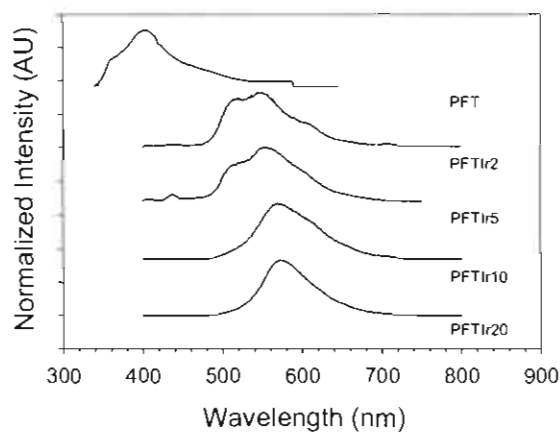
Figure 2.13: EL spectra PFTIr-based devices.
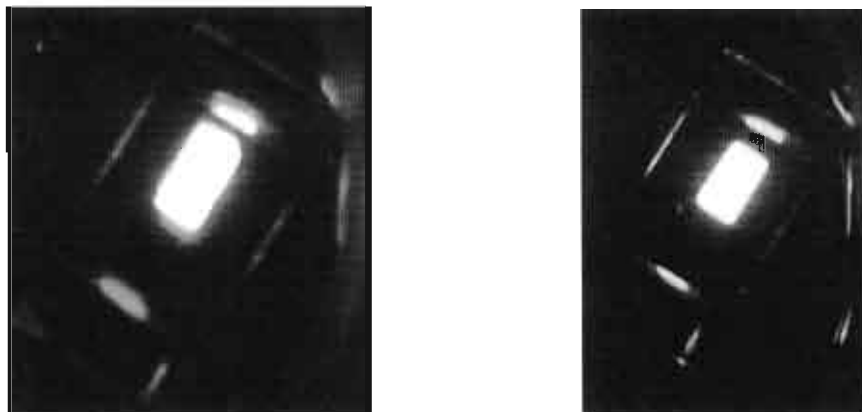
Figure 2.14: Photo of an operating LED made from PFTIr5 (left) and PFTIr10 (right).

2.3.8 LED Performance of PFPyIr and PFTIr

Devices were fabricated using the following two configurations: ITO|PEDOT:PSS| Polymer|CsF|Al and ITO|PEDOT:PSS| Polymer|TPBI|CsF|Al, where TPBI represents (1,3,5-tris(N-phenylbenzimidazol-2-yl)benzene). Polymers from the **PFPy** series containing iridium, **PFPyIr20** and **PFPyIr30** show better device performance than the host polymer (**PFPy**). **PFPyIr30** is twice as bright as the host at about $1/10^{th}$ the current density. However, the maximum brightness obtained for the **PFPyIr** series is only ~100 cd/m^2 and furthermore the efficiencies are low (~ 0.5 cd/A) (see Table 2.1 and Table 2.3). These values are nevertheless comparable to similar systems that have been published by Ito et. al..[70] They reported a maximum brightness of 74 cd/m^2 and maximum luminous efficiency of 0.04 cd/A for a similar iridium bound polyfluorene with the following device structure: ITO| PEDOT:PSS| Polymer| Ca| Al.

The **PFTIr** series also show much better device performances than their corresponding host polymers, i.e., in the absence or the Ir complex. The increase in performance is more drastic than the **PFPyIr** case because of the presence of the non-conjugated thiophene moiety in PFT. The host polymer, **PFT**, is a blue emitter but turn on voltages are high (as high as 27 V) and the maximum brightness was only 9.4 cd/m^2. However, when the Ir complex is incorporated into the polymer, a considerable improvement in device

64

performance is observed: the turn on voltage is reduced by greater than one half and the brightness increased by three orders of magnitude (see Table 2.3). When comparing the relative current densities and brightnesses of **PFTIr** polymers, it can be concluded that **PFTIr10** displays the best device performance and **PFTIr5**, the worst. At low current densities (0.04 A/cm^2), high brightnesses are obtained (1289 and 4541 cd/m^2) for **PFTIr10** for device structures with and without a TPBI layer, and the efficiencies are 2.69 and 4.11 cd/A, respectively (see Table 2.3 and *NM – not measured

Table 2.4).

Table 2.3: Summary of ITO| PEDOT:PSS| Polymer| CsF| Al device performance.

	λ_{max} PL	λ_{max} EL	Turn on voltage (V)	Max. Brightness (cd/m^2)	Luminous Efficiency (cd/A)	External Quantum Efficiency (%)
PFPy	428 (453)	490	4.6	77	0.08	0.05
PFPyIr5	613 (423,665)	609 (427)	NM	NM	NM	NM
PFPyIr10	613 (423,665,453)	610 (458)	NM	NM	NM	NM
PFPyIr20	613 (423,665,453)	NM	3.8	48	0.02	NM
PFPyIr30	613 (423,665,453)	610	6.6	150	0.48	0.32
PFT	390,410	402	27	1.80	0.003	NM
PFTIr2	553 (390,410)	550	4.8	1274	0.80	0.24
PFTIr5	554 (410)	550	6.1	230	0.33	0.10
PFTIr10	570	568	7.0	1289	2.69	0.84
PFTIr20	573	572	6.7	1552	1.35	0.41

*NM – not measured

Table 2.4: Summary of ITO| PEDOT:PSS| Polymer| TPBI| CsF| Al device performance.

	Turn on voltage (V)	Max. Brightness (cd/m^2)	Luminous Efficiency (cd/A)	External Quantum Efficiency (%)
PFT	21.5	9.39	0.02	NM
PFTIr2	8.3	3132	1.52	0.45
PFTIr5	6.4	291	0.66	0.21
PFTIr10	6.3	4541	4.11	1.29
PFTIr20	4.2	3462	1.94	0.59

*NM – not measured

For such a basic PLED structure, the performance of the **PFTIr** series is quite good and is attributed to the higher energy triplet energy of the polymer backbone. A study by Zhen et al.[68] reported a maximum brightness of 1730 cd/m^2 and a luminous efficiency 5.4 cd/A for a device with the following device structure: ITO| PEDOT:PSS| PVK| Polymer| Ba| Al, where the active polymer was poly(fluorene-co-carbazole) with alkyl-substituted ligands bound to the iridium complexes incorporated into the polymer backbone. A later study by Zhen et al.[99] reported a maximum brightness of 2010 cd/m^2 and a luminous efficiency 2.0 cd/A for a device with the following device structure: ITO| PEDOT:PSS| PVK| Polymer| Ba| Al. Their best performing polymer was poly(fluorene-co-carbazole) with 2-(1-naphthalene)-pyridine bicycloiridium complexes incorporated into the polymer backbone. Work by Yang et al.[80] described hyper-branched and linear substituted poly(*p*-phenylene)s based on Ir(ppy)$_3$ and (mppy)$_2$Ir(acac) complexes. Devices with the following structure: ITO| PVK| Polymer+PBD 30 wt.%| Ba| Al displayed luminous efficiencies of 3.6 cd/A.

From a materials perspective, it is reasonable to conclude that further improvements may be achieved by using a phosphorescent emitter that has a low triplet energy state. On the other hand, device performances may also be improved by modifying the device structure. In this case, TPBI was introduced

as a hole blocking layer with the intent to balance hole and electron flow. Typically, introduction of TPBI leads to a decrease in current densities[100] but in this case a significant increase was observed. It is possible that this is due to the TPBI layer acting as an electron injector as well as a hole blocker. Both brightness and efficiency were increased by a factor of ~ 2. The device data reported in this paper are preliminary and provide an indication of the materials properties – refinement of the device configuration can be used to further optimize the PLED device performance.

2.4 Conclusion

Two different synthetic methods have been successfully used to yield two different series of iridium-containing conjugated polymers. The first method involves a two step post-functionalization of a poly(fluorene-alt-pyridine) and the second involves a Suzuki polycondensation of a fluorene boronic ester and an iridium complex with a dibrominated ligand. The optical properties of the polymers vary significantly depending on the polymer structure. The former synthetic method produces a red-emitting conjugated polymer and the latter a greenish-yellow emitter, λ_{max} = 613 and ~ 560 nm in the film, respectively. A mechanism of energy transfer from the polymer backbone to the iridium complex, intersystem crossing, and phosphorescence from the Ir complex is assumed to be operating. Photoluminescence data indicates that emission quenching from the polymer triplet state is occurring: The quantum yields of phosphorescence from the polymer films decreases from 0.22 to 0.05, for PFTIr10 and PFPyIr10, respectively. It was found that increasing the triplet energy of the conjugated backbone by incorporation of a 3,4-linked thienyl group raises the energy of the triplet state of the polymer by lowering the conjugation length of the polymer backbone, thereby decreasing triplet energy transfer from the phosphorescent emitter to the non-emitting polymer backbone. It is surmised that changing the energy level of the polymer triplet relative to the triplet of the phosphor, changes the rate of back energy transfer. Electroluminescence data indicates that charge

67

trapping is most probably the dominant mechanism occurring in the PLEDs, resulting in tunable emission colour depending on the polymer structure.

CHAPTER 3: EFFECT OF IRIDIUM COMPLEXES BOUND TO A CONJUGATED POLYMER ON CHARGE GENERATION IN PHOTOVOLTAIC DEVICES

3.1 Introduction

The use of conjugated polymers as active materials in photovoltaic (PV) devices is an area of increasing interest.[101] This interest is motivated, in part, by their solution processability and low fabrication costs. Polythiophenes have been extensively used in organic photovoltaics for various reasons. One reason is the existence of previously proven synthetic techniques to make regio-specific poly(3-hexylthiophene) (P3HT).   Using methods developed by McCullough (section 1.2.1.2) or Rieke[102] a high level of structural control is possible. It has been shown that by controlling the percent regioregularity of P3HT it is possible to red-shift polymer absorption of films from 450 to 550 nm.[39, 103] The correlation between polymer absorption and photovoltaic properties is one area that continues to be under investigation. In addition it has been shown that films of regio-regular P3HT have a highly ordered semi-crystalline structure in comparison to their regio-random analogues.[38, 39] The formation of semi-crystalline domains has been used to explain the high mobility observed in blends of P3HT and [6,6]-phenyl C_{61} butyric acid methyl ester (PCBM). Hole mobility is another important property of materials that are intended to be used as electron donors in PV. State-of-the-art devices have been made from blends of

P3HT and PCBM (1:0.8 wt. ratio), producing devices with power conversion efficiencies (PCEs) > 5 % and external quantum efficiencies (EQEs) > 80 %.[46]

One of the primary limitations of a heterojunction photovoltaic device is that singlet excitons have short diffusion lengths (~ 10 nm), thus only the fraction of incident light absorbed in a thin region near the donor/acceptor interface results in the conversion of excitons into charges, i.e., charge generation is low. The relatively short diffusion length (L_D) of singlet excitons is illustrated in Figure 3.1a by the thin black lines separating the donor and acceptor phases. Hence the short L_D of singlet conjugated polymers has resulted in much research being devoted to the formation of nano-phase binary morphologies of donor (D) and accepter (A) so that the singlet exciton has only to travel a short distance (tens of nm) to a D/A interface; the negative consequence is that morphologies are restricted. The requirement for small phase separation might be lifted if triplet excitons are formed. Triplet *excited states* possess inherently longer lifetimes and triplet *excitons* are expected to possess longer diffusion lengths. The longer L_D of triplet excitons will result in increased charge generation assuming the mobility of the exciton is not compromised. The L_D of an exciton is determined by its mobility (μ) and lifetime (τ),[104] as shown in Equation 3.1. This work examines the use of a triplet forming conjugated polymer to increase the exciton lifetime which is expected to increase the L_D, as illustrated by the thicker black lines in Figure 3.1b.

Equation 3.1: $$L_D \propto \mu \times \tau$$
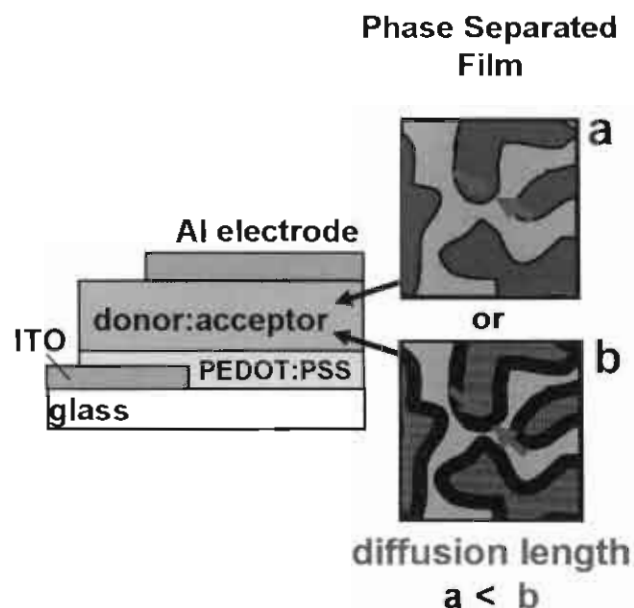
Figure 3.1: Illustration showing the phase separated morphology of a singlet material and its diffusion length represented by the thin black lines at the donor acceptor interface (a) and a triplet material with a longer diffusion length represented by the thicker black lines (b).

Figure 3.2 depicts some of the triplet materials that have been previously studied in PV devices. As part of the body of work on triplet-forming materials for PV devices, Köhler *et al.*[105] describe the photophysics of an organometallic polymer, Pt-poly-yne blended with C_{60}, reporting that electron transfer occurs from the Pt-poly-yne to C_{60} *via* triplet excitons. PV devices give external quantum efficiencies (EQE) up to 1.6 % under monochromatic illumination. Shao *et al.*[106] report the performance of a bilayer device using 2,3,7,8,12,13,17,18-octaethyl-21H,23H-phorphineplatinum(II) (PtOEP) and C_{60} as the electron donor and acceptor, respectively. They report power conversion efficiencies (PCE) of 1.2 %. Guo *et al.* report that photoinduced charge transfer from Pt-acetylide to C_{60} occurs *via* the triplet excited state (EQE = 9 %, PCE = 0.27 %),[107] as does photoinduced charge transfer in Pt acetylide triads end-capped with fullerene (EQE = 22 %, PCE = 0.05 %).[44] Yang *et al.* studied poly(fluorene) (PF) and poly(thiophene) (P3HT) blended with molecular Ir(mppy)$_3$ using CdSe as an acceptor,[108] and demonstrate an increase in the triplet exciton population, attributed to the increased rate of intersystem crossing (ISC) from the PF singlet

71

state to the triplet state. The short-circuit photocurrent subsequently doubled and the open circuit voltage (Voc) increased by 50 % upon addition of the phosphor.

Figure 3.2: Representative chemical structures of phosphorescent polymers for PV.

Blends of polymers and small molecules generally suffer from gross phase segregation, if not initially, then over a period of time. Noh et. al. report on the formation of aggregates in films of $Ir(ppy)_3$ doped in poly(fluorene-alt-phenylene), where aggregation was found to prevent dopant molecules from being in close proximity with host molecules, thereby inhibiting the energy transfer process.[109] However, this may be mitigated by chemically attaching the small molecule to the polymer backbone. This chapter examines the effect of tethering an Ir complex to the main chain of a conjugated polymer; its role in enhancing triplet formation (as evidence by increased phosphorescence); and its effect on charge generation in photovoltaic devices by giving rise to longer lived excited states and longer exciton diffusion lengths. The chemical structures of the polymers under investigation are shown in Figure 3.3. The work distinguishes itself from other reports in the field in that it is the first photovoltaic study where Ir complexes are covalently incorporated into a conjugated polymer.
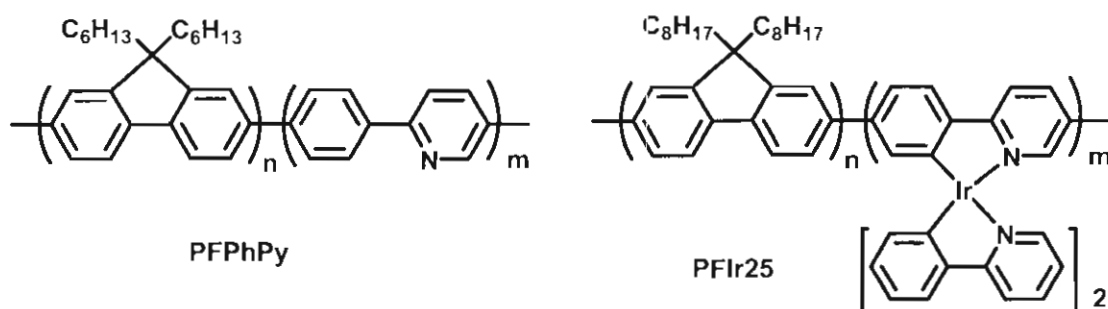
Figure 3.3: Chemical structures of polymers used in this study, PFPhPy and PFIr25.

3.2 Experimental

3.2.1 Materials

9,9-Dihexylfluorene-2,7-bis(trimethyleneborate), 9,9-dihexyl-2,7-dibromofluorene, 9,9-dioctyllfluorene-2,7-bis(trimethyleneborate), 9,9-dioctyl-2,7-dibromofluorene, 2,5-dibromopyridine, 4-bromophenylboronic acid, phenyl boronic acid, 2,5-dibromobenzene, 2-phenylpyridine, tetrakis(triphenylphosphine)palladium (Pd(PPh$_3$)$_4$), iridium (III) chloride trihydrate, iridium (III) acetylacetonate were purchased from either Sigma-Aldrich Co. or Strem Chemicals, Inc.. THF, ether and chlorobenzene were dried and freshly distilled before use. Poly(styrene sulfonic acid)-doped poly(ethylenedioxythiophene) (PEDOT:PSS, Baytron VP AI 4063) was purchased from Bayer Corp. PCBM was purchased from American Dye Source, Inc.. Indium tin oxide (ITO) coated glass was purchased from Merck Display Technologies Ltd.

Poly(9,9-dihexylfluorene-co-2-phenyllpyridine) **(PFPhPy)** was synthesized *via* Suzuki polycondensation according to Figure 3.4.[87] 9,9-Dihexylfluorene-2,7-bis(trimethyleneborate) (0.324 g, 0.64 mmol), 9,9-dihexyl-2,7-dibromofluorene (0.159, 0.32 mmol) and 5-bromo-2-(4-bromophenyl)pyridine) (0.102 g, 0.32 mmol) were dissolved in THF (12.5 mL, deoxygenated); to which, a solution of K$_2$CO$_3$ (2 M, 2 mL) was added, together with Pd(PPh$_3$)$_4$ (0.022 g, 3 mol % based on fluorene). The resulting mixture was sealed in a glass vial and heated for 2 days at 80°C in an oil bath. End capping of the polymer was carried

out as the last step in synthesis. Phenyl boronic acid (0.0039 g, 5 mol %) was added and the solution was heated (80˚C, 12 h). This was followed by the addition of bromobenzene (0.0067 g, 5 mol %), at the same temperature. Once cooled to room temperature, THF was removed and the residue dissolved in chloroform. This was followed by washing with water (3 times) and drying over anhydrous magnesium sulfate. After filtration, the volume of chloroform was reduced and the concentrated solution was passed through an alumina column. The volume of the resulting solution was again reduced and precipitated in methanol (~50 mL) to yield **PFPhPy** (0.386 g, 68%). A weight average molecular weight (M_w) of 32 700 Daltons and a PDI of 2.0 was obtained. δ_H (600 MHz, CDCl$_3$, Me$_4$Si) 9.1 (1H, s), 8.20-7.75 (29 H, m), 2.13 (12 H, br. β-CH$_2$), 1.15-0.78 (66 H, m, CH$_2$ and CH$_3$). δ_C (150 MHz, CDCl$_3$, Me$_4$Si) 155.50, 152.13, 148.30, 140.52, 140.02, 135.10, 128.82, 127.58, 127.23, 126.18, 121.53, 120.27, 120.01 (aromatic) 55.35 (C$_9$-fluorene ring) 40.38, 31.49, 29.72, 23.86, 22.59, 14.06 (aliphatic). Anal. Calcd for C$_{86}$H$_{103}$N: C, 89.8; H, 9.0; N, 1.2 %. Found: C, 87.8; H, 9.0; N, 0.7 %.

Poly(9,9-dioctylfluorene-co-tris(2-phenylpyridine)   iridium   (III))) **(PFIr25)** was synthesized *via* Suzuki polycondensation according to Figure 3.4.[46] 9,9-Dioctylfluorene-2,7-bis(trimethyleneborate) (0.178 g, 0.32 mmol), 9,9-dioctyl-2,7-dibromofluorene   (0.88,   0.16   mmol)   and   (5-bromo-2-(4-bromophenyl)pyridine))Ir(III)bis(2-phenylpyridine) (0.130 g, 0.16 mmol) were dissolve in THF (12.5 mL, deoxygenated); to which, a solution of Na$_2$CO$_3$ (2 M, 2 mL) was added, together with Pd(PPh$_3$)$_4$ (0.011 g, 3 mol % based on fluorene). The resulting mixture was sealed in a glass vial and heated for 5 days at 80˚C in an oil bath. End capping of the polymer was carried out as the last step in synthesis. Phenyl boronic acid (0.002 g, 5 mol %) was added and the solution was heated (80˚C, 12 h). This was followed by the addition of bromobenzene (0.0068 g, 10 mol %), at the same temperature. Once cooled to room temperature, THF was removed and the residue dissolved in chloroform. This was followed by washing with water (3 times) and drying over anhydrous magnesium sulfate. After filtration, the volume of chloroform was reduced and

the concentrated solution was passed through an alumina column. The volume of the resulting solution was again reduced and precipitated in methanol (~50 mL). The resulting precipitated solid was washed with acetone for 12 hours to remove residual oligomer, yielding **PFIr25** (0.073 g, 51%). A weight average molecular weight (M_w) of 12 200 Daltons and a PDI of 1.4 was obtained. δ_H (600 MHz, $CDCl_3$, Me_4Si) 8.3-6.6 (m, aromatic H), 2.12 (12 H, br. β-CH_2), 1.16-0.81 (m, CH_2 and CH_3). δ_C (150 MHz, $CDCl_3$, Me_4Si) 151.79, 140.47, 140.00, 128.77, 127.20, 126.14, 121.47, 119.95 (aromatic) 55.32 (C_9-fluorene ring) 40.37, 31.78, 30.03, 29.21, 23.90, 22.60, 14.06 (aliphatic). Anal. Calcd for $C_{120}H_{142}N_3Ir$: C, 79.2; H, 7.9; N, 2.3 %. Found: C, 82.4; H, 9.1; N, 0.5 %. Iridium content (XRF) 5.3 wt. %.

[(ppy)$_2$IrCl]$_2$ and **(ppy)$_2$Ir(BrPhPyBr)** were synthesized according to a previously published procedure.[37]

5-bromo-2-(4-bromophenyl)pyridine) was synthesized according to published procedure.[110] 4-Bromophenylboronic acid (2.54 g, 12.7 mmol) and 2,5-dibromopyridine (3.00 g, 12.7 mmol) were added to a degassed solution of THF; to which, a solution of Na_2CO_3 (2 M, 2 mL) was added, together with Pd(PPh$_3$)$_4$ (0.145 g, 1 mol % based on dibromopyridine). The resulting mixture was refluxed at 80°C for 48 hours. The reaction flask was cooled to room temperature and the solvent was removed, water was added to the residue (100 mL), followed by dilute HCl until the pH of the solution reached 5. The product was extracted with chloroform (3 x 30 mL), washed with water and dried over anhydrous magnesium sulfate. Column chromatography was used to isolate the product (silica gel, hexane and a mixture of hexane and ether, 50:2), which was recrystallized from a mixture of chloroform and hexane. Fluffy, white crystals were obtained (2.4 g, 60%). δ_H (500 MHz, $CDCl_3$, Me_4Si) 8.73 (1 H, d), 7.88 (1 H, dd), 7.85 (1 H, s), 7.83 (1 H, s), 7.59-7.61 (3 H, s). m/z (EI) 314.90, 312.80, 310.95 (M^+, 1:2:1, $C_{11}H_7NBr_2$ requires 314.98, 312.98, 310.98) 234.00, 231.90 (M^+- Br, $C_{11}H_7NBr$ requires 234.06, 232.06) 153.00 (M^+- 2Br, $C_{11}H_7N$ requires 153.06).

3.2.2 Methods and Instrumentation

Chloroform (spectro-grade, Caledon Laboratories Ltd.) was used to prepare solutions (4 mg/mL) for film casting. Films were spin-cast on either quartz or glass slides at 1000 rpm for 60 s, shortly before acquisition of absorption and photoluminescence spectra. NMR spectroscopy was performed using a 500 MHz Varian Inova500 spectrometer or a 600 MHz Brucker Avance QNP cryoprobe spectrometer. Elemental analyses were performed by Canadian Microanalytical Service Ltd. Mass spectrometry was performed using a Voyager DE Perceptive biosystems MALDI Spectrometer. Ir content was determined using a Kristalloflex 2H X-ray fluorescence (XRF) spectrometer made by Siemens. Samples were excited with Mo X-rays, operated at 40 kV and 5 mA. A calibration curve was made using $Ir(acac)_3$ as a standard and yttrium as an internal standard. Samples were prepared by drop casting films on ultra thin mylar sheets. Molecular weight determinations were performed using gel permeation chromatography (Waters Model 1515 isocratic pump) calibrated against PS standards. Polymers were eluted with THF using a flow rate of 1 mL/min and monitored with a UV-vis detector (Waters 2487). Microwave synthesis was performed using an in-house modified Panasonic Inverter Microwave (model no NN-S614, see Appendix C). Absorption and fluorescence spectra were collected using Cary 3E and Photon Technology International (PTI) spectrophotometers, respectively. Quantum yield measurements were performed using an integrating sphere instrument from PTI. Emission lifetimes were measured using a time correlated single photon counting system. Cyclic voltammograms were measured on polymer films drop cast on glassy carbon electrode (1.5 mm diameter). The electrolyte was dissolved in acetonitrile (0.1 M Bu_4NClO_4). Pt wire was used for the counter electrode. The reference electrode consisted of Pt wire in acetonitrile (0.1 M tetrabutylammonium iodine, 0.05 M I_2). Potentials were measured against ferrocene/ferrocenium redox couple using a PAR potentiostat/galvanostat 263A at a scan rate of 50 mV/s.

PV devices were prepared in the following manner: ITO was patterned by masking the pieces with tape and immersion in concentrated HCl, followed by

sequential sonication in isopropyl alcohol, acetone, a mixture of H_2O, H_2O_2 and NH_4OH (5:1:1 vol. ratio), prior to rinsing with H_2O. PEDOT:PSS (Baytron VP AI 4083) was spin coated at 5000 rpm and annealed for 10 minutes at 140°C under air. Polymer:PCBM blends (1:4 wt. ratio, ~ 15 mg/mL) in chlorobenzene were spin coated at 700 rpm in air. An Al layer was thermally evaporated on the polymer surface at a pressure < 2×10^{-6} Torr, yielding thicknesses of 100 nm. Current-voltage characteristics were measured using a Keithley source meter (model 2400). Polymer thicknesses were determined using a KLA Tencor Alpha-Step IQ surface profiler. The active area of the device was ~10 mm^2. I-V curves were obtained using a solar simulator, supplied by Newport, equipped with a 300 W Xenon lamp and a 1.5 AM filter at an irradiation intensity of 80 mW/cm^2. The reflection of light by the ITO was taken into account by placing a piece of ITO coated glass in front of the power meter when measuring the irradiation intensity.

3.3 Results and Discussion

3.3.1 Synthesis and Properties of PFPhPy and PFIr25

Figure 3.4 depicts the Suzuki polycondensation reaction that yielded polymers **PFPhPy** and **PFIr25**. The feed ratios of dibromo-9,9-dialkylfluorene to 5-bromo-2-(4-bromophenyl)pyridine or (5-bromo-2-(4-bromophenyl)pyridine))Ir(III)bis(2-phenylpyridine) were 1:1. The molar feed ratio of iridium in the **PFIr25** was calculated to be 25 %. X-ray fluorescence (XRF) spectroscopy determined the actual amount incorporated was 13 mol%. ^{1}H and ^{13}C NMR spectra were collected for both polymers and are shown in Appendix A. Peak assignments were carried out using the ^{1}H and ^{13}C NMR spectra of the monomers and polymer spectra from the literature. The weight average molecular weights of **PFPhPy** and **PFIr25** were determined by GPC (chromatograms shown in Figure 3.5), and found to be 32 700 and 12 200 Daltons with polydispersities of 2.0 and 1.4, respectively.
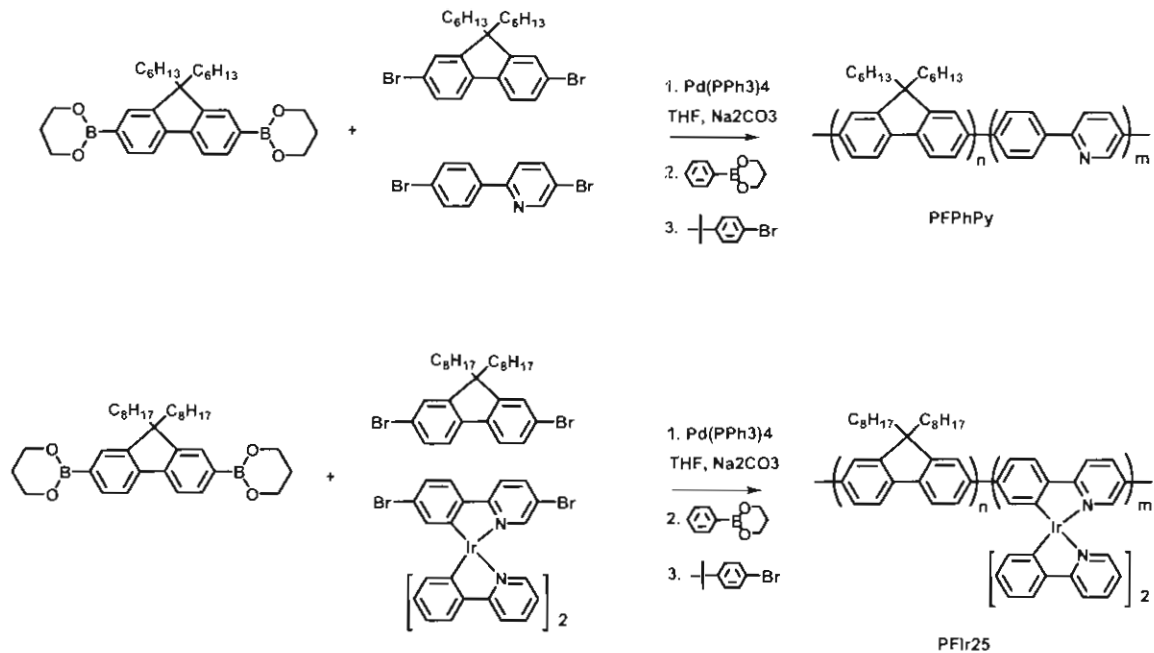
Figure 3.4: Synthesis of PFPhPy and PFIr25.
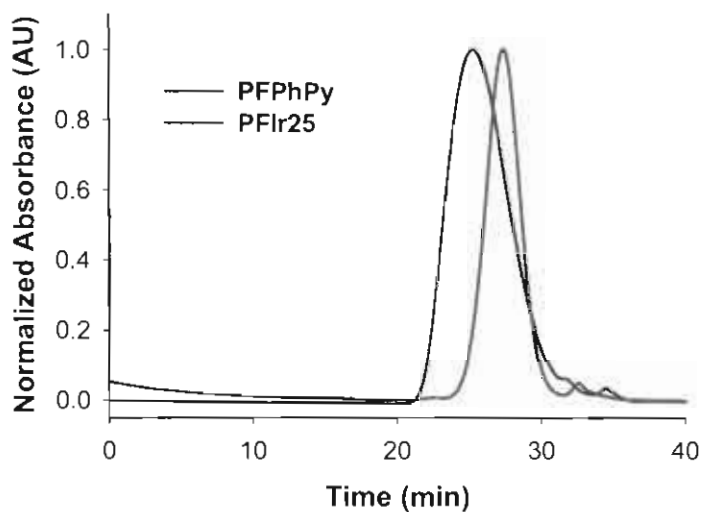
Figure 3.5: GPC trace of PFPhPy and PFIr25.

3.3.2 Absorption and Photoluminescent Properties of PFPhPy and PFPhPyIr

Absorption and photoluminescence spectra of films of **PFPhPy** and **PFIr25** are shown in Figure 3.6 and Figure 3.7, respectively. λ_{max} for both

78

PFPhPy and **PFIr25** occurs at ~ 385 nm, due to the absorption of the poly(fluorene-co-phenylpyridine) main chain. The longer absorption tail observed in **PFIr25**, between 400-450 nm, is due to absorption by the iridium complex. Figure 3.6 shows the absorption profile of Ir(ppy)$_3$, to further illustrate this point. The photoluminescence spectrum of **PFPhPy** exhibits a maximum at 422 nm whereas **PFIr25** exhibits a maximum at 596 nm (Figure 3.7). The former is due to fluorescence from the main chain, whereas the latter is due to phosphorescence from the iridium complex. The transient luminescent decay monitored at ~ 600 nm revealed the PL lifetime of **PFIr25** to be 0.26 μs (Figure 3.8, Table 3.1), indicating the triplet nature of the long wavelength emission. This result is consistent with previously reported lifetimes of iridium-bound conjugated polyfluorene copolymers, where it was shown that phosphorescent lifetimes decreased with increasing iridium content.[111] Fluorescent emission of **PFIr25** at 422 nm is very weak compared to its phosphorescence, due to energy transfer from the polymer backbone to the iridium complex, as observed for analogous host-guest polymer systems in light emitting devices (LEDs).[35, 37, 55] Phosphorescence from **PFIr25** is completely quenched upon blending [6,6]-phenyl C$_{61}$ butyric acid methyl ester (PCBM) into the film, as illustrated in Figure 3.7.
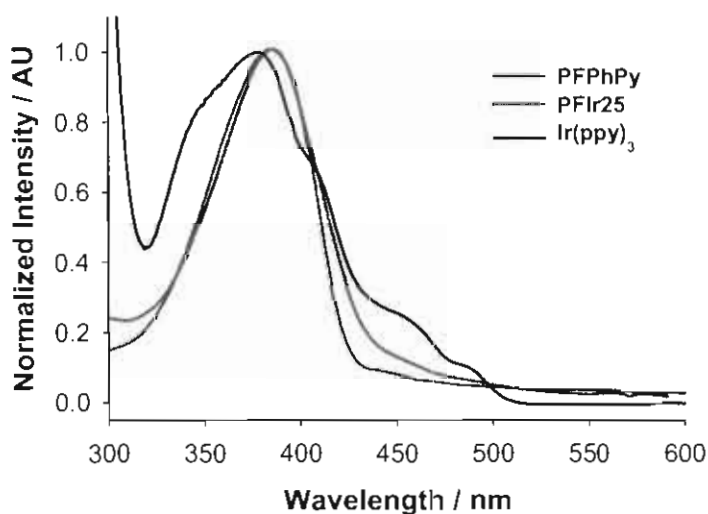
Figure 3.6: Absorption spectra of PFPhPy, PFIr25 films and Ir(ppy)$_3$ in THF.

The quantum yield of fluorescence from **PFPhPy** and phosphorescence from **PFIr25** was measured to be 0.04 and 0.02, respectively. Polymer **PFIr25** was designed to contain a significant amount of the iridium complex (25 mol %), to facilitate triplet exciton migration to an electron acceptor site. Hence the phosphorescence quantum yield of **PFIr25** is partially "concentration quenched"[68] or quenched by back energy transfer from the triplet state of the iridium complex by the triplet state of the polymer backbone. The quantum yield of **PFIr25** is much lower in magnitude than analogous poly(fluorene-co-thiophene) iridium complexes prepared with lower Ir content.[37]
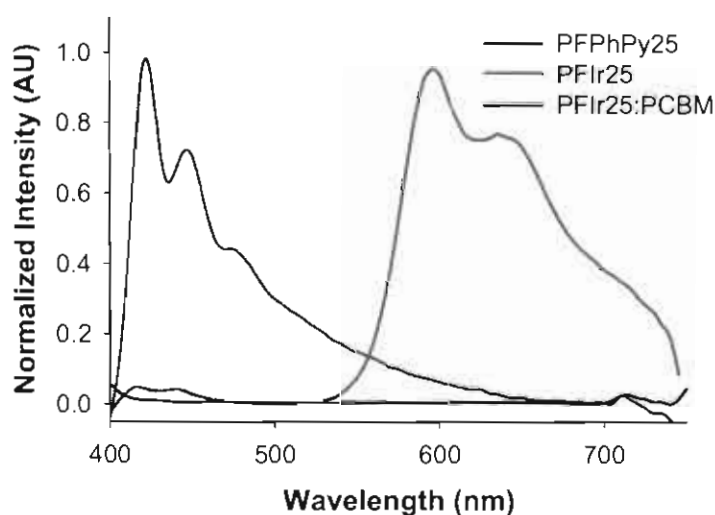
Figure 3.7: Photoluminescence spectra of PFPhPy, PFIr25 and a PFIr25:PCBM blend (1:4 wt. ratio). λ_{ex} = 380 nm.

Table 3.1: Photophysical properties of films of PFPhPy and PFIr25.

Polymer	Absorption λ_{max} (nm)	Emission λ_{max} (nm)	Φ	τ (μs)
PFPhPy	385	422	0.04	-
PFIr25	385	596	0.02	0.26
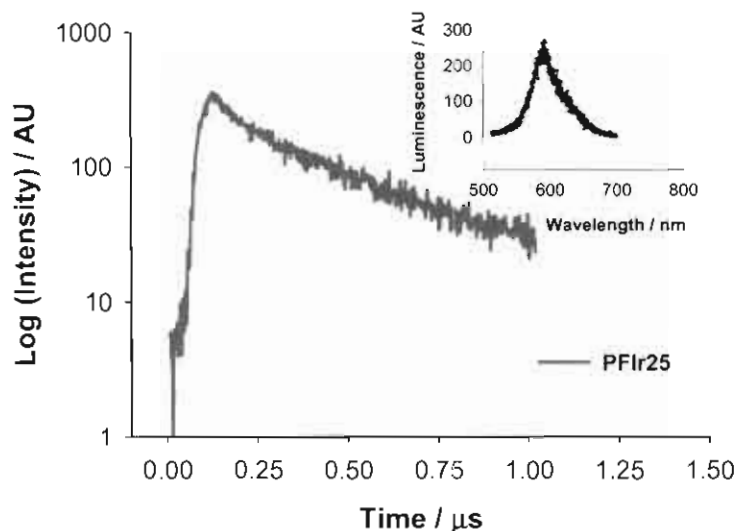
Figure 3.8: Transient luminescent decay of a thin film of PFIr25. λ_{ex} = 355 nm. Inset shows the corresponding luminescence spectrum.

3.3.3 Energy levels of PFPhPy and PFPhPyIr

Electronic energy levels of the compounds were estimated using a combination of absorption spectroscopy and cyclic voltammetry (CV), as described in section 1.4.3 in the introduction. CVs of thin films deposited on a glassy-carbon working electrode were obtained, Figure 3.9, and potentials were measured relative to the ferrocene/ferrocenium redox couple, as described in section 1.4.3. Using the onset of the oxidation peak, the HOMO levels of **PFPhPy** and **PFIr25** were estimated to be 5.73 and 5.68 eV (+/- 0.05), respectively. Using the onset of the absorption spectra, the band gap was estimated to be 2.94 and 2.88 eV (+/- 0.05), resulting in a LUMO level estimation for **PFPhPy** and **PFIr25** of 2.79 and 2.80 eV (+/- 0.10), respectively. The HOMO levels were within 0.05 eV of each other and assumed to be similarly dominated by the poly(fluorene-co-phenylpyridine) backbone. The HOMO and LUMO levels of **PFPhPy** are depicted in Figure 3.10. The triplet energy gap of the polymer was estimated using the following equation: $T_1 = (1.13\ S_1 - 1.43) \pm 0.25$ eV.[92] Given the similarity of the energy levels, it is expected that PV devices prepared

from **PFPhPy** and **PFIr25** blended with PCBM will possess similar open circuit potentials.
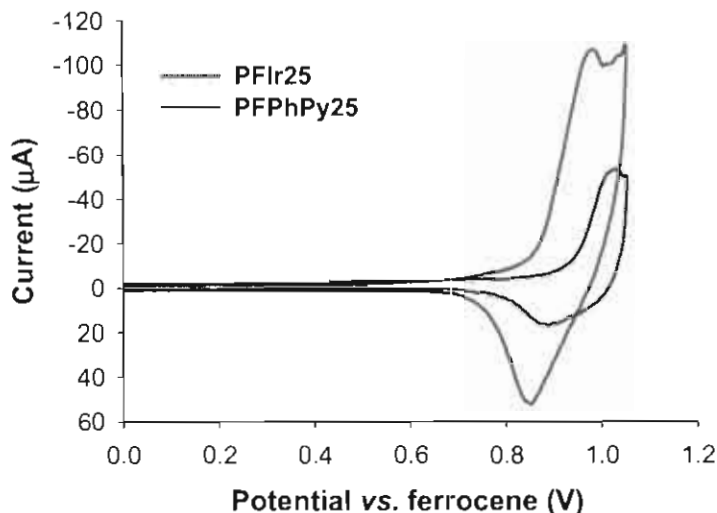
Figure 3.9: Cyclic voltammograms of films of PFPhPy and PFIr25. Scans recorded at 50 mV/s in 0.1 M Bu₄NClO₄ in acetonitrile.

Figure 3.10 demonstrates representative processes that may occur upon excitation of **PFIr25** in the presence of PCBM. Energy transfer from poly(fluorene-alt-pyridine) (**PFPhPy**) to the phosphorescent group, Ir(ppy)$_3$, is depicted as process (a). The triplet excited state may be quenched by the polymer backbone (b), by concentration quenching (c), by phosphorescence (d), or by electron transfer to PCBM (e), the latter being essential for PV activity. The relative rates of these photophysical processes determine the fate of the triplet state. For an analogous system, polyspirobifluorene and a substituted derivative of Ir(ppy)$_3$, the rate of (b) occurs within ~ 10 ns.[112] Rates of photoelectron transfer (process (e)) typically occur in the ps time domain,[44] i.e., three orders of magnitude faster. It is thus believed that self-quenching of the Ir(ppy)$_3$ triplet state in **PFIr25** by the main chain is unlikely to compete with electron transfer, if the triplet exciton can reach an electron acceptor site. Therefore, in contrast to highly phosphorescent polymers of similar structure, designed for LED applications, the triplet energy level of the conjugated polymer is deemed to be of less significance in the design of such polymers for PVs. As discussed above,

PL from a **PFIr25**:PCBM blend (1:4 wt. ratio) shown in Figure 3.7 is completely quenched, which is indicative of electron transfer from the excited state polymer to PCBM.
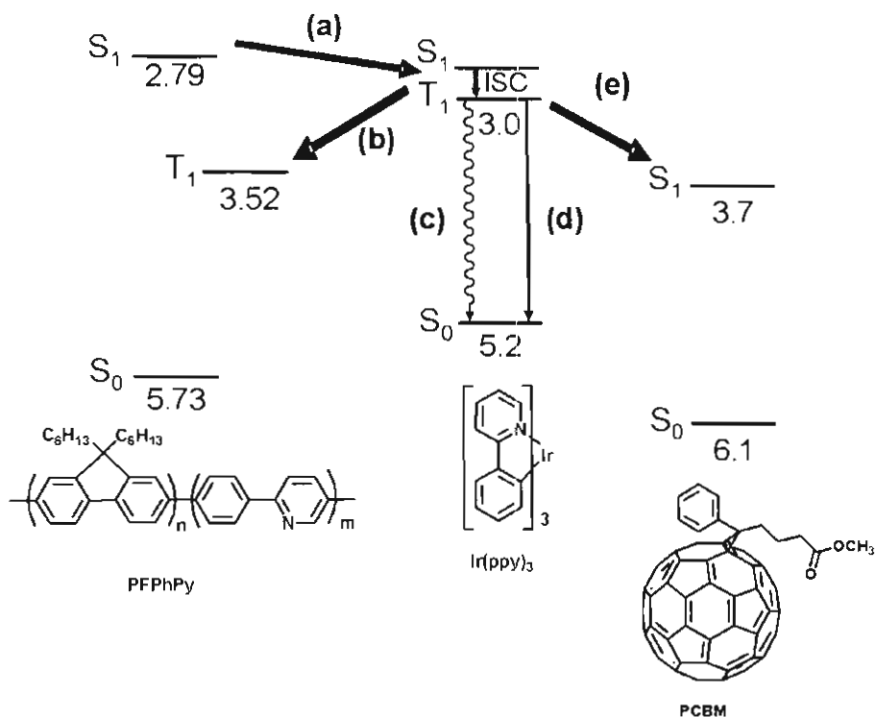
Figure 3.10: **Energy level diagram showing (a) energy transfer from the PFPhPy main chain to the bound Ir complex, (b) triplet quenching of the Ir complex by the PFPhPy main chain, (c) concentration quenching of the triplet state, (d) phosphorescence of the Ir complex and (e) photo-induced electron transfer (PET) from the Ir complex to PCBM.**

3.3.4 Photovoltaic Devices of PFPhPy and PFPhPyIr

Photovoltaic devices were fabricated by blending **PFPhPy** and **PFIr25** with PCBM in order to examine the effect of triplet formation on charge generation as observed by the PV response. Although the solar PV efficiencies of devices based on **PFPhPy** and **PFIr25** are much lower than current state-of-the-art devices,[46] **PFIr25** clearly exhibits an improved device performance as shown in Figure 3.11 and listed in Table 3.2. The short circuit current densities (Jsc) are 0.01 and 0.44 mA/cm^2 for devices prepared with **PFPhPy** and **PFIr25**, respectively, and the power conversion efficiency improves from 0.002 for **PFPhPy** to 0.07 % for **PFIr25**. The fill factors of the two systems, while relatively

low, are similar, which indicates that that the overall cell resistances to charge transport, once charges are formed, are similar, and that this is unlikely to account for the differences in photovoltaic efficiency.
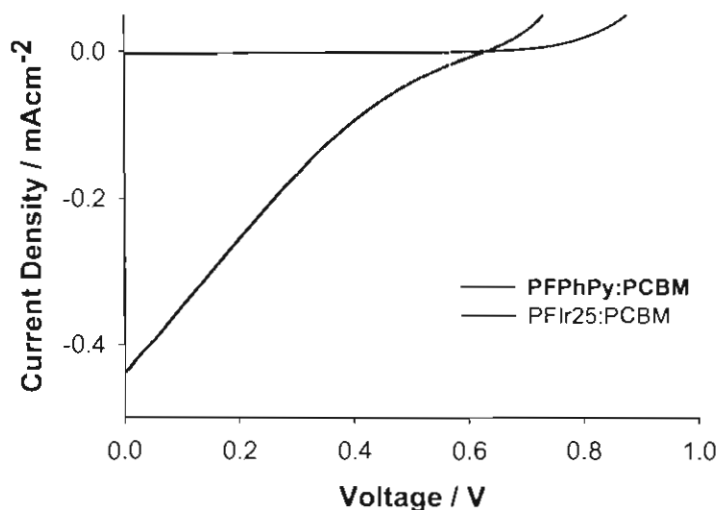
Figure 3.11: I-V curves obtained from PFIr25:PCBM (1:4) and PFPhPy:PCBM (1:4) solar cells under AM 1.5 illumination (80 mW/cm^2). Device configuration: ITO|PEDOT:PSS| (PFPhPy or PFIr25):PCBM| Al.

Table 3.2: Summary of device performance data plotted in Figure 3.11.

	Voc (V)	Jsc (mA/cm^2)	FF	PCE (%)
PFPhPy:PCBM	0.60	0.01	0.24	0.002
PFIr25:PCBM	0.63	0.44	0.19	0.07

External quantum efficiencies (EQE) of the devices are shown in Figure 3.12. Incorporating the Ir complex into the polymer increases the EQE by ~ a factor of 10, from 1.1 to 10.3 %. The maximum EQE observed at ~ 350 nm is attributed to absorption by the poly(fluorene-co-phenylpyridine) main chain and the small peak observed at ~ 715 nm is attributed to absorption by PCBM. An approximation of the internal quantum efficiency (IQE), i.e., the conversion efficiency of photons absorbed to current produced, was obtained by dividing the EQE by the light absorbed in the device. The absorption of **PFPhPy** and **PFIr25** at 350 nm is 0.62 and 0.59, respectively, from which it is calculated that 76 and

74 % of the incident irradiation is absorbed. The reflection by the ITO was measured to be ~ 20 % at 350 nm, thus IQEs were estimated to be 2 and 19 % for **PFPhPy** and **PFIr25**, respectively, indicating that the conversion of photons absorbed to electrons produced increased by almost a factor of 10.
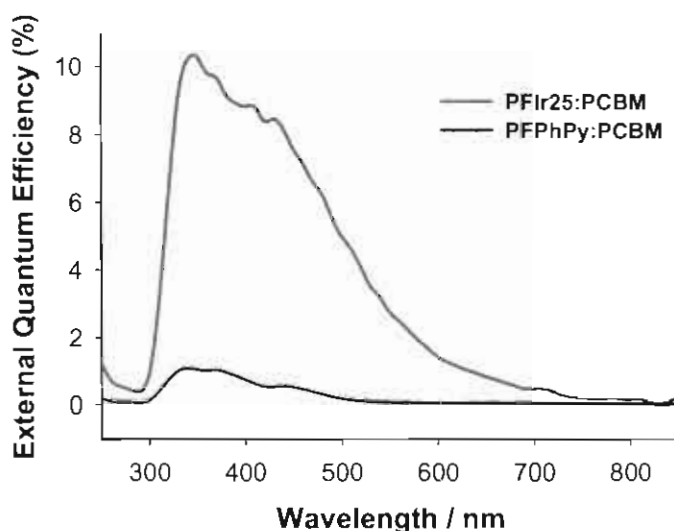
Figure 3.12: External quantum efficiency (EQE) of PFIr25:PCBM (1:4) and PFPhPy:PCBM (1:4) versus wavelength. Device configuration: ITO| PEDOT:PSS| Polymer:PCBM| Al.

3.4 Conclusion

Suzuki polycondensation was used to synthesize two polyfluorene derivatives, one with and without bound iridium complexes. It was found that incorporation of iridium into the **PFPhPy** backbone led to minor changes in the absorption spectrum. The fluorescence intensity decreased significantly upon incorporation of iridium and phosphorescence was observed at ~ 600 nm. Blending of **PFIr25** with the electron acceptor (PCBM) resulted in quenching of all the photoluminescence and was attributed to electron transfer from the polymer to the PCBM. Cyclic voltammetry revealed the HOMO energy levels to be similar, 5.73 and 5.68 eV for **PFPhPy** and **PFIr25**, respectively, which resulted in similar open circuit potentials.

85

This work demonstrates that introducing triplet forming Ir complexes into a polyfluorene-based polymer blended with an electron acceptor considerably enhances photovoltaic conversion efficiencies, as evidenced by an increase in external quantum efficiency from 1.1 to 10.3 % and an increase in internal quantum efficiencies from 2 to 20 %. The improved performance of **PFIr25** over **PFPhPy** is believed due to the formation of the triplet state, and by inference, the longer diffusion length of the triplet exciton, compared to the singlet exciton formed in **PFPhPy**. Power conversion efficiencies are lower than many polymer:PCBM systems based on singlet exciton charge generation, but this is in part due to the unfavorable absorption cross-section of **PFIr25**. Further improvements in conversion efficiencies are expected upon optimizing the iridium content in the system, and choosing a main chain that possess an absorption spectrum that overlaps more fully with the solar spectrum. Furthermore, in contrast to highly phosphorescent polymers of similar structure, designed for LED applications, the triplet energy level of the conjugated polymer is deemed to be of less significance in the design of such polymers for PVs.

CHAPTER 4: RED-SHIFTING THE ABSORPTION SPECTRUM OF IRIDIUM-BOUND CONJUGATED POLYMERS FOR PHOTOVOLTAIC APPLICATIONS

4.1 Introduction

As described in the introduction to Chapter 3, triplet excited states possess inherently longer lifetimes relative to singlet excited states and triplet excitons are expected to possess longer diffusion lengths, thereby increasing the percentage of excitons that reach a donor/acceptor interface, *i.e.*, increasing the efficiency of charge generation. As part of the body of work on triplet-forming materials for PV devices, Köhler *et al.*[105] describe the photophysics of an organometallic polymer, Pt-poly-yne blended with C_{60}, reporting that electron transfer occurs from the Pt-poly-yne to C_{60} *via* triplet excitons. PV devices give external quantum efficiencies (EQE) up to 1.6 % under monochromatic illumination. Shao *et al.*[106] report the performance of a bilayer device using 2,3,7,8,12,13,17,18-octaethyl-21H,23H-phorphineplatinum(II) (PtOEP) and C_{60} as the electron donor and acceptor, respectively. They report power conversion efficiencies (PCE) of 1.2 %. Guo *et al.* report that photoinduced charge transfer from Pt-acetylide to C_{60} occurs *via* the triplet excited state (EQE = 9 %, PCE = 0.27 %),[107] as does photoinduced charge transfer in Pt acetylide triads end-capped with fullerene (EQE = 22 %, PCE = 0.05 %).[44] Yang *et al.* studied poly(fluorene) (PF) and poly(thiophene) (P3HT) blended with molecular Ir(mppy)$_3$ using CdSe as an acceptor,[108] and demonstrate an increase in the triplet exciton population, attributed to the increased rate of intersystem crossing (ISC) from the PF singlet state to the triplet state. The short-circuit photocurrent subsequently doubled and the open circuit voltage (Voc) increased by 50 % upon addition of the phosphor. It was shown in Chapter 3 that tethering an Ir complex onto the main chain of a conjugated polymer (**PFIr25**) results in increased charge

generation in photovoltaic devices, as by the increase in EQE from 1.1 to 10.3 %, i.e., by a factor of 10.
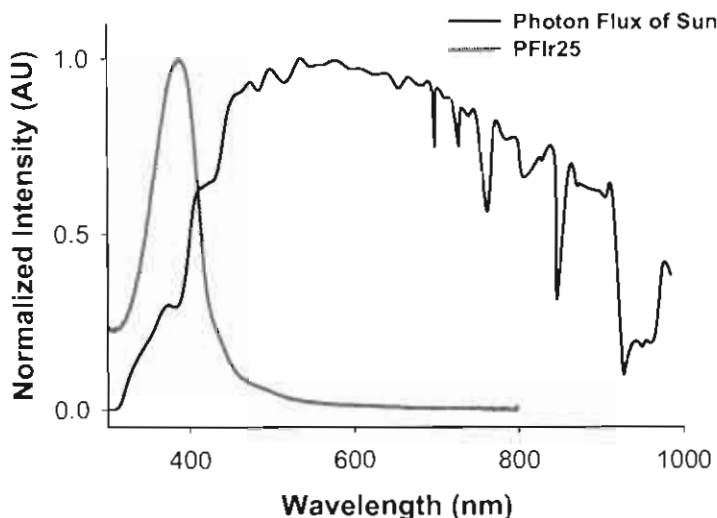
Figure 4.1: Absorption profile of PFIr25 and the solar spectrum.

Figure 4.1 compares the absorption profile of **PFIr25** with the photon flux of the sun. The poor photovoltaic performance of **PFIr25** described in Chapter 3, was in part attributed to the poor spectral overlap shown in Figure 4.1. A solution to this dilemma may be found by red-shifting the absorption of the iridium containing polymers. To this end, the synthesis of two different conjugated polymers was proposed; **PTIr** and **F8T2Ir**.

Poly(alkylthiophene)s, most commonly poly(3-hexylthiophene) (P3HT) have been extensively studied in organic photovoltaics (PV).[113] State-of-the-art devices have been made from blends of P3HT and [6,6]-phenyl C_{61} butyric acid methyl ester (PCBM) (1:0.8 wt. ratio), producing devices with power conversion efficiencies (PCEs) > 5 % and external quantum efficiencies (EQEs) > 80 %. The high efficiencies observed in these devices are attributed to the hole transporting ability of P3HT which results from its semi-crystalline morphology and the nano-sized phase separation of P3HT and PCBM.[47] **PTIr** was modeled after the extensively studied P3HT. The synthesis of **PTIr** using Suzuki polycondensation was unsuccessful (structure shown in Figure 4.2) and is

described in Appendix B. As a result, an alternative polymer, also shown in Figure 4.2, poly(fluorene-co-bithiophene-co-iridium), **F8T2Ir** was investigated.

PTIr

PFIr25

F8T2Ir
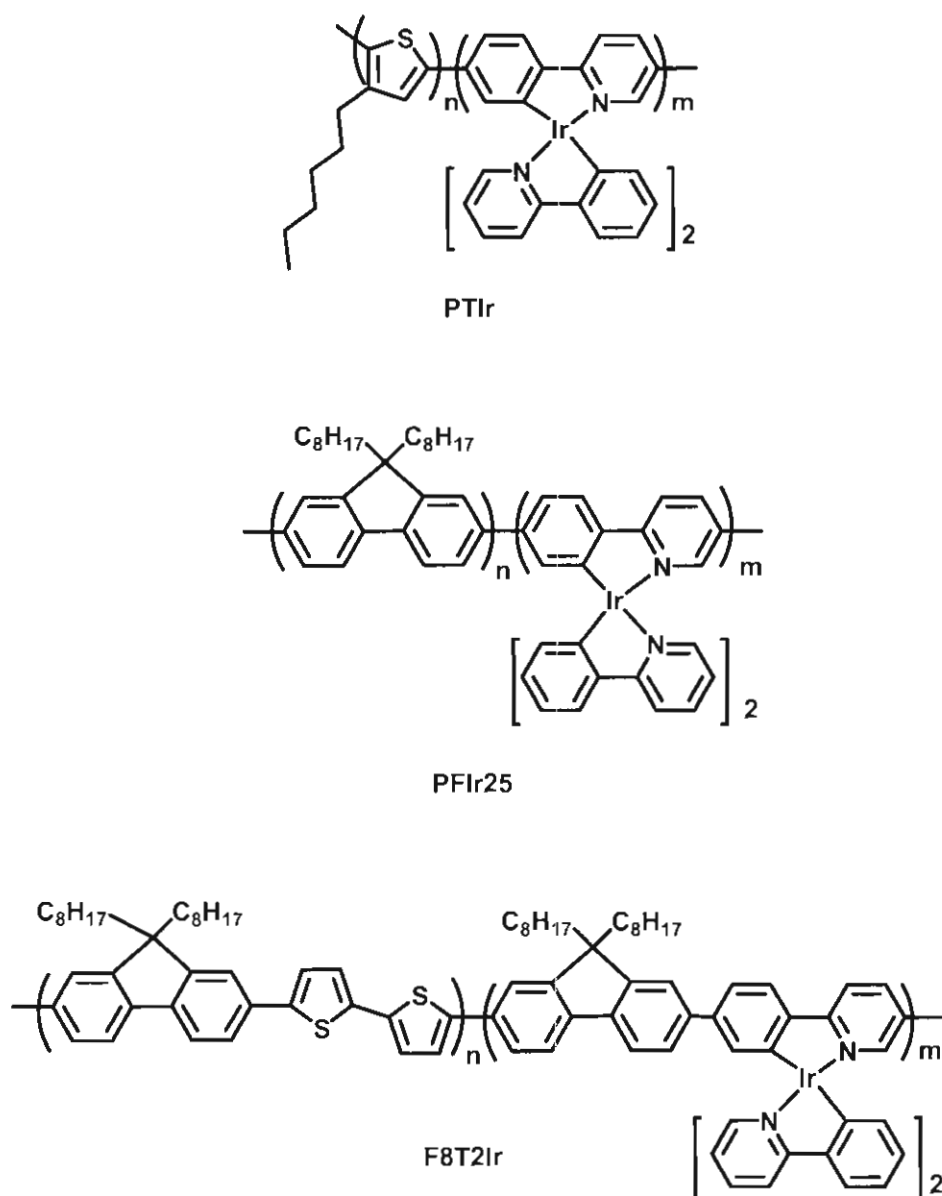
Figure 4.2: Proposed structures for Ir bound CPs, including PFIr25.

The non-iridium containing poly(fluorene-alt-bithiophene), **F8T2**, has been extensively studied in field effect transistors (FETs) due to its high charge mobility[114, 115] and has shown initial promise in hybrid photovoltaic devices. For example, Nelson and Durrant studied **F8T2** with TiO_2 as the electron acceptor,

they obtained PCEs of 0.2 %[116] and EQEs of 13 %[117] and demonstrated that photovoltaic performance was primarily limited by the rate of photogeneration and quality of the donor/acceptor interfaces rather than by hole transport in the polymer.

This chapter describes the Suzuki polycondensation of a series of fluorene, bithiophene and iridium containing polymers to investigate the effect of red shifting the absorption of the polymer backbone, which will improve the spectral overlap. This was expected to result in increasing the number of absorbed photons, thereby increasing the overall photovoltaic performance. The effect of varying the iridium content from 0 to 40 mol % in the polymer was investigated in an attempt to determine a correlation between PV performance and iridium content. The properties of the polymers are studied using UV-vis absorption and photoluminescence spectroscopy, gel permeation chromatography, cyclic voltammetry and with photovoltaic devices.

4.2 Experimental

4.2.1 Materials

2,5-dibromopyridine, 4-bromophenylboronic acid, phenyl boronic acid, 2,5-dibromobenzene, 2-phenylpyridine, 9,9-dioctyllfluorene-2,7-bis(trimethyleneborate), 5,5'-dibromo-2,2'-bithiophene, tetrakis(triphenylphosphine)palladium (Pd(PPh3)4), iridium (III) chloride trihydrate, iridium (III) acetylacetonate were purchased from either Sigma-Aldrich Co or Strem Chemicals, Inc. THF, ether and chlorobenzene were dried and freshly distilled before use. Poly(styrene sulfonic acid)-doped poly(ethylenedioxythiophene) (PEDOT:PSS, Baytron VP AI 4063) was purchased from Bayer Corp. PCBM was purchased from American Dye Source, Inc. Indium tin oxide (ITO) coated glass was purchased from Merck Display Technologies Ltd.

[(ppy)₂IrCl]₂ and (ppy)₂Ir(BrPhPyBr) were synthesized according to a previously published procedure and described in Chapter 3.[37]

5-Bromo-2-(4-bromophenyl)pyridine) was synthesized according to the published procedure and described in Chapter 3.[110]

Poly(9,9-dioctylfluorene-alt-2,2'-bithiophene) (F8T2) was synthesized *via* Suzuki polycondensation according to Figure 4.3.[87] 9,9-Dioctylfluorene-2,7-bis(trimethyleneborate) (0.419 g, 0.75 mmol) and 5,5'-dibromo-2,2'-bithiophene (0.243, 0.75 mmol) were dissolve in THF (12.5 mL, deoxygenated); to which, a solution of K_2CO_3 (2 M, 2 mL) was added, together with $Pd(PPh_3)_4$ (0.026 g, 3 mol % based on fluorene). The resulting mixture was sealed in a round bottom and heated for 48 hours at 80°C in an oil bath. End capping of the polymer was carried out as the last step in synthesis. Phenyl boronic acid (0.009g, 10 mol %) was added and the solution was heated (80°C, 12 h). This was followed by the addition of bromobenzene (0.024 g, 15 mol %), for 12 hours at the same temperature. Once cooled to room temperature, THF was removed and the residue dissolved in chloroform. This was followed by washing with water (3 times) and drying over $MgSO_4$. After filtration, the volume of chloroform was reduced and the concentrated solution was passed through an alumina column. The volume of the resulting solution was again reduced and precipitated in methanol (~300 mL) to yield 0.28 g **F8T2**. Soxhlet extraction was performed using methanol and hexanes. A weight average molecular weight (M_w) of 50 800 Daltons and a PDI of 1.7 was obtained. δ_H (500 MHz, CD_2Cl_2, Me_4Si) 7.74-7.38 (10 H, m), 2.08 (4 H, br. β-CH_2), 1.10 (20 H, br. CH_2), 0.80 (6 H, t CH_3), 0.71 (4 H, br., γ-CH_2). Anal. Calcd for $C_{37}H_{44}S_2$: C, 80.4; H, 8.0 %. Found: C, 80.2; H, 7.7 %.

General Procedure for the Synthesis of F8T2Ir10, F8T2Ir20 and F8T2Ir40 Using F8T2Ir10 as an Example. F8T2Ir10 was synthesized *via* Suzuki polycondensation according to Figure 4.3. 9,9-Dioctylfluorene-2,7-bis(trimethyleneborate) (0.279 g, 0.5 mmol) and 5,5'-dibromo-2,2'-bithiophene (0.129, 0.4 mmol) and (ppy)$_2$Ir(BrPhPyBr) (0.081 g, 0.1 mmol) were dissolve in THF (10 mL, deoxygenated); to which, a solution of K_2CO_3 (2 M, 2 mL) was added, together with $Pd(PPh_3)_4$ (0.017 g, 3 mol % based on fluorene). The resulting mixture was sealed in a round bottom flask and heated for 4 days at

80°C in an oil bath. End capping of the polymer was carried out as the last step in synthesis. Phenyl boronic acid (0.006 g, 10 mol %) was added and the solution was heated (80°C, 12 h). This was followed by the addition of bromobenzene (0.016 g, 15 mol %), at the same temperature. Once cooled to room temperature, THF was removed and the residue dissolved in chloroform. This was followed by washing with water (3 times) and drying over MgSO$_4$. After filtration, the volume of chloroform was reduced and the concentrated solution was passed through an alumina column. The volume of the resulting solution was again reduced and precipitated in methanol (~300 mL) to yield 0.165 g **F8T2Ir10**. Soxhlet extraction was performed using methanol, hexanes and acetone. A weight average molecular weight (M$_w$) of 18 900 Daltons and a PDI of 1.8 was obtained. δ$_H$ (500 MHz, CDCl$_3$, Me$_4$Si) 7.70-7.24 (11 H, m), 2.05 (4 H, br. β-CH$_2$), 1.08 (20 H, br. CH$_2$), 0.81 (6 H, t CH$_3$), 0.71 (4 H, br., γ-CH$_2$). δ$_C$ (150 MHz, CDCl$_3$, Me$_4$Si) 152.0, 144.0, 140.5, 136.7, 133.2, 129.0, 127.4, 124.7, 123.9, 120.3, 119.9 (aromatic) 55.5 (C$_9$-fluorene ring) 40.6, 32.0, 30.0, 29.4, 29.3, 24.0, 22.8, 14.3 (aliphatic). Anal. Calcd for **F8T2Ir10**: C, 78.6; H, 7.6; N, 0.8 %. Found: C, 78.4; H, 7.4; N, 1.3 %.

F8T2Ir20 was synthesized in the same manner as **F8T2Ir10** and according to Figure 4.3. A weight average molecular weight (M$_w$) of 8500 Daltons and a PDI of 1.4 was obtained. δ$_H$ (500 MHz, CDCl$_3$, Me$_4$Si) 8.25-6.60 (18 H, m), 2.05 (4 H, br. β-CH$_2$), 1.08 (20 H, br. CH$_2$), 0.81 (6 H, t CH$_3$), 0.71 (4 H, m, γ-CH$_2$). Anal. Calcd for **F8T2Ir20**: C, 76.8; H, 7.2; N, 1.6 %. Found: C, 76.7; H, 7.2; N, 2.0 %.

F8T2Ir40 was synthesized in the same manner as **F8T2Ir10** and according to Figure 4.3. A weight average molecular weight (M$_w$) of 7500 Daltons and a PDI of 1.3 was obtained. δ$_H$ (500 MHz, CDCl$_3$, Me$_4$Si) 8.25-6.60 (16 H, m), 1.92 (4 H, br. β-CH$_2$), 1.03 (10 H, br. CH$_2$), 0.73 – 0.6 (6 H, m, CH$_2$ and CH$_3$). Anal. Calcd for **F8T2Ir40**: C, 73.3; H, 6.4; N, 3.2 %. Found: C, 72.8; H, 7.0; N, 2.8 %.

4.2.2 Methods and Instrumentation

Chloroform (spectro-grade, Caledon Laboratories Ltd.) was used to prepare solutions (4 mg/mL) for film casting. Films were spin-cast on either quartz or glass slides at 1000 rpm for 60 s, shortly before acquisition of absorption and photoluminescence spectra. NMR spectroscopy was performed using a 500 MHz Varian Inova500 spectrometer or a 600 MHz Brucker Avance QNP cryoprobe spectrometer. Elemental analyses were performed using a Carlo Erba model 1106 C H N analyzer. Mass spectrometry was performed using a Voyager DE Perceptive biosystems MALDI Spectrometer. Ir content was determined using a Kristalloflex 2H X-ray fluorescence (XRF) spectrometer made by Siemens. Samples were excited with Mo X-rays, operated at 40 kV and 5 mA. A calibration curve was made using $Ir(acac)_3$ as a standard and yttrium as an internal standard. Samples were prepared by drop casting films on ultra thin mylar sheets. Molecular weight determinations were performed using gel permeation chromatography (Waters Model 1515 isocratic pump) calibrated against PS standards. Polymers were eluted with THF using a flow rate of 1 mL/min and monitored with a UV-vis detector (Waters 2487). Microwave synthesis was performed using an in-house modified Panasonic Inverter Microwave (model no NN-S614, see Appendix C). Absorption and fluorescence spectra were collected using Cary 3E and Photon Technology International (PTI) spectrophotometers, respectively. Quantum yield measurements were performed using an integrating sphere instrument from PTI. Time-resolved fluorescence measurements were made using a Horiba-JobinYvon Fluorolog spectrometer equipped with an IBH deterctor and electronics for time correlated single photon counting (TCSPC). Cyclic voltammograms were measured on polymer films drop cast on glassy carbon electrode (1.5 mm diameter). The electrolyte was dissolved in acetonitrile (0.1 M Bu4NClO4). Pt wire was used for the counter electrode. The reference electrode consisted of Pt wire in acetonitrile (0.1 M tetrabutylammonium iodine, 0.05 M I_2). Potentials were measured against ferrocene/ferrocenium redox couple using a PAR potentiostat/galvanostat 263A at a scan rate of 50 mV/s.

PV devices were prepared in the following manner: ITO was patterned by masking desired area with tape and immersion in concentrated HCl to remove the unprotected area, followed by sequential sonication in isopropyl alcohol, acetone, a mixture of H_2O, H_2O_2 and NH_4OH (5:1:1 vol. ratio), prior to rinsing with H_2O. PEDOT:PSS (Baytron VP AI 4083) was spin coated at 5000 rpm and annealed for 10 minutes at 140°C under air. Polymer:PCBM blends (1:4 wt. ratio, ~ 20 mg/mL) in chlorobenzene were spin coated at 700 rpm in a glovebox. Ca (25 nm) followed by AI (~ 70 nm) was thermally evaporated on the polymer surface at a pressure < $2x10^{-6}$ Torr. Current-voltage characteristics were measured using a Keithley source meter (model 2400). Polymer thicknesses were determined using a KLA Tencor Alpha-Step IQ surface profiler. The active area of all the devices were ~10 mm^2. I-V curves were obtained using a solar simulator, supplied by Newport, equipped with a 300 W Xenon lamp and a 1.5 AM filter with an irradiation intensity of 100 mW/cm^2.

4.3 Results and Discussion

4.3.1 Synthesis and Properties of F8T2Ir

Suzuki polycondensation was used to prepare a series of poly(fluorene-co-bithiophene)s with varying amounts of iridium incorporated into the polymer backbone, as shown in Figure 4.3. The feed ratios of iridium complexes to fluorene monomer in the polycondensation were 0, 10, 20 and 40 mol %; the corresponding polymers are termed **F8T2**, **F8T2Ir10**, **F8T2Ir20** and **F8T2Ir40**, respectively. X-ray fluorescence (XRF) spectroscopy determined the amount of Ir incorporated into the polymer and was found to be 0, 7, 21 and 30 mol %, respectively. ^{1}H NMR spectra were collected for all of the polymers. ^{13}C NMR were measured for novel polymers only, i.e., iridium containing. Examples spectra for **F8T2** and **F8T2Ir10** are shown in Appendix A. Peak assignments were done using the ^{1}H and ^{13}C NMR spectra of the monomers and polymer spectra from the literature. The weight average molecular weights were determined to be 50 800, 18 900, 8 500 and 7 500 Daltons with polydispersities

of 1.7, 1.8, 1.4 and 1.3 for **F8T2**, **F8T2Ir10**, **F8T2Ir20** and **F8T2Ir40**, respectively. The molecular weights of the polymers decreased with increasing iridium content, most likely due to the lower reactivity of the iridium containing monomer relative to the dibromobithiophene.
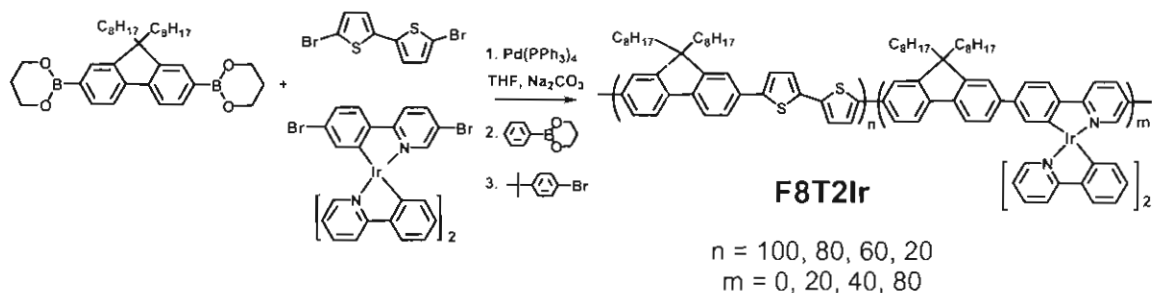
Figure 4.3: General reaction scheme for F8T2Ir.

Gel permeation chromatography (GPC) was used to estimate the molecular weight of the polymers. For polymers **F8T2Ir10 – F8T2Ir40**, the measurement was straight forward and mono-modal GPC traces were obtained. However, that was not the case for **F8T2**, Figure 4.4 shows the GPC trace for **F8T2** at various concentrations. The inset shows the trace of a dilute solution of **F8T2** in THF at a typical concentration for a conjugated polymer (~ 0.5 mg/mL). Under these conditions, a multi-modal peak is observed. It was found that upon sample dilution the intensity of the peak observed at ~ 20 min decreased relative to the peak at ~ 24 min. In GPC analysis, the faster the elution time, the higher the molecular weight of the polymer. It is reasoned that aggregates of polymers over-estimates the molecular weight, i.e., the onset of the peak is observed earlier than it should if it were a single molecule, as seen in Figure 4.4. This observation supports the hypothesis that **F8T2** forms aggregates.
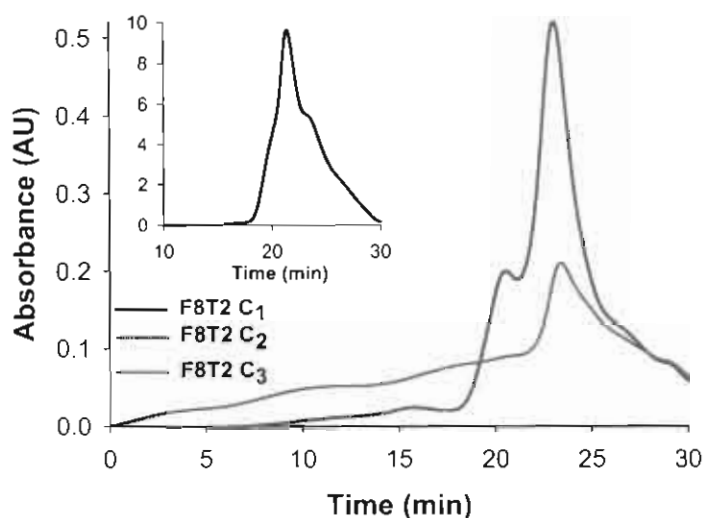
Figure 4.4: GPC traces for F8T2 for various sample concentrations, where $C_1 > C_2 > C_3$.

4.3.2 Absorption and Photoluminescent Properties of F8T2Ir

Absorption spectra of the polymers in THF and as films are shown in Figure 4.5, Figure 4.6, and summarized in Table 4.1. λ_{max} of absorption for **F8T2** is 457 and 459 nm, in the solution and solid state, respectively, which is red-shifted relative to polyfluorene (385 nm) due to incorporation of the bithiophene moiety, as a result of planarization of the polymer backbone. In general, the absorption and emission maximum is red-shifted in the solid state compared to in solution. Upon close examination of the absorption profile of **F8T2** in Figure 4.6, a well defined peak at 480 nm is visible. This peak could be attributed to aggregation in the polymer film.[118] Grell et. al. have induced aggregation in films of PFO which has resulted in red-shifting and the appearance of well-defined structure in the absorption spectrum. Increasing iridium content in the polymer results in blue shifting the λ_{max} of absorption from 443 to 427nm in solution and 457 to 423 nm in films, due to twisting of the polymer backbone. Increasing the Ir content also results in broadening of the absorption profiles and a loss of fine structure.

96
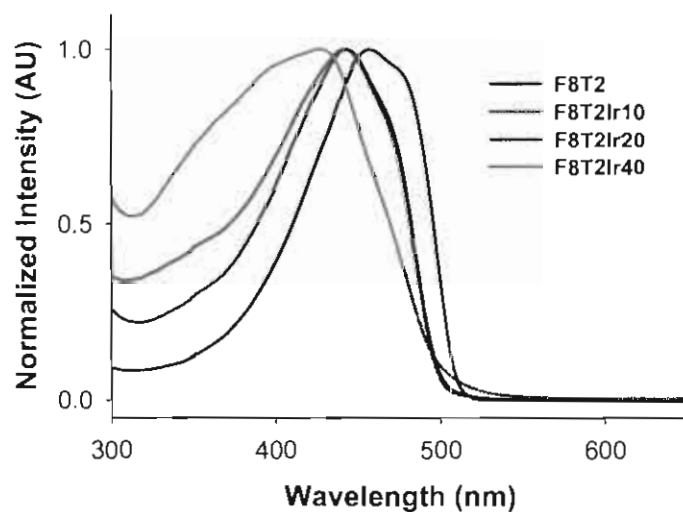
Figure 4.5: Absorption profile of F8T2, F8T2Ir10, F8T2Ir20 and F8T2Ir40 in THF.
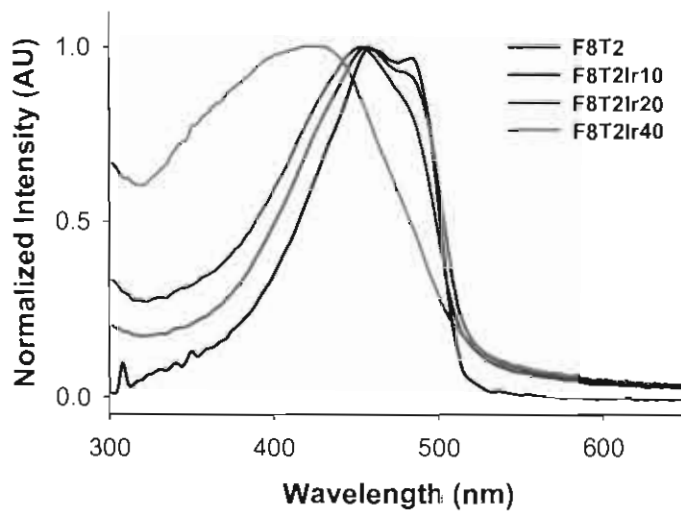
Figure 4.6: Absorption profile of films of F8T2, F8T2Ir10, F8T2Ir20 and F8T2Ir40.

Table 4.1: Optical properties of films of F8T2, F8T2Ir10, F8T2Ir20 and F8T2Ir40.

Polymers	Solution			Film		
	Absorption λ_{max} (nm)	Emission λ_{max} (nm)	Φ	Absorption λ_{max} (nm)	Emission λ_{max} (nm)	Φ
F8T2	457	502	0.55	459	506	0.08
F8T2Ir10	443	493	0.33	457	509	0.01
F8T2Ir20	443	493	0.26	453	537	0.01
F8T2Ir40	427	493	0.02	423	-	-
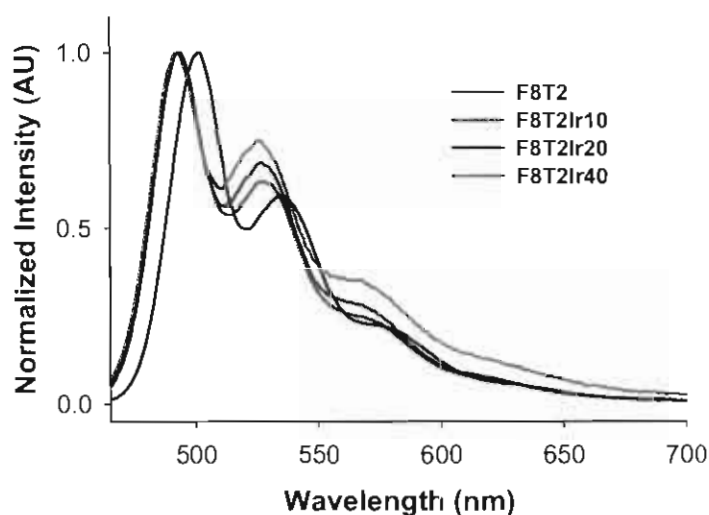
Figure 4.7: Photoluminescence of F8T2, F8T2Ir10, F8T2Ir20 and F8T2Ir40 in THF. λ_{ex}=450 nm.

Photoluminescence spectra of the polymers in THF and as films were obtained and are shown in Figure 4.7, Figure 4.9, and summarized in Table 4.1. The maximum fluorescence of **F8T2** is observed at 502 and 506 nm in solution and films, respectively, which is comparable to previously reported values.[119] The relative intensity of the emission from the vibronic transition of **F8T2Ir10** and **F8T2Ir20** vary with increasing iridium content, but the main difference in the spectrum, compared to that of **F8T2,** is the relative intensities of the emission. In general, the fluorescence intensity decreases with increasing iridium content, see

Figure 4.9. Films of **F8T2Ir40** display no observable fluorescence. Figure 4.8 depicts some of the possible processes that may occur upon excitation of **F8T2**. Energy transfer from poly(fluorene-alt-bithiophene) (**F8T2**) to the phosphorescent group, Ir(ppy)$_3$, is depicted as process (a). The triplet excited state may be quenched by the polymer backbone (b), by concentration quenching (c), or undergo phosphorescence (d). The absence of fluorescence from **F8T2Ir40** is thus attributed to complete energy transfer (process (a) in Figure 4.8) from the polymer main chain to the iridium complex.

Transient luminescence measurements of **F8T2** and **F8T2Ir10** in THF (see Figure 4.10) reveal the lifetime of the emission monitored at 540 nm to be 0.49 and 0.47 ns respectively, thus confirming that the emission seen in Figure 4.9 is due to fluorescence. Unfortunately it was not possible to obtain transient luminescence measurements of the polymers as films.

The absence of phosphorescence of the **F8T2Ir** polymers is attributed to quenching of the triplet state of the iridium complex by the triplet state of the polymer backbone (process (b) in Figure 4.8), analogous to the **PFPyIr** series presented in Chapter 2.
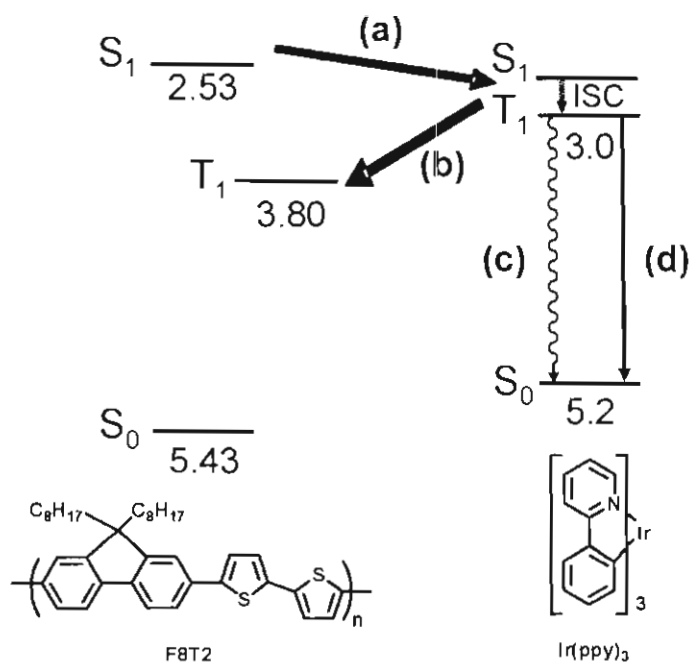
Figure 4.8: Energy level diagram showing (a) energy transfer from the F8T2 main chain to the bound Ir complex, (b) triplet quenching of the Ir complex by F8T2 main chain, (c) concentration quenching of the triplet state and (d) phosphorescence of the Ir complex.
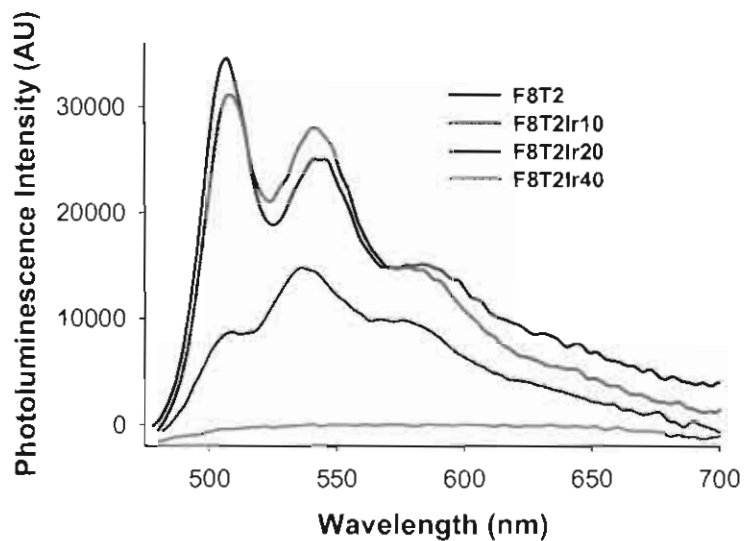
Figure 4.9: Photoluminescence of films of F8T2, F8T2Ir10, F8T2Ir20, F8T2Ir40. λ_{ex}=450 nm.
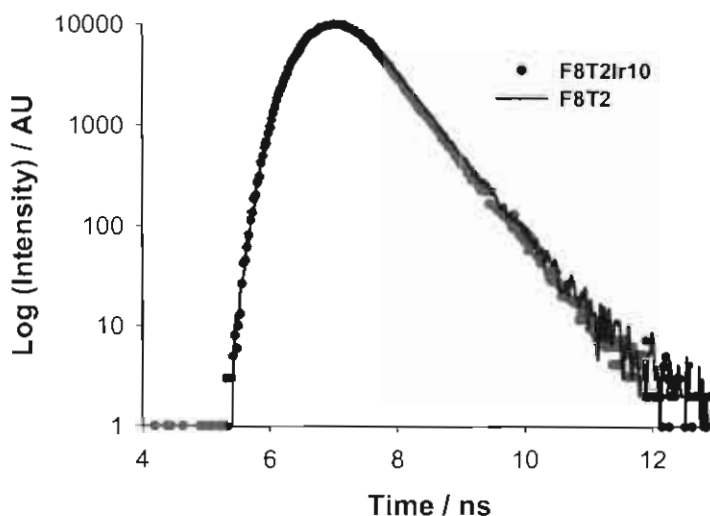
Figure 4.10: Transient luminescent decay of F8T2 and F8T2Ir10 in THF. λ_{ex} = 463 nm.

The quantum yield of fluorescence from **F8T2** was measured to be 0.55 and 0.08 in the solution and solid state, respectively, (Table 4.1) and is comparable to previously reported values.[119] Incorporation of iridium into the polymer main chain results in a decrease in quantum yield from 0.55 to 0.02 and 0.08 to 0, in the solution and solid state for **F8T2** through **F8T2Ir40**, respectively. The decrease of quantum yield s of **F8T2** upon incorporation of iridium could be explained by increased energy transfer from the **F8T2** backbone to the iridium complex with increasing iridium content (depicted as process (a) in Figure 4.8).[37]

Many reports in the literature have shown that very small amounts of a guest moiety in a conjugated polymer is required for efficient energy transfer in polymer films.[36] In addition, it was shown in Chapter 2 that when as little as 2 mole % of the guest (3,4-linked-thienyl moiety) was incorporated into the polymer, energy transfer was occurring.

Figure 4.11 shows the normalized absorption spectra of **F8T2Ir10** and **PFIr25**, the Ir-containing polymer described in Chapter 2, in comparison to the photon flux of the sun. The larger the spectral overlap between the polymer absorption and the solar irradiation, the more excitons can be produced in the PV device. As expected, poly(fluorene-co-bithiophene-co iridium) (**F8T2Ir10**) has a

broad absorption between 400 and 525 nm (λ_{max} = 457 nm) in the solid state, which is red-shifted relative to poly(fluorene-co-(2-phenylpyridine(iridium(III)))) (λ_{max} = 385 nm for **PFIr25** from Chapter 3). Since the red shift in the absorption spectrum of **F8T2Ir10** results in improved spectral overlap, it is expected based on the absorption spectra alone, that PV devices made from **F8T2Ir10** will generate more excitons and most likely have higher overall efficiencies, than those made from **PFIr25** from Chapter 2.
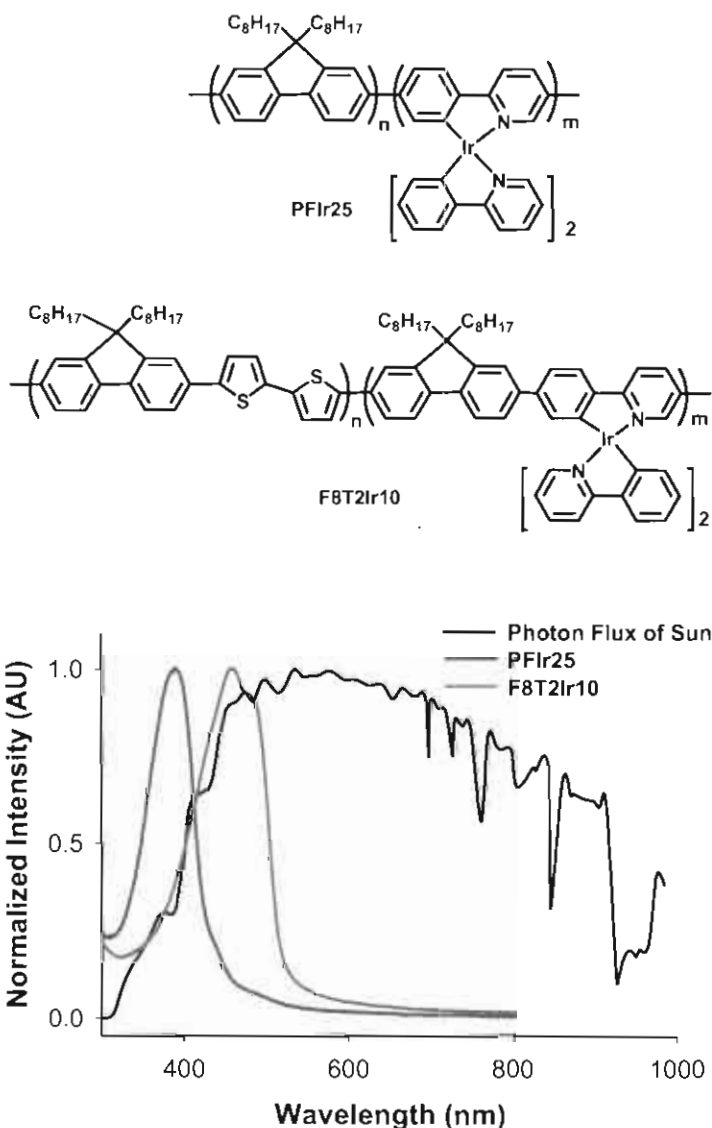
Figure 4.11: Absorption profile of PFIr25, F8T2Ir10 and photon flux of the sun.

102

4.3.3 Energy Levels of F8T2Ir

Electronic energy levels of the **F8T2Ir** series of polymers were estimated using the cyclic voltammograms shown in Figure 4.12. CVs of thin films deposited on a glassy-carbon working electrode were obtained and potentials were measured relative to the ferrocene/ferrocenium redox couple (see Table 4.2 and Figure 4.12), as described in section 1.4.2. Using the onset of the oxidation peaks for the p-doping process, the HOMO levels of **F8T2 – F8T2Ir40** were estimated to be 5.43, 5.39, 5.40 and 5.29 eV (+/- 0.05), respectively. Using the onset of the reduction peaks for the n-doping process, the LUMO levels of **F8T2 – F8T2Ir40** were estimated to be 2.53, 2.51, 2.59 and 2.72 eV (+/- 0.05), respectively. The HOMO level of F8T2 is higher than that of PF (5.5 eV) and lower than that of P3HT (5.0 eV). Incorporation of the iridium into the polymer increases the HOMO level from 5.43 to 5.29 eV and decreases the LUMO level from 2.53 to 2.72 eV. These values are approaching the HOMO and LUMO level of Ir(ppy)$_3$ which has been reported to be 5.2 and 3.0 eV, respectively.[93] The optical band gaps were also estimated using the onset of absorption profiles shown in Figure 4.6 and are tabulated in Table 4.2. The general trend seen in the magnitude of the electrochemical band gaps and the optical band gaps are the same but overall the optical band gaps are smaller. The band gap of the polymers is decreasing with increasing iridium content, due to the increase in the HOMO level and decrease of the LUMO level of the polymers with increasing iridium content. Therefore, since the open circuit potentials (V_{oc}) of the PV devices is related to the energy difference between the HOMO of the donor (polymer) and the LUMO of the acceptor (PCBM), the Voc is expected to decrease with increasing iridium content. This will be discussed in the following section.
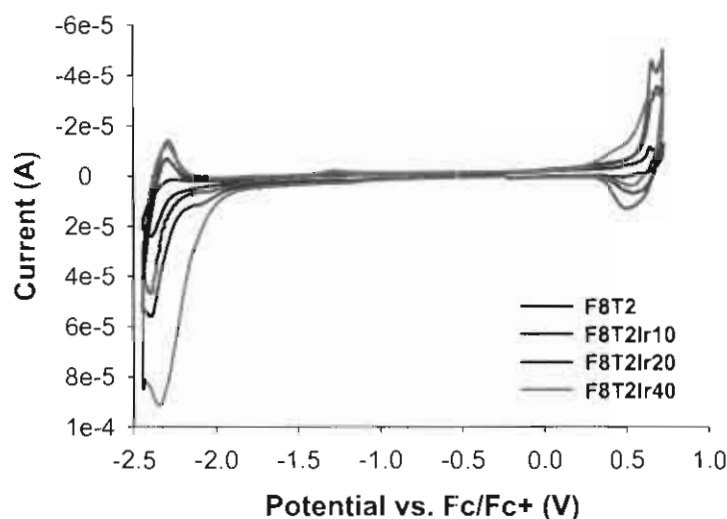
Figure 4.12: Cyclic voltammagrams of films of F8T2, F8T2Ir10, F8T2Ir20, F8T2Ir40. Scans recorded at 50 mV/s in 0.1 M Bu$_4$NClO$_4$ in acetonitrile.

Table 4.2: Energy levels of films of F8T2, F8T2Ir10, F8T2Ir20, F8T2Ir40.

	HOMO (eV)	LUMO (eV)	E_g(eV, Echem)	E_g(eV, UV)
F8T2	-5.43	-2.53	2.90	2.43
F8T2Ir10	-5.39	-2.51	2.88	2.40
F8T2Ir20	-5.40	-2.59	2.81	2.39
F8T2Ir40	-5.29	-2.72	2.57	2.38
Ir(ppy)$_3$	5.2	3.0	-	-

Figure 4.13 demonstrates representative processes that may occur upon excitation of a **F8T2Ir** polymer in the presence of PCBM. Energy transfer from poly(fluorene-alt-bithiophene) (**F8T2**) to the phosphorescent group, Ir(ppy)$_3$, is depicted as process (a). The triplet excited state may be quenched by the polymer backbone (b), by concentration quenching (c), by phosphorescence (d), or by electron transfer to PCBM (e), the latter being essential for PV activity. The relative rates of these photophysical processes determine the fate of the triplet state. For an analogous system, polyspirobifluorene and a substituted derivative

104

of Ir(ppy)$_3$, the rate of (b) occurs within ~ 10 ns.[112] Rates of photoelectron transfer (process (e)) typically occur in the ps time domain,[44] i.e., three orders of magnitude faster. It is thus believed that self-quenching of the Ir(ppy)$_3$ triplet state in **F8T2Ir10** by the main chain is unlikely to compete with electron transfer, if the triplet exciton can reach an electron acceptor site. Therefore, in contrast to highly phosphorescent polymers of similar structure designed for LED applications, and similar to the system presented in Chapter 2, the triplet energy level of the conjugated polymer is deemed to be of less significance in the design of such polymers.
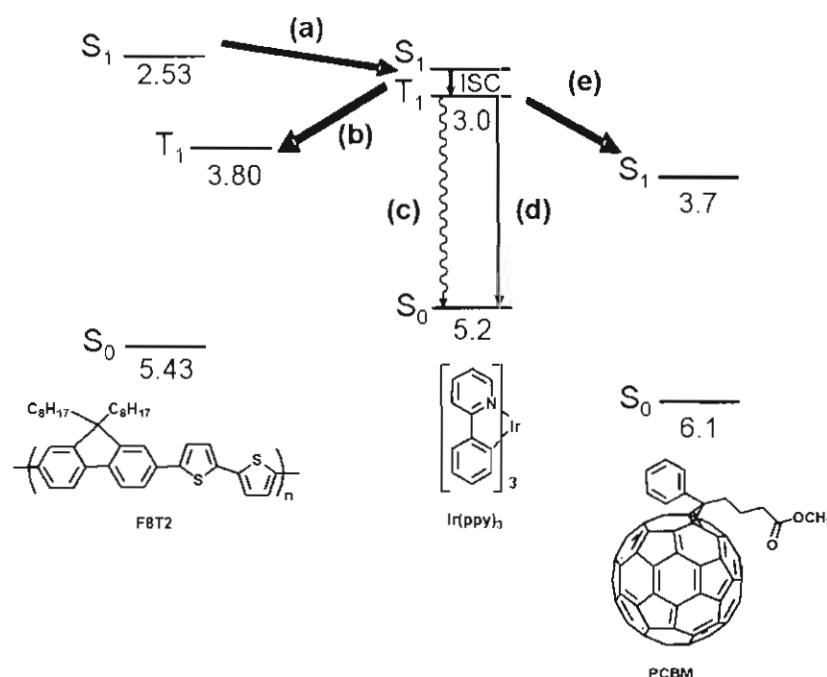
Figure 4.13: **Energy level diagram showing (a) energy transfer from the F8T2 main chain to the bound Ir complex, (b) triplet quenching of the Ir complex by the F8T2 main chain, (c) concentration quenching of the triplet state, (d) phosphorescence of the Ir complex and (e) photo-induced electron transfer (PET) from the Ir complex to PCBM.**

4.3.4 Photovoltaic Devices using F8T2Ir

In order to investigate the effect of the iridium complexes in the polymer on charge generation and to examine the effect of triplet exciton formation, photovoltaic devices were fabricated using the following device configuration: ITO|PEDOT:PSS| **Polymer**:PCBM (1:4)| Ca| Al. It is presumed that triplet

excitons are formed on the iridium complexes, despite the lack of phosphorescence observed in the photoluminecent measurements, because fluorescence is quenched. This is discussed further in section 4.3.2. When the polymer is blended with PCBM and operating in the PV device, it is expected that electron transfer will occur on a faster time scale than back energy transfer from the Ir complex to the triplet state of the polymer, as described in section 4.3.3, as long as the triplet exciton can reach the donor-acceptor interface. The I-V plot and photovoltaic properties are shown in Figure 4.14 and summarized in Table 4.3. The short-circuit current density (Jsc) was found to decrease an order of magnitude from 3.94 (for **F8T2**) to 0.35 mA/cm^2, with increasing the iridium content from 0 to 40 mol %. Similarly, the fill factor (FF) decreased from 0.51 to 0.26 and the open circuit potential (V_{OC}) decreased from 0.94 to 0.59 V. The reduction in the J_{SC}, the V_{OC} and the FF resulted in the reduction in the power conversion efficiency (PCE) from 1.9 to 0.05 % upon increasing iridium content from 0 to 40 mol %.
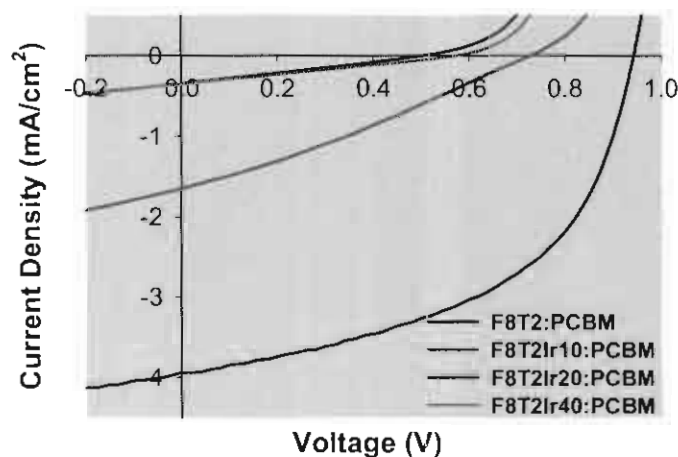
Figure 4.14: I-V curves obtained from Polymer:PCBM (1:4) solar cells under AM 1.5 illumination (100 mW/cm^2). Device configuration: ITO|PEDOT:PSS| Polymer:PCBM| Ca| Al.

Table 4.3: Summary of device performance data plotted in Figure 4.14.

	Voc (V)	Jsc (mA/cm^2)	FF	PCE (%)	EQE (%)*	IQE (%)
F8T2:PCBM	0.94	3.94	0.51	1.9	24	43
F8T2Ir10:PCBM	0.73	1.65	0.29	0.35	17	33
F8T2Ir20:PCBM	0.55	0.35	0.26	0.05	3	6
F8T2Ir40:PCBM	0.59	0.35	0.26	0.05	4	9

* reported at 455 nm
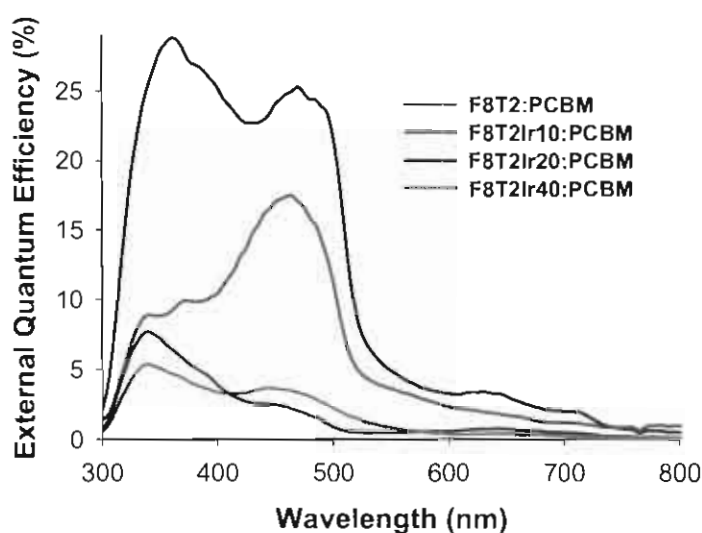
Figure 4.15: External quantum efficiency (EQE) of Polymer:PCBM (1:4) versus wavelength. Device configuration: ITO| PEDOT:PSS| Polymer:PCBM| Ca| Al.

External quantum efficiencies (EQEs), shown in Figure 4.15 and tabulated in Table 4.3, clearly show the absorption by the polymer at ~ 450 nm and that of the PCBM at ~ 330 nm. **F8T2** blended with PCBM (1:4 wt. ratio) resulted in a EQE of 24 % at the λ_{max} of absorption (455nm). With increasing Ir content from 10 to 40 mol % the EQE at 455 nm decreased from 17 to 3 %. The EQE is calculated using the short circuit current (I_{SC}, see equation 1.15 in section 1.4.5) and the J_{SC} was found to decrease with increasing iridium content from 0 to 40 mol %, therefore the EQE also decreased with increasing iridium content.

An approximation of the internal quantum efficiency (IQE), i.e., the conversion efficiency of photons absorbed to current produced, was obtained by dividing the EQE by the light absorbed in the device. The absorption of of **F8T2** – **F8T2Ir40** at 455 nm is 0.51, 0.35, 0.37 and 0.32, respectively, from which it is calculated that 65, 55, 57 and 52 % of the incident irradiation is absorbed. The reflection by the ITO was measured to be ~ 20 % at 455 nm. IQEs were estimated to be 43, 33, 6 and 9 % for **F8T2**, **F8T2Ir10**, **F8T2Ir20**, and **F8T2Ir40**, respectively. These results parallel the I-V characteristics, in that the trend observed in the obtained J_{SC} are reflected in the calculated values of the EQE and IQEs.

A possible explanation for this reduction in photovoltaic performance could be that incorporation of iridium into the polymer main chain distorts the backbone (indicated in the blue-shifting of the absorption maximum, shown in Figure 4.6) to such an extent that holes cannot be transported efficiently to the electrodes. The lower fill factors for **F8T2Ir10-40**, shown in Table 4.3, were 0.29-0.26 relative to 0.51 for **F8T2**, indicate that the PV devices are indeed limited by charge mobility. Further investigation into the transport properties of the polymer is necessary to investigate this particular effect.

4.4 Conclusion

Two approaches to synthesize iridium-bound conjugated polymers with red-shifted absorption relative to the iridium-bound polyfluorene reported in Chapter 3 were investigated. A series of fluorene-alt-bithiophene polymers were prepared containing 0 to 40 mol % iridium bound to the polymer main chain *via* Suzuki polycondensation. It was found that incorporation of iridium into the **F8T2** polymer led to a blue-shift in absorption from 459 to 423 nm. The fluorescence intensity decreased with increasing iridium content, which was illustrated in the decreased quantum yield. Back energy transfer from the triplet state of the iridium complex to the triplet state of the polymer explains the lack of observed phosphorescence. Cyclic voltammetry revealed an decrease in the HOMO energy levels with increasing iridium content from 5.43 to 5.29 eV, explaining in

part, the decrease of the Voc from 0.94 to 0.55 V. Short circuit current densities, fill factors and open circuit potentials all decreased with increasing iridium content. This resulted in an overall decrease in power conversion efficiency from 1.9 to 0.05 % and a decrease in external quantum efficiency from 24 to 3 %. The decrease in photovoltaic performance is attributed to a combination of the following: a blue-shift in polymer absorption and poor charge transport. Although incorporation of iridium complexes into the **F8T2** polymer backbone has resulted in decreased photovoltaic performance, it remains unclear whether this is due to the lack of formation of triplet excitons or simply a change in polymer transport properties. Further investigation into the exciton transport, hole transport and polymer:PCBM blend morphology is necessary to address these questions.

CHAPTER 5: THESIS SUMMARY AND FUTURE WORK

5.1 Summary

Chapter 2 presents the synthesis of conjugated fluorene-alt-pyridine and fluorene-alt-thiophene polymers containing phosphorescent iridium complexes. Exchanging the 2,5-linked pyridine group with the 3,4-linked thiophene group resulted in a blue shift in the absorption and emission spectra of the conjugated polymers. Upon incorporation of the thienyl unit, phosphorescent quantum yields of films increased from 0.05 to 0.20 and electrophosphorescent external quantum efficiencies increased from 0.32 to 0.84%. These results are attributed to raising the triplet energy of the main chain polymer, with respect to the Ir phosphor, thereby reducing triplet quenching of the phosphor by the main chain. In general, attaching phosphorescent groups to conjugated polymers have shown better device stability at higher current densities, however device efficiencies for polymers of this class are still lower than devices made using "small molecule" host-guest blend systems.[35]

The aim of the work presented in Chapter 3 is to investigate the effect of incorporating an iridium complex into a conjugated polymer backbone on photovoltaic properties such as charge generation, power conversion efficiency and external quantum efficiency. Poly(9,9-dihexylfluorene-co-2-phenylpyridine) (**PFPhPy**) and poly(9,9-dioctylfluorene-co-tris(2-phenylpyridine) iridium (III))) (**PFIr25**) were synthesized using Suzuki polycondensation. An increase in percent EQE for **PFIr25** over **PFPhPy**, from 1.1 to 10.3, is attributed to the formation of the triplet state in **PFIr25**, and by inference, longer diffusion lengths of the triplet exciton, compared to the singlet exciton that is formed in **PFPhPy**. Furthermore, in contrast to highly phosphorescent polymers of similar structure, designed for LED applications, like those presented in Chapter 2, the triplet

energy level of the conjugated polymer is deemed to be of less significance in the design of polymers for PVs.

Chapter 4 investigates two methods to red-shift the absorption spectrum of the polymers relative to **PFIr25**. A series of fluorene-alt-bithiophene polymers were prepared containing varying amounts of iridium bound to the polymer main chain *via* Suzuki polycondensation. It was found that incorporation of iridium into the **F8T2** polymer led to a blue-shift in absorption from 459 to 423 nm, decreased fluorescence intensity with no observed phosphorescence. Cyclic voltammetry revealed an increase in the HOMO energy levels with increasing iridium content from 5.43 to 5.29 eV, explaining in part, the decrease of the Voc from 0.94 to 0.55 V. Overall, the photovoltaic performance decreased with increasing iridium content from 1.9 to 0.05 %, possibly due to a combination of the following: the blue-shift in absorption and poor charge transport. This work has been successful, in that, the absorption of the **F8T2Ir** polymers were red shifted with respect to **PFIr25**. However, there was no observed increase in photon to electron conversion because other factors inherent to the polymer structure, dominated.

5.2 New Directions

5.2.1 Triplet polymers

The impact of incorporating triplet materials in PV devices still remains unclear from the work presented in chapters 3 and 4. In order to prove the underlying principle on which this study was based, it is necessary to consider more than the presence of a phosphorescent moiety. It was hoped that by comparing an iridium-containing and a non-iridium-containing polymer, the effect of increasing the lifetime of the exciton, i.e., extending the diffusion length, would increase the charge generation and in turn, the conversion of photons to electrons. However, despite the formation of triplet excitons in **PFIr25** and **F8T2Ir**, there was not always a correlation between their presence and increased charge generation. The iridium complex has an octahedral geometry and

incorporation of one of its ligands into the polymer backbone induces twisting in the main chain, as evidenced by the blue-shifting of the polymer absorption profile with increasing iridium content in the polymer (see Figure 4.6). In order to isolate the effect of triplet formation, the polymer could be designed in such a way that the incorporation of the phosphorescent moiety does not significantly alter the geometry of the polymer nor its absorption profile. Figure 5.1 depicts the polymers studied in Chapter 4 (**F8T2**, **F8T2Ir**) and, a new polymer, **F8T2Co**, that would be of interest to study. In Chapter 4, **F8T2** was compared with **F8T2Ir** but it was unclear whether their differences in properties were a result of the formation of triplets or the change in polymer geometry induced by the iridium complex. Therefore, it is proposed that a polymer such as **F8T2Co** be synthesized, and its properties compared with **F8T2Ir**. When the iridium center is replaced with cobalt, the polymer is not expected to phosphoresce upon electronic excitation, yet it will retain its main chain geometry. **F8T2Co** would serve as a modified version of **F8T2**, i.e., a reference material that does not form triplet-excited states.
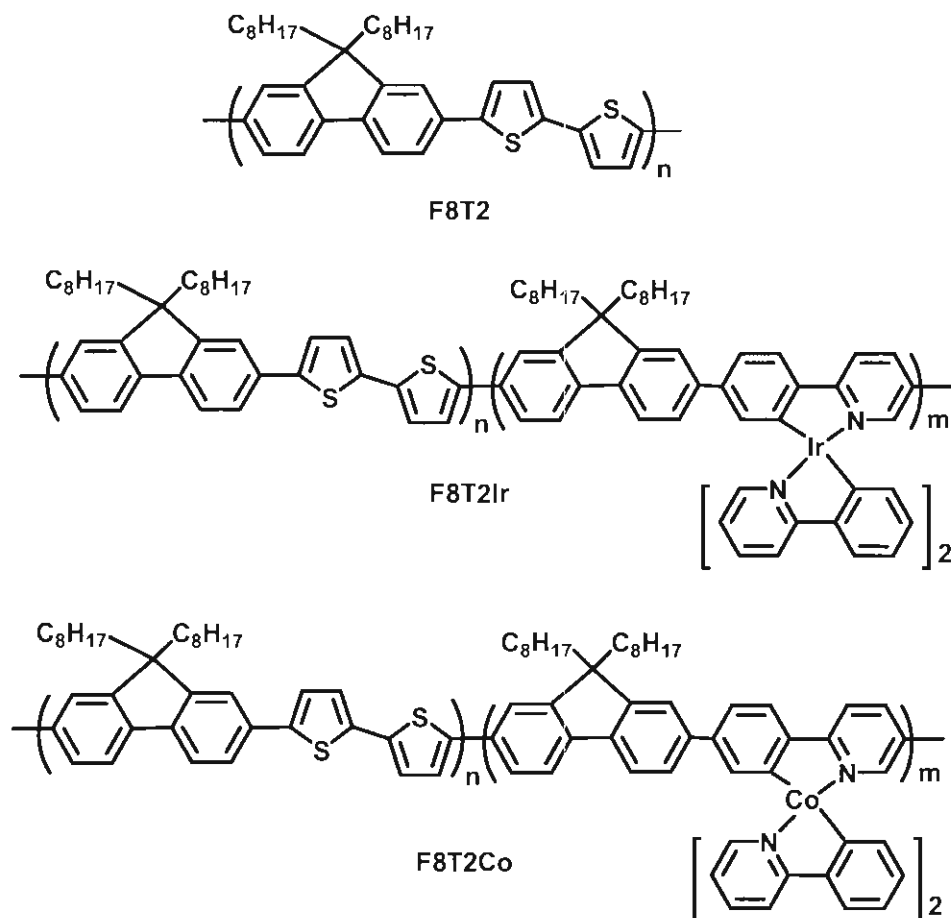
Figure 5.1 Structure of F8T2, F8T2Ir and a new polymer, F8T2Co.

The synthesis of the Co-containing polymer could be carried out using Suzuki polycondensation. The photophysical properties of the two polymers shown in Figure 5.1 can be examined in terms of their effect on photovoltaic performance in bilayer devices. One advantage of using a bilayer device structure is that it should allow for the estimation of the diffusion length of the excitons. This method of estimating triplet exciton diffusion lengths has been reported by Shao et. al. for bilayer devices of a Pt porphyrin complex.[106] Bilayer devices are different than bulk heterojunction devices in that the donor and acceptor form two distinct layers as shown in Figure 5.2.

113
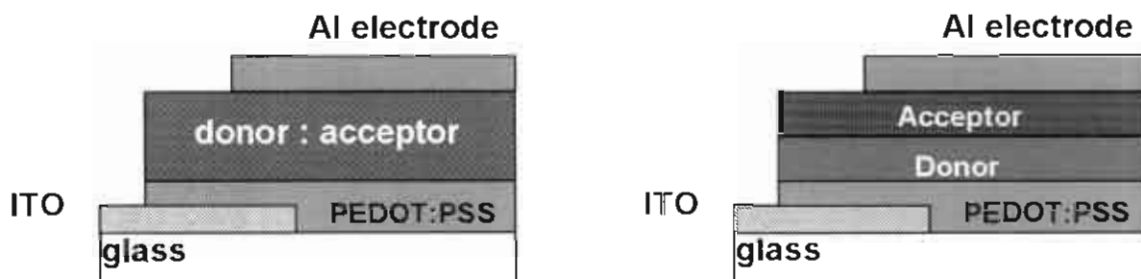
Figure 5.2: Bulk heterojunction (left) and bilayer PV device structure (right).

5.2.2 Poly(fluorene-alt-bithiophene)s

The efficiency of organic PV devices is often limited by poor overlap of the absorption spectrum and solar spectrum, and, because the charge transport properties of conjugated polymers are generally low, the active layers must be thin. In an attempt to overcome these limitations, tandem[120], stacked[121] or folded[122] photovoltaic devices are being investigated, wherein materials of different absorption profiles are combined in an attempt to capture light over a wider range of the solar spectrum.

Despite recent progress in low band gap polymers, there is still a need to capture higher energy light more efficiently, i.e., wavelengths between 300-500 nm. Recently, Tvingstedt et. al. reported the use of folded tandem solar cells, where single cells are reflecting the non-absorbed light onto the adjacent cell. The cells are configured in a V-shaped geometry and allow for the use of multiple band gap materials. Since materials with different band gaps can be employed, thinner absorbing layers can be used and charge mobility will increase. Using folded tandem solar cells, photoconversion efficiencies were found to increase by a factor of 1.8.[122] To date, only a few polymers have shown promise of high PCE/EQE in the 300-500 nm absorption region. Hou et al. reported a series of 2-dimensional polythiophenes with bi(thienylenevinylene) side chains that exhibit a broad absorption extending from 350-700 nm.[123] Within this series, the polymer with the strongest absorption between 350-500 nm yielded a PCE and EQE of 1.71 % and 80 %, respectively. Brabec et al reported a PCE of 3.3 % for films of

poly(2-methoxy-5-(3',7'-dimethyl-octyloxy))-*p*-phenylene vinylene (MDMO-PPV) blended with PCBM,[124] but absorption between 300-450 nm was minimal.

Although the incorporation of iridium into the fluorene-alt-bithiophene polymer resulted in decreased PV performance, poly(fluorene-alt-bithiophene) (**F8T2**) displayed quite promising power conversion efficiencies, i.e., ~ 2 %, when blended with PCBM (as shown in Chapter 4). **F8T2** can be considered a high band gap polymer because it absorbs light from 400-500 nm and could therefore be used in combination with medium and low band gap materials in tandem or folded photovoltaic devices. Recently, Bradley et al. have reported the effect of alkyl side chain length (octyl *vs*. 2-methylbutyl) of fluorene copolymers on hole mobilities, demonstrating shorter alkyl chains result in higher mobilities.[125] An analogous effect may be found with **F8T2** vs. F6T2 (the dihexyl analogue of **F8T2**). The synthesis of F6T2 could be easily performed using Suzuki polycondensation.

APPENDICES

Appendix A
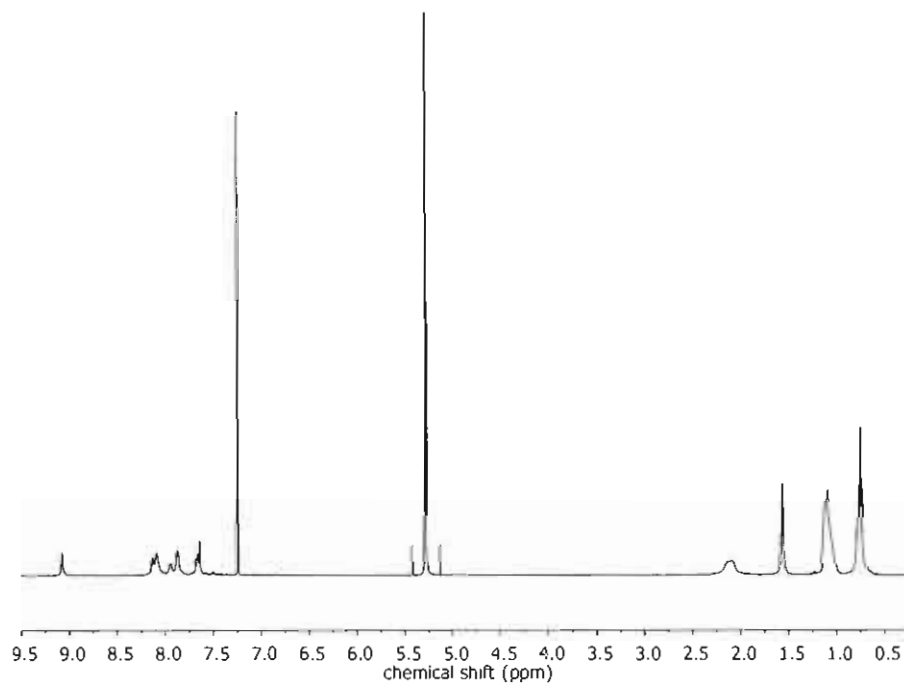
Figure A.1: ^{1}H NMR of PFPy in CD$_2$Cl$_2$.
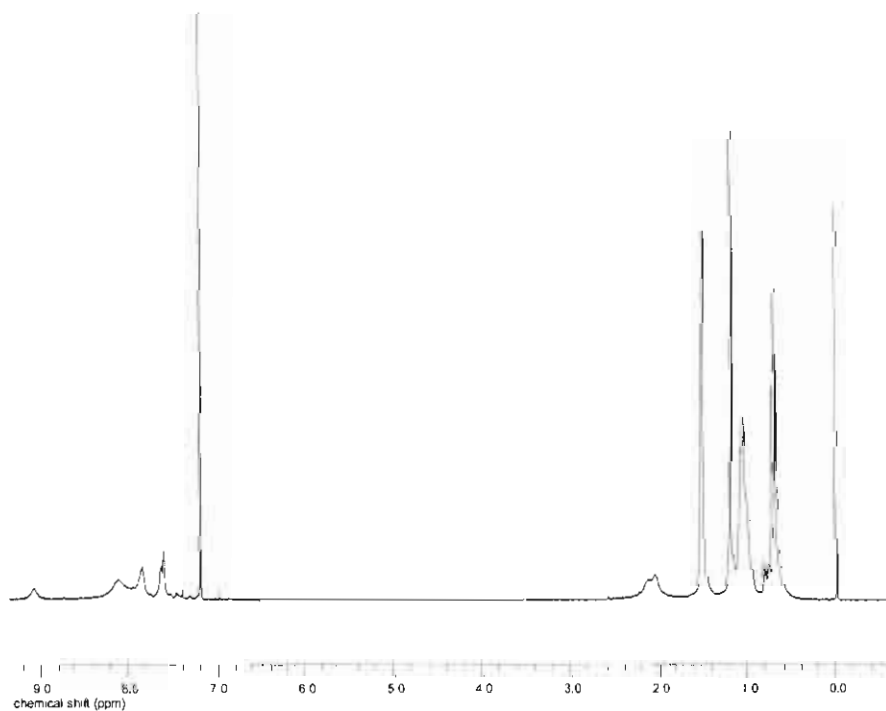
Figure A.2: ^{1}H NMR of PFPyIr15 in CDCl$_3$.
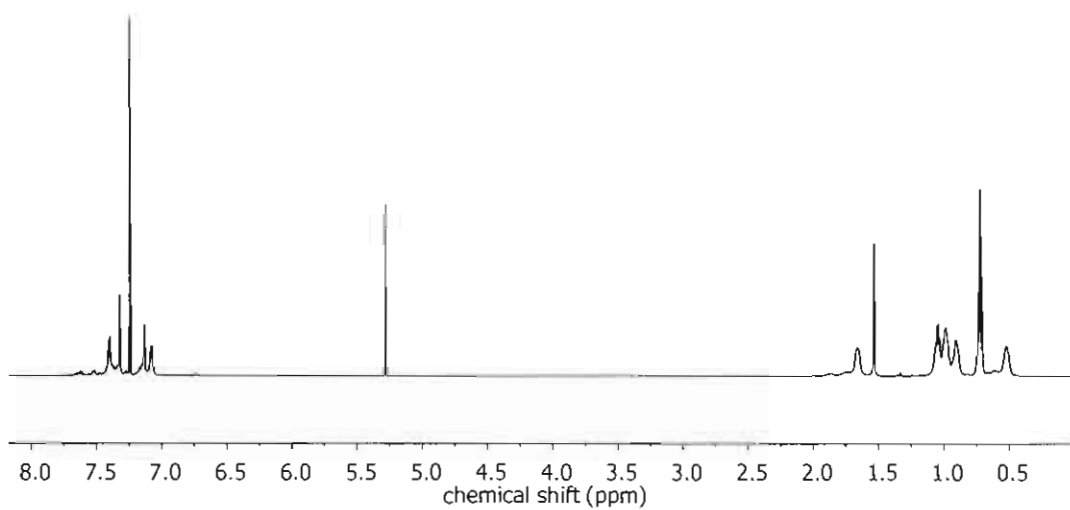
Figure A.3: ^{1}H NMR of PFT in CDCl$_3$.
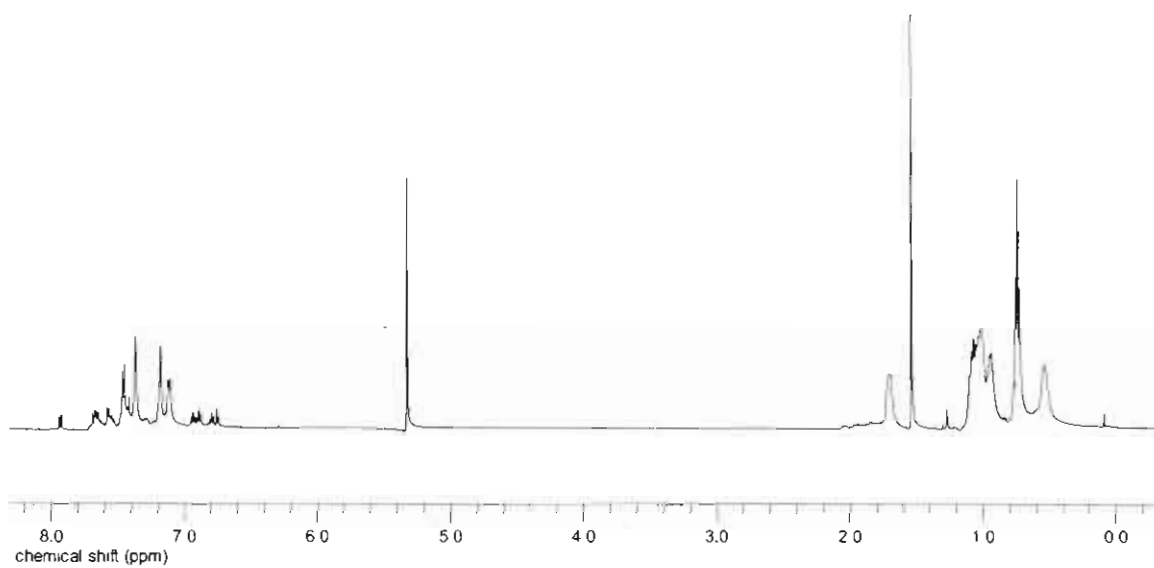
Figure A.4: ^{1}H NMR of PFTIr10 in CD$_2$Cl$_2$.

118
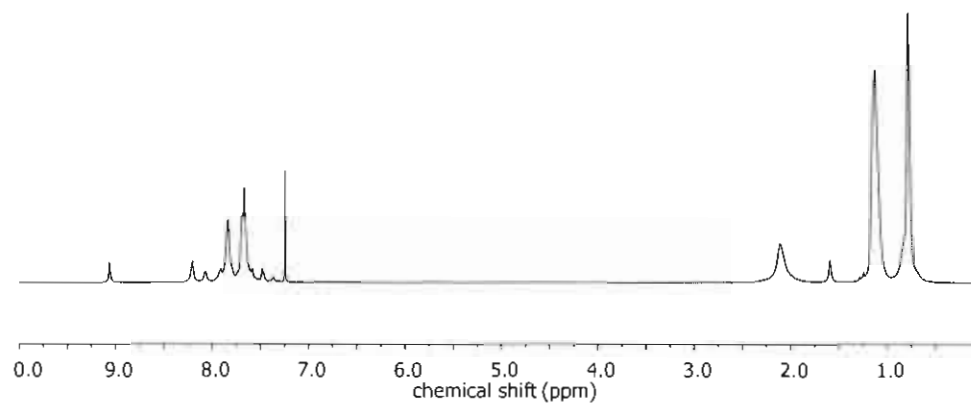
Figure A.5: ^{1}H NMR of PFPhPy in CDCl$_3$.
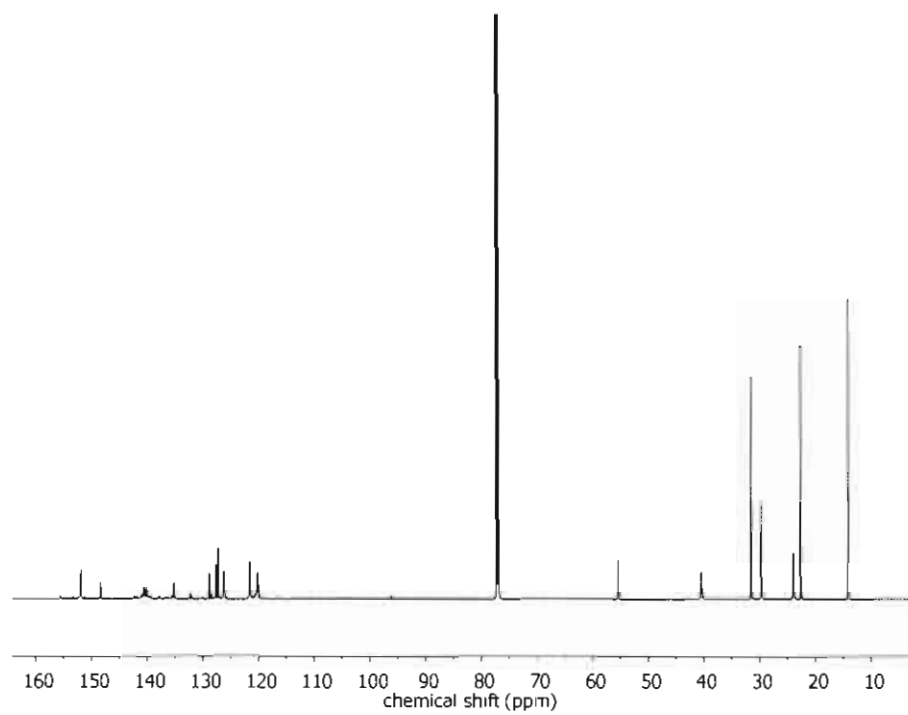
Figure A.6: ^{13}C NMR of PFPhPy in CDCl$_3$.
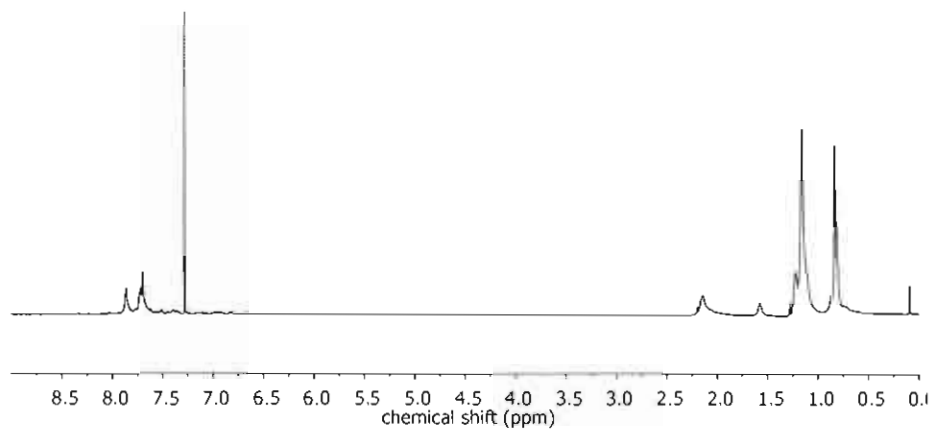
Figure A.7: ^{1}H NMR of PFIr25 in CDCl$_3$.
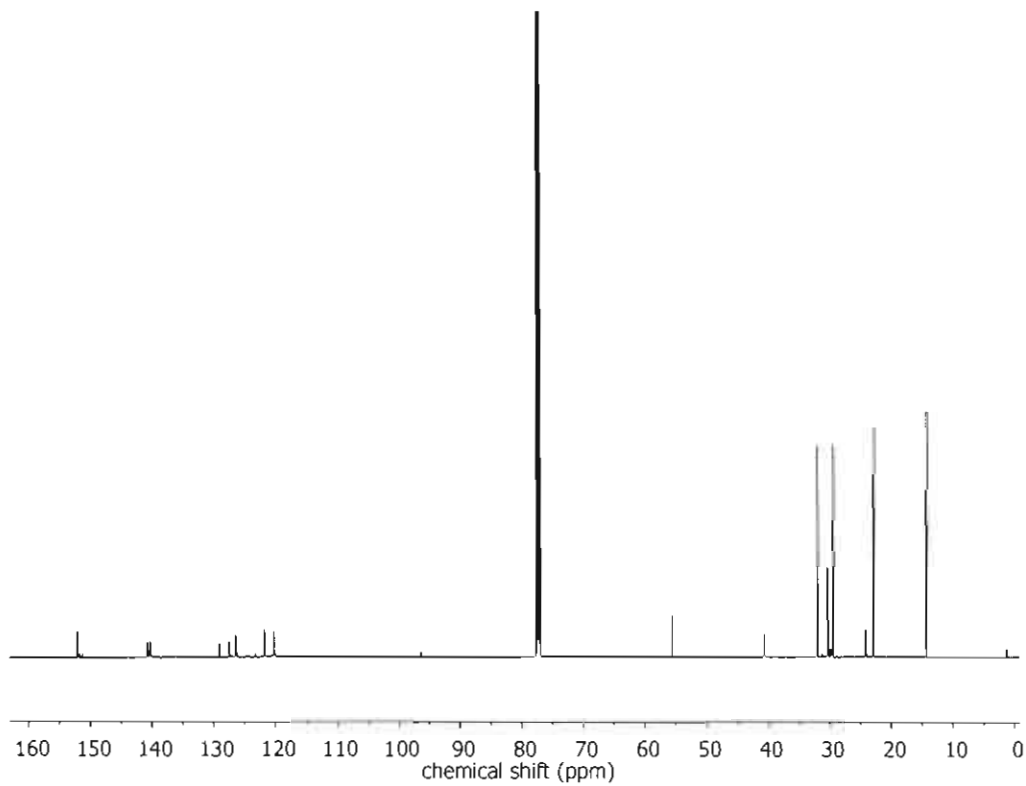
Figure A.8: ^{13}C NMR of PFIr25 in CDCl$_3$.
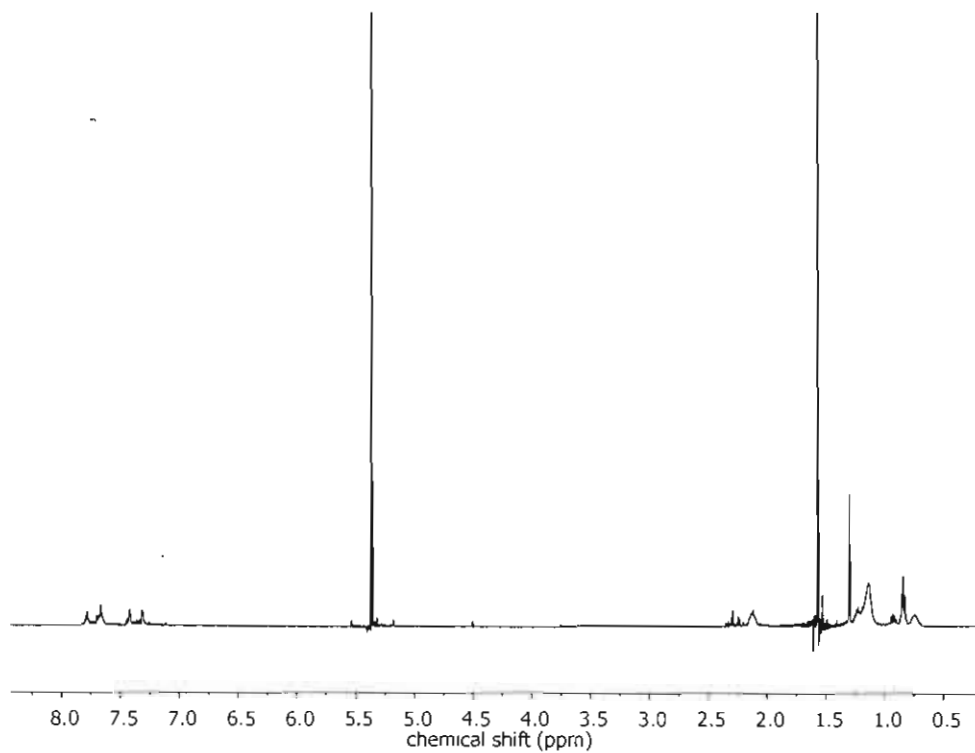
Figure A.9: ^{1}H NMR of F8T2 in CD_2Cl_2.
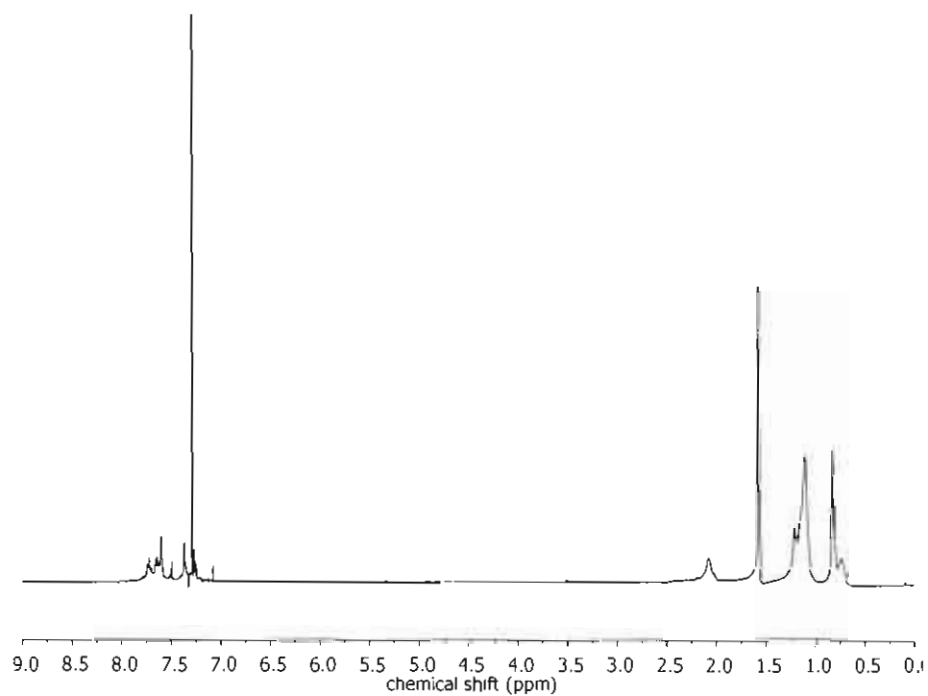
Figure A.10: ^{1}H NMR of F8T2Ir10 in $CDCl_3$.

121
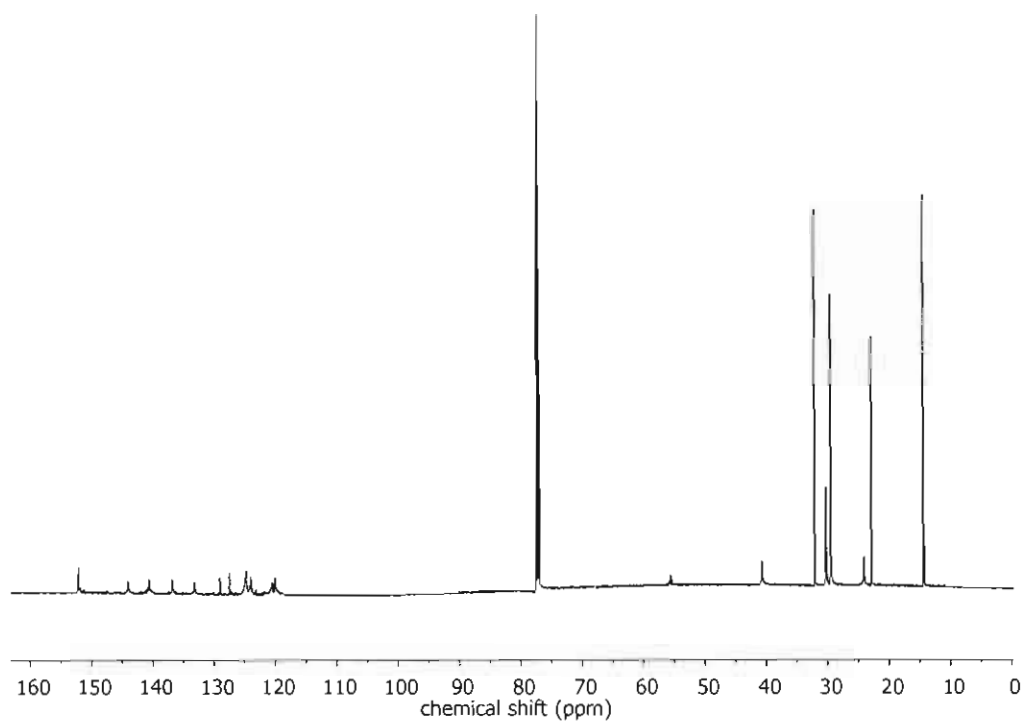
Figure A.11: ^{13}C NMR of F8T2Ir10 in CDCl$_3$.

Appendix B

With the aim of combining the red-shifted absorption of regio-random P3HT (450 nm) relative to **PFIr25** (385 nm) and the expected longer diffusion length of triplet excited states, the synthesis of a regio-random poly(thiophene-co-irdium) (**PTIr**) was proposed and is shown in Figure B.1.

PTIr
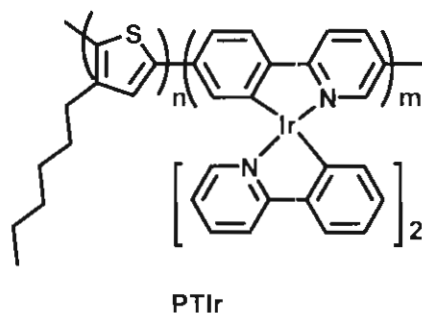
Figure B.1: Proposed structures for red-shifted Ir bound CP relative to PFIr25.

Experimental

3-Bromothiophene, hexylmagnesium bromide, N-bromosuccinimide, 2-isopropoxy-4,4,5,5-tetramethyl-1,3,2-dioxaborolane,, tetrakis(triphenylphosphine)palladium (Pd(PPh3)4), iridium (III) chloride trihydrate, iridium (III) acetylacetonate were purchased from either Sigma-Aldrich Co or Strem Chemicals, Inc. THF, ether and chlorobenzene were dried and freshly distilled before use.

3-Hexylthiophene (1) was synthesized under standard Grignard reaction conditions. Hexylmagnesium bromide (2.0 M in diethyl ether) was added dropwise to a solution of 3-bromothiophene (18.5 g, 0.113 mol) and Ni(dppp)Cl$_2$ (82 mg, 0.151 mmol) in ether (120 mL). The mixture began to reflux after ~ ¼ of the hexylmagnesium bromide was added. The mixture was refluxed for an additional 3 h. The reaction mixture was cooled in an ice bath then poured slowly into 2 M HCl (150 mL). The layers were separated and the aqueous layer was washed with 3 x 100 mL of ether. The combined organic layers were washed with 3 x 100 mL of a saturated solution of NaCl. The crude product was

distilled under vacuum, the fraction boiling at 48°C was collected. Yield: 15.1 g (79%). δ_H (500 MHz, CDCl$_3$, Me$_4$Si) 7.15 (1 H, d), 6.84 (2 H, dd), 2.55 (2 H, t), 1.54 (2 H, t), 1.24 (6 H, m), 0.81 (3 H, t).

2,5-Dibromo-3-hexylthiophene (**2**) was synthesized from (**1**). 3-Hexylthiophene (**1**, 15 g, 0.089 mol) was dissolved in 1:1 (v/v) acetic acid/CHCl$_3$ (150 mL). N-bromosuccinimide (36.4 g, 0.20 mol) was added to the solution and stirred overnight. The reaction mixture was washed with 3 x 100 mL of 0.5 M NaHCO$_3$ and the organic fraction was dried over MgSO$_4$. The solvent was removed by rotary evaporation, the crude product was distilled under vacuum, and the fraction boiling at 120°C was collected as a pale yellow liquid. Yield: 23.5 g (81%). δ_H (500 MHz, CDCl$_3$, Me$_4$Si) 6.78 (1 H, s), 2.51 (2 H, t), 1.54 (2 H, t), 1.31 (6 H, m), 0.90 (3 H, t).

2,5-Bis(4,4,5,5-tetramethyl-1,3,2-dioxaborolan-2-yl)-3-hexylthiophene (**3**) was synthesized according to a modified published procedure.[126] To a solution of 2,5-dibromo-3-hexylthiophene (2, 6g, 18.3 mmol) in THF (75 mL) at -78°C, 43 mL (73.5 mmol) of tert-butyllithium (1.7 M in pentane) was added dropwise. The mixture was stirred at -78°C, allowed to slowly warm up to 10°C. A small fraction was removed, quenched with H$_2$O and analyzed using GC, revealing one peak at 4.67 minutes. The signal at 4.67 min corresponded to 3-hexylthiophene, the product expected when 2,5-dilithium-3-hexylthiophene is quenched with H$_2$O. The reaction mixture was cooled to -78°C, followed by the rapid addition of 2-isopropoxy-4,4,5,5-tetramethyl-1,3,2-dioxaborolane (5.3g, 28 mmol). The reaction mixture was allowed to come to room temperature slowly and stirred for an additional 12 h. The contents of the reaction flask were poured into 100 mL of H$_2$O and extracted with 3 x 100 mL of ether. The organic extracts were washed with 3 x 100 mL of a saturated solution of NaCl and dried over MgSO$_4$. The solvent was removed by rotary evaporation; the residue was purified by column chromatography (silica gel, 1% ethyl acetate in hexane) resulting in a pale orange viscous liquid. Yield: 4.9 g (65%). δ_H (500 MHz, CDCl$_3$, Me$_4$Si) 7.5 (1 H, s), 2.87 (2 H, t), 1.58 (2 H, m), 1.32 (30 H, m), 0.88 (3 H,

t). m/z (CI) 421.1 (M$^+$, C$_{22}$H$_{38}$B$_2$O$_4$S requires 420.2) 377.6 (M$^+$- C$_3$H$_7$, C$_{19}$H$_{31}$B$_2$O$_4$S requires 377.2) 256.0 (M$^+$- C$_9$H$_{13}$, C$_{10}$H$_{18}$B$_2$O$_4$S requires 256.1).

Poly(3-hexylthiophene)s (PT) synthesis was attempted *via* Suzuki polycondensation according to Figure B.2.[87] 2,5-Bis(4,4,5,5-tetramethyl-1,3,2-dioxaborolan-2-yl)-3-hexylthiophene **(3)** (0.304 g, 0.71 mmol) and 2,5-dibromo-3-hexylthiophene **(2)** (0.256, 0.71 mmol) were dissolved in THF (12 mL, deoxygenated), to which, a solution of K$_2$CO$_3$ (2 M, 2 mL) was added, together with Pd(PPh$_3$)$_4$ (0.025 g, 3 mol % based on the thiophene boronic ester). The resulting mixture was sealed in a round bottom flask and heated for 5 days at 80°C in an oil bath. End capping of the polymer was carried out as the last step in synthesis. Phenyl boronic acid (0.008.7 g, 10 mol %) was added and the solution was heated (80°C, 12 h), followed by the addition of bromobenzene (0.023 g, 15 mol %), at the same temperature. Once cooled to room temperature, THF was removed and the residue dissolved in chloroform, followed by washing with water (3 times) and drying over anhydrous MgSO$_4$. After filtration, the volume of chloroform was reduced and the concentrated solution was passed through an alumina column. The volume of the resulting solution was again reduced and precipitated in methanol (~50 mL) to yield a small quantity of gel.

Results and Discussion
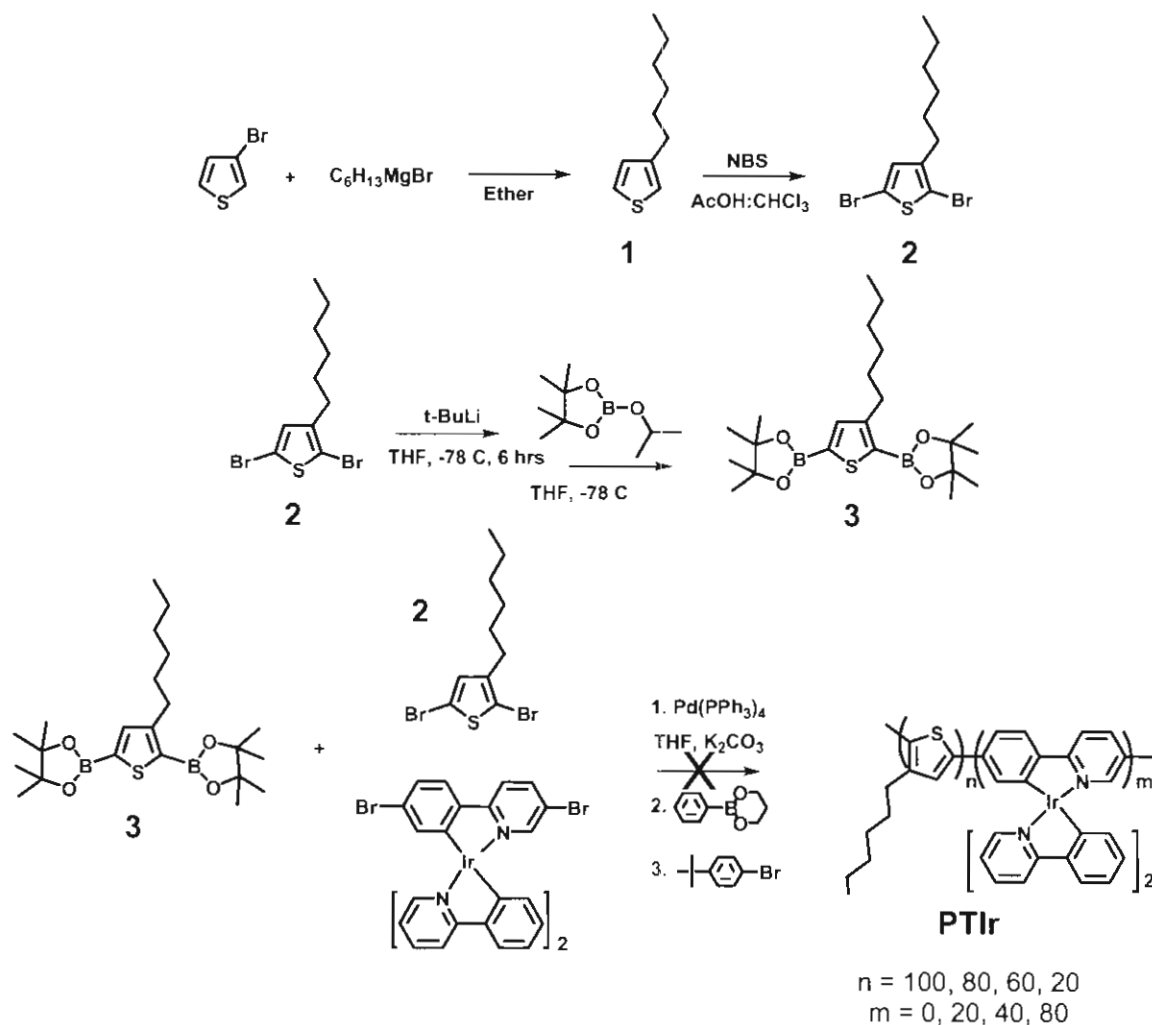
Figure B.2: Proposed reaction scheme for PTIr.

Figure B.2 shows the proposed reaction route for the synthesis of the PTIr series. The first step of the reaction involves the coupling of n-hexylmagnesium bromide with 3-bromothiophene, which afforded **1** in 75 % yield. Compound **1** was dibrominated upon addition of 2.25 molar equivalents of N-bromosuccinimide, to yield **2** as a pale liquid in 81 % yield. Compound **2** was further reacted with 4 molar equivalents of tert-butyllithium, followed by addition of 2-isopropoxy-4,4,5,5-tetramethyl-1,3,2-dioxaborolane. This afforded the desired monomer, **3**, in 65 % yield.

The synthesis of **PTIr** using Suzuki polycondensation as shown in Figure B.2 was unsuccessful. A small quantity of gel was obtained as opposed to a fibrous polymer. The reaction was attempted multiple times, while varying the reaction conditions, for example using a different bases such as Na_2CO_3, K_2CO_3 or NaOH. Suzuki and Miyaura reported that both the strength of the base and changing the ligands of the palladium catalyst can effect the reactivity and yield of palladium-catalyzed cross-coupled reactions between organoboron and dihaloaryl compounds.[127] The failure of the polymerization is believed to be attributed to the lower reactivity of the 2,5-diboronic ester of 3-hexyl thiophene. In electrophilic aromatic substitution (EAS), it has been established that alkyl groups are *ortho* and *para* directors and that the *meta* position is deactivated. The lower reactivity of the 2,5-diboronic ester of 3-hexyl thiophene could therefore arise from the deactivation of the 5-position due to its position "*meta*" to the hexyl chain. Another strategy that could be employed in the future to polymerize 3-hexylthiophene using Suzuki polycondensation, include the use of a more active catalyst such as Ni(II)-aryl complexes.[128]

Appendix C

Some of the iridium complexes described in this thesis were synthesized using an in-house modified Panasonic Inverter Microwave (model no NN-S614). All reactions were carried out under N_2 in an open system. It should be noted that microwave reactions done in closed systems are potentially dangerous due to pressure build up. Figure C.1 shows a photograph of the microwave reactor before operation.

Figure C.1: Photograph of the modified microwave oven.

A hole was drilled through the top of the oven by the SFU machine shop to allow for attachment of a water condenser. Upon compromising the body of the microwave, the over would short circuit after only a few seconds of operation, which was attributed to a safety feature put in by the manufacturers.

REFERENCES

[1]   C. K. Chiang, C. R. Fincher, Y. W. Park, A. J. Heeger, H. Shirakawa, E. J. Louis, S. C. Gau, A. G. Macdiarmid, *Physical Review Letters* **1977**, *39*, 1098.

[2]   R. H. Friend, R. W. Gymer, A. B. Holmes, J. H. Burroughes, R. N. Marks, C. Taliani, D. D. C. Bradley, D. A. Dos Santos, J. L. Bredas, M. Logdlund, W. R. Salaneck, *Nature* **1999**, *397*, 121.

[3]   L. S. Hung, C. H. Chen, *Mater. Sci. Eng. R-Rep.* **2002**, *39*, 143.

[4]   C. D. Dimitrakopoulos, D. J. Mascaro, *IBM J. Res. Dev.* **2001**, *45*, 11.

[5]   E. Bundgaard, S. E. Shaheen, F. C. Krebs, D. S. Ginley, *Sol. Energy Mater. Sol. Cells* **2007**, *91*, 1631.

[6]   S.-S. a. S. N. S. Sun, *Organic Photovoltaics*, CRC Press, Florida **2005**.

[7]   C. J. Brabec, N. S. Sariciftci, J. C. Hummelen, *Adv. Func. Mater.* **2001**, *11*, 15.

[8]   R. D. McCullough, *Adv. Mater.* **1998**, *10*, 93.

[9]   P. Kovacic, C. Wu, *Journal of Polymer Science* **1960**, *47*, 45.

[10]   M. Leclerc, F. M. Diaz, G. Wegner, *Makromolekulare Chemie-Macromolecular Chemistry and Physics* **1989**, *190*, 3105.

[11]   R. D. McCullough, R. D. Lowe, M. Jayaraman, D. L. Anderson, *Journal of Organic Chemistry* **1993**, *58*, 904.

[12]   M. Fukuda, K. Sawada, K. Yoshino, *Japanese Journal of Applied Physics Part 2-Letters* **1989**, *28*, L1433.

[13]   T. Yamamoto, A. Yamamoto, *Chemistry Letters* **1977**, 353.

[14]   M. Rehahn, A. D. Schluter, G. Wegner, W. J. Feast, *Polymer* **1989**, *30*, 1054.

[15]   Z. N. Bao, W. K. Chan, L. P. Yu, *Chemistry of Materials* **1993**, *5*, 2.

[16]   G. L. Schulz, X. Chen, H. S., *Appl. Phys. Lett.* **2009**, *94*, 023302.

[17]   R. E. Peierls, *Quantum Theory of Solids*, Oxford University Press, **1955**.

[18]   A. J. Heeger, *Angewandte Chemie-International Edition* **2001**, *40*, 2591.

[19]   J. Guillet, *Polymer photophysics and photochemistry*, Cambridge University Press, Cambridge **1985**.

[20]   J. Liu, Y. J. Shi, Y. Yang, *Appl. Phys. Lett.* **2001**, *79*, 578.

[21]   I. P. Kaminow, L. W. Stulz, Chandros.Ea, C. A. Pryde, *Applied Optics* **1972**, *11*, 1563.

[22]   M. A. Baldo, D. F. O'Brien, Y. You, A. Shoustikov, S. Sibley, M. E. Thompson, S. R. Forrest, *Nature* **1998**, *395*, 151.

[23]   D. F. O'Brien, C. Giebeler, R. B. Fletcher, A. J. Cadby, L. C. Palilis, D. G. Lidzey, P. A. Lane, D. D. C. Bradley, W. Blau, *Syn. Met.* **2001**, *116*, 379.

[24]   Y. G. Ma, H. Y. Zhang, J. C. Shen, C. M. Che, *Syn. Met.* **1998**, *94*, 245.

[25]   J. Yang, K. C. Gordon, *Syn. Met.* **2005**, *152*, 213.

[26]   J. Kido, H. Hayase, K. Hongawa, K. Nagai, K. Okuyama, *Appl. Phys. Lett.* **1994**, *65*, 2124.

[27]   M. D. McGehee, T. Bergstedt, C. Zhang, A. P. Saab, M. B. O'Regan, G. C. Bazan, V. I. Srdanov, A. J. Heeger, *Adv. Mater.* **1999**, *11*, 1349.

[28]   M. Zhang, P. Lu, X. Wang, L. He, H. Xia, W. Zhang, B. Yang, L. Liu, L. Yang, M. Yang, Y. Ma, J. Feng, D. Wang, N. Tamai, *Journal of Physical Chemistry B* **2004**, *108*, 13185.

[29]   C. L. Lee, K. B. Lee, J. J. Kim, *Appl. Phys. Lett.* **2000**, *77*, 2280.

[30]   C. Jiang, W. Yang, J. Peng, S. Xiao, Y. Cao, *Adv. Mater.* **2004**, *16*, 537.

[31]   E. B. Namdas, A. Ruseckas, I. D. W. Samuel, S. C. Lo, P. L. Burn, *Journal of Physical Chemistry B* **2004**, *108*, 1570.

[32]   Y. Kawamura, K. Goushi, J. Brooks, J. J. Brown, H. Sasabe, C. Adachi, *Appl. Phys. Lett.* **2005**, *86*, 071104/1.

[33]   X. Gong, J. C. Ostrowski, G. C. Bazan, D. Moses, A. J. Heeger, M. S. Liu, A. K. Y. Jen, *Adv. Mater.* **2003**, *15*, 258.

[34]   F. C. Chen, G. F. He, Y. Yang, *Appl. Phys. Lett.* **2003**, *82*, 1006.

[35]   J. X. Jiang, W. Yang, Y. Cao, *Journal of Inorganic and Organometallic Polymers and Materials* **2007**, *17*, 37.

[36]   G. Vamvounis, S. Holdcroft, *Adv. Mater.* **2004**, *16*, 716.

[37]   G. L. Schulz, X. W. Chen, S. A. Chen, S. Holdcroft, *Macromolecules* **2006**, *39*, 9157.

[38]   W. Luzny, M. Trznadel, A. Pron, *Syn. Met.* **1996**, *81*, 71.

[39]   H. Y. Mao, B. Xu, S. Holdcroft, *Macromolecules* **1993**, *26*, 1163.

[40]   U. Scherf, E. J. W. List, *Adv. Mater.* **2002**, *14*, 477.

[41]   N. Blouin, A. Michaud, D. Gendron, S. Wakim, E. Blair, R. Neagu-Plesu, M. Belletete, G. Durocher, Y. Tao, M. Leclerc, *J. Amer. Chem. Soc.* **2008**, *130*, 732.

[42]   H. Spanggaard, F. C. Krebs, *Sol. Energy Mater. Sol. Cells* **2004**, *83*, 125.

[43]   V. D. Mihailetchi, P. W. M. Blom, J. C. Hummelen, M. T. Rispens, *J. Appl. Phys.* **2003**, *94*, 6849.

[44]   F. Q. Guo, K. Ogawa, Y. G. Kim, E. O. Danilov, F. N. Castellano, J. R. Reynolds, K. S. Schanze, *Physical Chemistry Chemical Physics* **2007**, *9*, 2724.

[45]   H. Hoppe, N. S. Sariciftci, *Journal of Materials Research* **2004**, *19*, 1924.

[46]   W. L. Ma, C. Y. Yang, X. Gong, K. Lee, A. J. Heeger, *Adv. Func. Mater.* **2005**, *15*, 1617.

[47]   X. Yang, J. Loos, S. C. Veenstra, W. J. H. Verhees, M. M. Wienk, J. M. Kroon, M. A. J. Michels, R. A. J. Janssen, *Nano Letters* **2005**, *5*, 579.

[48]   D. A. Skoog, F. J. Holler, T. A. Nieman, *Principles of Instrumental Analysis*, Hardcourt Brane College Publishers, Florida **1998**.

[49]   D. F. Eaton, *Pure and Applied Chemistry* **1988**, *60*, 1107.

[50]   D. Magde, J. H. Brannon, T. L. Cremers, J. Olmsted, III, *Journal of Physical Chemistry* **1979**, *83*, 696.

[51]   E. P. Bertin, *Principles and Practise of X-Ray Spectometric Analysis*, Plenum Press, New York **1975**.

[52]   J. Wang, *Analytical Electrochemistry*, VCH Publishers, **1994**.

[53]   R. Cervini, X. C. Li, G. W. C. Spencer, A. B. Holmes, S. C. Moratti, R. H. Friend, *Syn. Met.* **1997**, *84*, 359.

[54]   H. R. Allcock, F. W. Lampe, J. E. Mark, *Contemporary Polymer Chemistry*, Pearson Education, Inc., **2003**.

[55]   X. Chen, J. L. Liao, Y. Liang, M. O. Ahmed, H. E. Tseng, S. A. Chen, *J. Amer. Chem. Soc.* **2003**, *125*, 636.

[56]   K. Waldermar, Vol. 1 (Ed: K. Waldermar), CRC Press, **2006**, 3728.

[57]   D. A. Atchison, G. Smith, *Optic of the Human Eye*, Elsevier Health Sciences, **2000**.

[58]   K. a. S. U. Mullen, *Organic Light Emitting Devices*, Wiley_VCH, Weinheim **2006**.

[59]   X. Gong, M. R. Robinson, J. C. Ostrowski, D. Moses, G. C. Bazan, A. J. Heeger, *Adv. Mater.* **2002**, *14*, 581.

[60]   M. C. Scharber, D. Muehlbacher, M. Koppe, P. Denk, C. Waldauf, A. J. Heeger, C. J. Brabec, *Adv. Mater.* **2006**, *18*, 789.

[61]   Z. Chiguvare, V. Dyakonov, *Phys. Rev. B* **2004**, *70*, 5207.

[62]   P. Lampert M. A. and Mark, *Current Injection in Solids*, Academic, New York **1970**.

[63]   I. F. Perepichka, D. F. Perepichka, H. Meng, F. Wudl, *Adv. Mater.* **2005**, *17*, 2281.

[64]   Y. Q. Mo, R. Y. Tian, W. Shi, Y. Cao, *Chemical Communications* **2005**, 4925.

[65]   E. Bundgaard, F. C. Krebs, *Sol. Energy Mater. Sol. Cells* **2007**, *91*, 954.

[66]   C. J. Brabec, S. E. Shaheen, T. Fromherz, F. Padinger, J. C. Hummelen, A. Dhanabalan, R. A. J. Janssen, N. S. Sariciftci, *Syn. Met.* **2001**, *121*, 1517.

[67]   A. J. Sandee, C. K. Williams, N. R. Evans, J. E. Davies, C. E. Boothby, A. Koehler, R. H. Friend, A. B. Holmes, *J. Amer. Chem. Soc.* **2004**, *126*, 7041.

[68]   H. Zhen, C. Jiang, W. Yang, J. Jiang, F. Huang, Y. Cao, *Chemistry--A European Journal* **2005**, *11*, 5007.

[69]   J. Jiang, C. Jiang, W. Yang, H. Zhen, F. Huang, Y. Cao, *Macromolecules* **2005**, *38*, 4072.

[70]   T. Ito, S. Suzuki, J. Kido, *Polymers for Advanced Technologies* **2005**, *16*, 480.

[71]   G. Li, Y. Yao, H. Yang, V. Shrotriya, G. Yang, Y. Yang, *Adv. Func. Mater.* **2007**, *17*, 1636.

[72]   M. M. Koetse, J. Sweelssen, K. T. Hoekerd, H. F. M. Schoo, S. C. Veenstra, J. M. Kroon, X. Yang, J. Loos, *Appl. Phys. Lett.* **2006**, *88*, 083504/1.

[73]   A. J. Heeger, *Solid State Communications* **1998**, *107*, 673.

[74]   P. K. H. Ho, D. S. Thomas, R. H. Friend, N. Tessler, *Science* **1999**, *285*, 233.

[75]   S. Lamansky, P. Djurovich, D. Murphy, F. Abdel-Razzaq, H. E. Lee, C. Adachi, P. E. Burrows, S. R. Forrest, M. E. Thompson, *J. Amer. Chem. Soc.* **2001**, *123*, 4304.

[76]   Y. H. Niu, Y. L. Tung, Y. Chi, C. F. Shu, J. H. Kim, B. Chen, J. Luo, A. J. Carty, A. K. Y. Jen, *Chemistry of Materials* **2005**, *17*, 3532.

[77]   F. Li, M. Zhang, G. Cheng, J. Feng, Y. Zhao, Y. G. Ma, S. Y. Liu, J. C. Shen, *Appl. Phys. Lett.* **2004**, *84*, 148.

[78]   J. Brooks, Y. Babayan, S. Lamansky, P. I. Djurovich, I. Tsyba, R. Bau, M. E. Thompson, *Inorganic Chemistry* **2002**, *41*, 3055.

[79]   M. Sudhakar, P. I. Djurovich, T. E. Hogen-Esch, M. E. Thompson, *J. Amer. Chem. Soc.* **2003**, *125*, 7796.

[80]   W. Yang, H. Y. Zhen, C. Y. Jiang, L. J. Su, J. X. Jiang, H. H. Shi, Y. Cao, *Syn. Met.* **2005**, *153*, 189.

[81]   G. Vamvounis, G. L. Schulz, S. Holdcroft, *Macromolecules* **2004**, *37*, 8897.

[82]   M. Ranger, M. Leclere, *Canadian Journal of Chemistry-Revue Canadienne De Chimie* **1998**, *76*, 1571.

[83]   S. S. Tokito, M; Tanaka, I; Inoue, Y.; Shirane, K.; Takeuchi, M; Ito, N, **2003**.

[84]   H. Konno, Y. Sasaki, *Chemistry Letters* **2003**, *32*, 252.

[85]   T. Yamamoto, Z. h. Zhou, T. Kanbara, M. Shimura, K. Kizu, T. Maruyama, Y. Nakamura, T. Fukuda, B. L. Lee, *J. Amer. Chem. Soc.* **1996**, *118*, 10389.

[86]   A. B. Tamayo, B. D. Alleyne, P. I. Djurovich, S. Lamansky, I. Tsyba, N. N. Ho, R. Bau, M. E. Thompson, *J. Amer. Chem. Soc.* **2003**, *125*, 7377.

[87]   M. Ranger, M. Leclerc, *Canadian Journal of Chemistry-Revue Canadienne de Chimie* **1998**, *76*, 1571.

[88]   D. Neher, *Macromolecular Rapid Communications* **2001**, *22*, 1366.

[89]   K. Saito, N. Matsusue, H. Kanno, Y. Hamada, H. Takahashi, T. Matsumura, *Japanese Journal of Applied Physics, Part 1: Regular Papers, Short Notes & Review Papers* **2004**, *43*, 2733.

[90]   S. Lamansky, P. Djurovich, D. Murphy, F. Abdel-Razzaq, R. Kwong, I. Tsyba, M. Bortz, B. Mui, R. Bau, M. E. Thompson, *Inorganic Chemistry* **2001**, *40*, 1704.

[91]   B. Liu, W. L. Yu, Y. H. Lai, W. Huang, *Chemistry of Materials* **2001**, *13*, 1984.

[92]   A. P. Monkman, H. D. Burrows, L. J. Hartwell, L. E. Horsburgh, I. Hamblett, S. Navaratnam, *Physical Review Letters* **2001**, *86*, 1358.

[93]   A. J. Makinen, I. G. Hill, Z. H. Kafafi, *J. Appl. Phys.* **2002**, *92*, 1598.

[94]   A. Donat-Bouillud, I. Levesque, Y. Tao, M. D'Iorio, S. Beaupre, P. Blondin, M. Ranger, J. Bouchard, M. Leclerc, *Chemistry of Materials* **2000**, *12*, 1931.

[95]   G. Klaerner, R. D. Miller, *Macromolecules* **1998**, *31*, 2007.

[96]   P. H. Aubert, M. Knipper, L. Groenendaal, L. Lutsen, J. Manca, D. Vanderzande, *Macromolecules* **2004**, *37*, 4087.

[97]   X. Gong, S. H. Lim, J. C. Ostrowski, D. Moses, C. J. Bardeen, G. C. Bazan, *J. Appl. Phys.* **2004**, *95*, 948.

[98]   M. S. Liu, J. D. Luo, A. K. Y. Jen, *Chemistry of Materials* **2003**, *15*, 3496.

[99]   H. Y. Zhen, C. Luo, W. Yang, W. Y. Song, B. Du, J. X. Jiang, C. Y. Jiang, Y. Zhang, Y. Cao, *Macromolecules* **2006**, *39*, 1693.

[100] T. H. Huang, J. T. Lin, Y. T. Tao, C. H. Chuen, *Chemistry of Materials* **2003**, *15*, 4854.

[101] S. Gunes, H. Neugebauer, N. S. Sariciftci, *Chem. Rev.* **2007**, *107*, 1324.

[102] T. A. Chen, R. D. Rieke, *Syn. Met.* **1993**, *60*, 175.

[103] R. D. McCullough, S. Tristramnagle, S. P. Williams, R. D. Lowe, M. Jayaraman, *J. Amer. Chem. Soc.* **1993**, *115*, 4910.

[104]   P. Schilinsky, C. Waldauf, C. J. Brabec, *Appl. Phys. Lett.* **2002**, *81*, 3885.

[105]   A. Kohler, H. F. Wittmann, R. H. Friend, M. S. Khan, J. Lewis, *Syn. Met.* **1996**, *77*, 147.

[106]   Y. Shao, Y. Yang, *Adv. Mater.* **2005**, *17*, 2841.

[107]   F. Q. Guo, Y. G. Kim, J. R. Reynolds, K. S. Schanze, *Chemical Communications* **2006**, 1887.

[108]   C. M. Yang, C. H. Wu, H. H. Liao, K. Y. Lai, H. P. Cheng, S. F. Horng, H. F. Meng, J. T. Shy, *Appl. Phys. Lett.* **2007**, *90*.

[109]   Y. Y. Noh, C. L. Lee, J. J. Kim, K. Yase, *Journal of Chemical Physics* **2003**, *118*, 2853.

[110]   S. W. Thomas, S. Yagi, T. M. Swager, *Journal of Materials Chemistry* **2005**, *15*, 2829.

[111]   S. J. Liu, Q. Zhao, R. F. Chen, Y. Deng, Q. L. Fan, F. Y. Li, L. H. Wang, C. H. Huang, W. Huang, *Chemistry-A European Journal* **2006**, *12*, 4351.

[112]   C. Rothe, S. King, A. Monkman, *Nat. Mater.* **2006**, *5*, 463.

[113]   B. C. Thompson, J. M. J. Frechet, *Angewandte Chemie-International Edition* **2008**, *47*, 58.

[114]   R. Rawcliffe, D. D. C. Bradley, A. J. Campbell, *Proc. SPIE* **2003**, *5217*.

[115]   L. Burgi, T. J. Richards, R. H. Friend, H. Sirringhaus, *J. Appl. Phys.* **2003**, *94*, 6129.

[116]   P. Ravirajan, S. A. Haque, J. R. Durrant, D. D. C. Bradley, J. Nelson, *Adv. Func. Mater.* **2005**, *15*, 609.

[117]   P. Ravirajan, S. A. Haque, J. R. Durrant, D. Poplavskyy, D. D. C. Bradley, J. Nelson, *J. Appl. Phys.* **2004**, *95*, 1473.

[118]   M. Grell, D. D. C. Bradley, X. Long, T. Chamberlain, M. Inbasekaran, E. P. Woo, M. Soliman, *Acta Polym.* **1998**, *49*, 439.

[119]   E. Lim, B. J. Jung, H. K. Shim, *Macromolecules* **2003**, *36*, 4288.

[120]   G. Dennler, H. J. Prall, R. Koeppe, M. Egginger, R. Autengruber, N. S. Sariciftci, *Appl. Phys. Lett.* **2006**, *89*, 073502.

[121]   K. Kawano, N. Ito, T. Nishimori, J. Sakai, *Appl. Phys. Lett.* **2006**, *88*, 073514.

[122]   K. Tvingstedt, V. Andersson, F. Zhang, O. Inganas, *Appl. Phys. Lett.* **2007**, *91*, 123514.

[123]   J. H. Hou, Z. A. Tan, Y. Yan, Y. J. He, C. H. Yang, Y. F. Li, *J. Amer. Chem. Soc.* **2006**, *128*, 4911.

[124]   C. J. Brabec, S. E. Shaheen, C. Winder, N. S. Sariciftci, P. Denk, *Appl. Phys. Lett.* **2002**, *80*, 1288.

[125] B. K. Yap, R. D. Xia, M. Campoy-Quiles, P. N. Stavrinou, D. D. C. Bradley, *Nat. Mater.* **2008**, *7*, 376.

[126] M. Ranger, D. Rondeau, M. Leclerc, *Macromolecules* **1997**, *30*, 7686.

[127] N. Miyaura, A. Suzuki, *Chem. Rev.* **1995**, *95*, 2457.

[128] C. Chen, L. M. Yang, *Tetrahedron Lett.* **2007**, *48*, 2427.